Alma Mater Studiorum – Università di Bologna

DOTTORATO DI RICERCA IN

Ingegneria Civile, Chimica, Ambientale e dei Materiali

Ciclo XXX

Settore Concorsuale: 09/D1

Settore Scientifico Disciplinare: ING-IND 22

CEMENT-FREE BUILDING MATERIALS: MIX DESIGN AND PROPERTIES IN VIEW OF THEIR APPLICATION IN CIVIL ENGINEERING

Presentata da: Lorenza Carabba

Coordinatore Dottorato

Prof. Luca Vittuari

Supervisore

Prof. Maria Chiara Bignozzi

Co-supervisore

Dott. Ing. Stefania Manzi

Esame finale anno 2018

Abstract

This PhD thesis deals with a new class of cement-free building materials also known as geopolymers. Geopolymers are obtained through the reaction of a low-calcium solid aluminosilicate source in alkaline conditions. In the last 20 years, the interest towards this class of materials has grown exponentially together with the growing concern on global warming due to greenhouse emissions in the atmosphere and the awareness of the detrimental contribution of the cement industry on this issue. This increasing interest is motivated by the fact that to produce geopolymers, waste powders can be used as amorphous aluminosilicate sources and Portland cement additions are not necessary.

With the aim to go forward on the research on geopolymers and to pursuit a sustainable product, this thesis investigates geopolymer systems obtained by room temperature alkali activation of Italian low-calcium fly ash for applications in civil engineering. In view of developing products potentially ready for the market, geopolymers were produced, characterized and tested according to the conventional procedures used for cementitious binders. Geopolymers were investigated as cement-free alternative binders for applications where cement-based materials can show critical issues (e.g. compatibility with existing structures and high temperature resistance). To do that, the mix design was changed by adding different types of aggregates depending on the application.

Geopolymer mortars were obtained using fine quartz aggregate. A preliminary investigation of using commercially available superplasticizers to improve the workability of geopolymer mortars and to facilitate the *in-situ* applications was carried out. The experimental findings showed that the addition of polycarboxylic ether-based superplasticizer improved the workability, without compromising the final strength of the hardened material. The feasibility of using geopolymer mortars for strengthening existing structures by using composites based on fibre reinforced geopolymer matrix (FRGM) technology was demonstrated. Furthermore, results showed that if galvanized steel fibres are used as reinforcement, a reduction in molar concentration of NaOH activating solution is preferable to increase the strengthening effect.

An extensive study on the mechanism of cracking of geopolymer matrix exposed to high temperature treatments was carried out. Results indicated crack formation for temperature higher than 550°C, mainly occurring during the cooling period. The thermal dimensional stability of geopolymers was improved by adding recycled refractory particles to the matrix, thus producing geopolymer composites. The recycled refractory particles did not hinder the alkali activation process, significantly reduced the heat induced cracking, increased the maximum temperature of dimensional stability, and improved the linear dimensional stability during heating.

Lightweight geopolymer mortars were developed using expanded perlite as fine lightweight aggregate and studied as passive fire protection systems for steel substrates. A comprehensive study was carried out starting from the optimization of the mix design up to the testing of the developed mortars by a medium-scale fire test setup. Experimental fire tests demonstrated that the developed lightweight geopolymer mortars were able to provide protection to the steel substrate for more than 30 minutes under cellulosic fire conditions, thus representing an important safety measure against accidental fires with no evidences of explosive spalling

during heating. This aspect is particularly advantageous compared to ordinary Portland cement-based materials, which can be prone to spalling phenomena.

The experimental findings highlighted the strong potential of geopolymers for all the investigated applications. In particular, geopolymers used as both FRGM composites and fireproofing materials showed performance comparable and even better than the commercial products currently used in these fields.

Graphical abstract
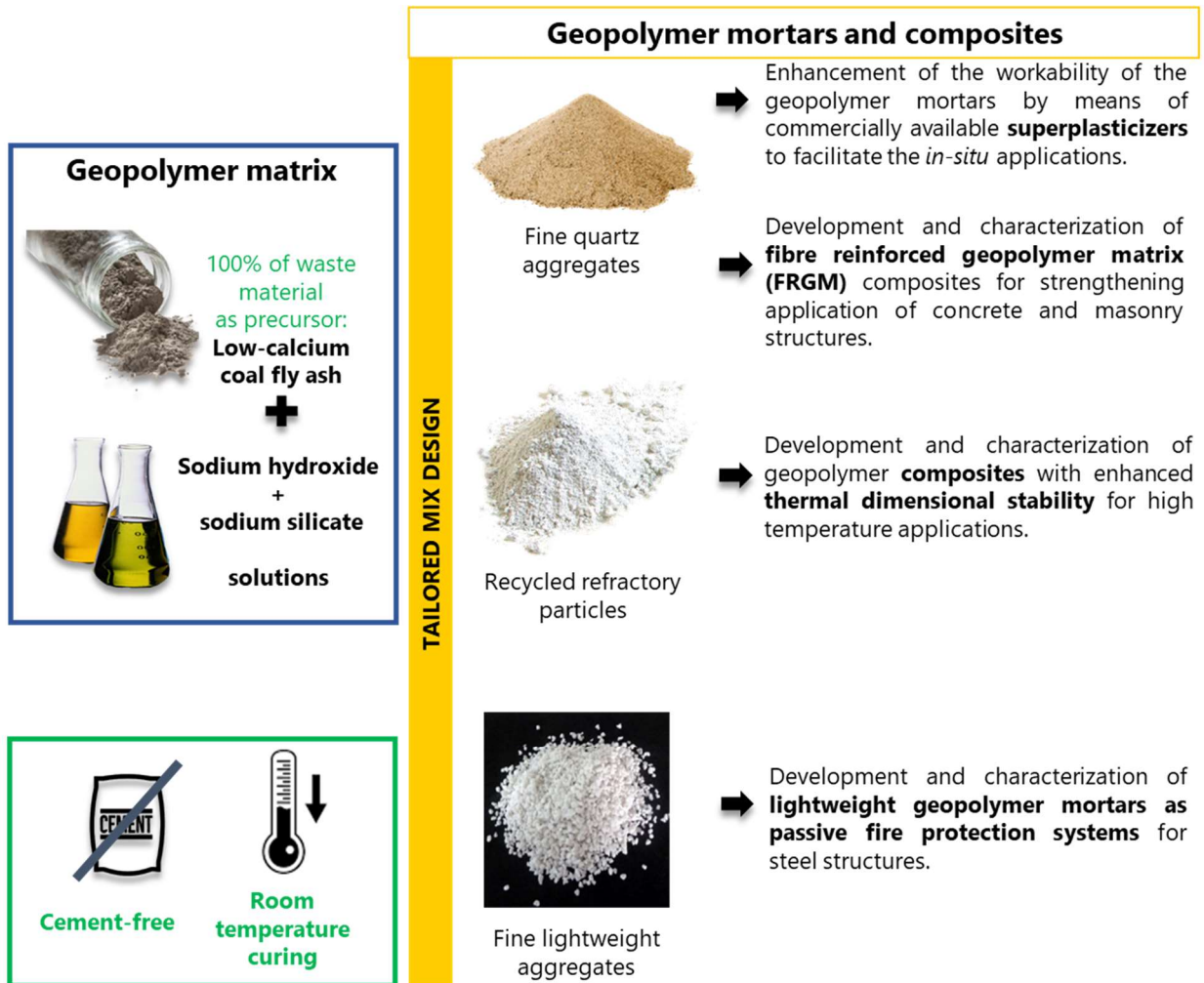
Keywords: Alkali Activated materials; Bond; Civil engineering; Composites; Cracking; Fibre reinforced cementitious matrix; Fire tests; Fireproofing material; Fly ash; Geopolymers; Heat exposure; Mechanical properties; Mix design; Passive fire protection; Porosity; Refractory; Room temperature curing; Single-lap direct-shear tests; Superplasticizers; Thermal conductivity; Thermal stability; Waste processing.

Acknowledgments

I would like to express my sincere gratitude to my advisor Professor Maria Chiara Bignozzi for giving me the opportunity to undertake a PhD and for her supervision, advice, and support during these years.

For the friendship and encouragement, I thank Dr. Stefania Manzi

Special thanks to Dr.-Ing. Hans-Carsten Kühne who gave access to the laboratory and research facilities of Bundesanstalt für Materialforschung und -prüfung (BAM) in Berlin, and to Dr.-Ing Gregor Gluth for his supervision during the months spent at BAM, a very inspiring and fruitful period that enriched my research and my life.

For their collaboration, my sincere thanks goes to Prof. Christian Carloni, Dr. Mattia Santandrea, Prof. Alessandro Tugnoli, and Ing. Raffaela Moricone (DICAM), Dr. Elisa Rambaldi and Dr. Giovanni Ridolfi (Centro Ceramico), and Dipl.-Ing. S.M. Pirskawetz and Dr.rer.nat. S. Krüger (BAM), who helped me achieve interesting results and improve the quality of this research.

I would like to extend my thanks to all the working groups in Bologna and in Berlin. I am grateful to all the students and the technicians who helped me with experiments, in particular to Mr. Paolo Carta who is always there for me with technical and personal advice.

I warmly thank my lab-mates who now I consider real friends. These years wouldn't have been the same without Giulia, my brilliant officemate and fellow adventurer. We went together all the way through the PhD, supporting each other in good and not-so-good days and, eventually, now we can proudly say that we made it! Thanks to Enrico and Gabriela, the HAP dream team, for the stimulating discussions and for their passion and love for science and research, which I found inspiring and motivating.

The greatest "thank you" goes to my family and all my friends for their unconditional love and support no matter the distance. You are constantly pushing me to become a strong and independent woman and for this, I really and sincerely thank you all.

Table of Contents

VII

Chapter 1:

General overview

1.1   Research objectives

Data recently presented at the UN Climate Change Conference (November 2017, Bonn, Germany) revealed that industrial emissions of carbon dioxide are projected to rise of 2 % in 2017 after a three-year plateau [1]. The control of CO_2 emissions to keep the global average temperature increases below 1.5 °C, as signed in the Paris agreement in 2015, is an urgent concern in all research fields. In the field of material science related to the civil engineering, this concern translates into the research of alternative and more sustainable building materials. Among all the building materials, concrete is by far the most widely used one and its consumption is constantly increasing for the increasing demand from developing countries such as China and India. It can be estimated that nowadays, the cement industry accounts for approximately 8% of global anthropogenic CO_2 emissions considering that the production of 1 t of cement releases about 0.73–0.99 t of carbon dioxide in atmosphere and cement consumption is expected to rise to more than 5000 Mt/year by 2050 [2].

In this scenario, a new class of cement-free materials known as geopolymers, considered part of the broad category of alkali activated materials, has raised some interest. This technology is based on the reaction between a solid aluminosilicate source and an alkali activator to obtain a mainly amorphous 3D network of aluminosilicates with binding properties. The remarkable growth of research interest on geopolymers over the last years can be ascribed to their widely advertised low CO_2 emissions when compared to ordinary Portland cement (OPC). Indeed, one of the main advantages of geopolymers consists in the possibility of using waste powders as amorphous aluminosilicate source, taking advantage of their reactivity in sodium and/or potassium hydroxide and silicate solutions. Furthermore, previous studies showed that, if industrial wastes are used as aluminosilicate source and reactions and relevant consolidation process take place at low temperature ($T \leq 100$ °C), these materials achieve a reduced greenhouse effect when compared to Portland cement-based products, in the range of 44-64% [3].

In the building sector, cementitious materials make up 30-50% of everything the human kind produce. Therefore, thinking about replacing them with geopolymers is an unrealistic prospective. However, the approach used in this research is instead investigating the possibility of using the alkali activation technology to provide a possible alternative to cement-based materials for some selected applications. More in detail, this research focuses on coal fly ash-based geopolymers activated at room temperature. The activation of fly ash at room temperature is particularly challenging. Indeed, fly ash originates from waste streams and, for this reason, its microstructure is much more complex than other geopolymer precursors such as calcined clays. In addition, when fly ash is used as precursor, the heat curing usually boosts the activation process, increasing the degree of reaction and final products performance. Nevertheless, it was chosen to use a waste as precursor and to avoid high temperature production processes in order to enhance the environmental and economic benefits for the obtained geopolymers.

The main objectives of this research can be summarized as follows:

–   improvement of the workability of the geopolymer mixture by means of commercially available superplasticizers to facilitate the *in-situ* applications;

–   development and characterization of fly ash-based geopolymers as mortars for strengthening application of concrete and masonry structures. Fibre reinforced geopolymer matrix (FRGM) composites were obtained by embedding continuous fibres on concrete or masonry surfaces through geopolymer mortars. The stress transfer mechanism between the composite and the substrate in FRGM-substrate joints was analysed;

–   development and characterization of fly ash-based geopolymers for high temperature applications. After an extensive study of thermal properties and high temperature behaviour, geopolymer composites were developed with enhanced dimensional thermal stability. In addition, lightweight geopolymer mortars were developed and tested as passive fire protection systems for steel structures.

Macroscopic results are discussed together with microstructural characterization in order to give a comprehensive overview of the final products properties.

The research project was developed at the Department of Civil, Environmental and Materials Engineering (DICAM) of the University of Bologna and, for a period of six months, at the Bundesanstalt für Materialforschung und -prüfung (BAM) in Berlin, Germany.

1.2   Organisation of the Thesis

An updated literature review of fly ash-based geopolymers is presented in Chapter 2.

In Chapter 3, details of the source materials used in this study as well as the mix design and the mixture procedures used for synthesizing the geopolymers are reported. In addition, the techniques adopted for characterizing fresh and hardened properties of the final products are also showed.

In Chapter 4, the influence of commercially available superplasticizers on properties of geopolymers and geopolymer mortars is investigated. Fresh and hardened properties of the final products are analysed with a special focus on porosity and its distribution.

In Chapter 5, an interdisciplinary approach to study newly developed fibre reinforced geopolymer matrix (FRGM) composites for strengthening applications of reinforced concrete and masonry structures is presented. Physical, mechanical, and microstructural properties of geopolymer mortars are measured to characterize completely the material. FRGM strips are bonded to concrete and masonry prisms and single-lap direct shear tests are performed to study the stress transfer mechanism between the composite and the substrates.

In Chapter 6, the behaviour of the geopolymers exposed to high temperature is investigated. Firstly, the damages induced by heat treatments on geopolymers are investigated in details through acoustic emission measurements, SEM and XRD analysis. Secondly, the mix design of the geopolymers is implemented by adding recycled refractory particles, thus obtaining composites with enhanced thermal dimensional stability.

In Chapter 7, the possibility of using fly ash-based geopolymers as passive fire protection (PFP) system for steel components is investigated. A comprehensive study is presented. The first part of the study aims at optimizing the mix design in order to produce lightweight geopolymer mortars with increased thermal insulation and low weight load. Physical, mechanical and thermal properties of the obtained lightweight mortars are investigated. According to the experimental findings, the behaviour of the fireproofing geopolymers during a fire accident is simulated through finite volume method simulations. In the second part of the study, experimental tests are conducted on prototypes of steel covered by the lightweight geopolymer mortars by means of medium-scale fire test setup. Cellulosic and hydrocarbon standard fire curves are adopted. Furthermore, acoustic emission measurements are used to analyse cracking phenomena occurring during the fire tests.

In Chapter 8, the main conclusions of this study and suggestions for future research are reported.

Chapter 2:

Literature review

In this Chapter, an updated overview of literature on low-calcium geopolymers technology is presented linking fundamental geopolymer chemistry to the use of these binders for producing construction materials. The state of the art regarding the processing, chemistry and performance of geopolymers is reported, followed by an overview on the applications. Major attention will be given to fly ash-based systems, since the thesis investigates materials based on them. Metakaolin-based systems will be also described as far as comparison between the two systems is considered useful.

2.1 Background and definition

Geopolymers are a new class of materials with the potential to become an important tool in the construction industry. Geopolymers are obtained through the reaction of a solid aluminosilicate (named the "precursor") under alkaline conditions (induced by the "alkaline activator") [4].

It was the French researcher J. Davidovits who in 1979 introduced the term geopolymer [5], indicating inorganic polymers consisting of chains or networks of mineral molecules linked with covalent bonds. Raw materials used in the synthesis were mainly calcined kaolinitic clay precursors, an aluminosilicate oxide better known under the generic term of metakaolin. For the chemical designation of geopolymers, Davidovits proposed the name "poly(sialate)" where sialate is an abbreviation for silicon-oxo-aluminate. The poly(sialate) has the following empiric formulae:

$$M_n\{-(SiO_2)_z - AlO_2\}_n \cdot wH_2O$$
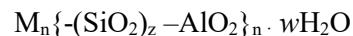
Where n is a degree of polycondensation, M is a cation (e.g., Na^+, K^+), z is 1, 2, or 3.

The reaction of an alkali source with an alumina- and silica-containing solid precursor to form a material comparable to hardened Portland cement, had been already investigated by the German cement chemist and engineer Kühl in 1908 [6,7]. Since then, the most important and pioneering investigations and developments in the field of alkali activation binders are represented by the studies of Purdon in 1940s [8] and Glukhovsky in the late 50s [9]. Purdon, by studying the activation of blast furnace slags with NaOH solutions concluded that the alkali hydroxides acted as catalysts. Glukhovsky developed the so-called "soil cements", discovering the possibility of producing binding materials using low-calcium or calcium-free aluinosilicates and solutions of alkali [10]. He also investigated the activation of blast furnace slag and identified the hydration products as being composed by calcium silicate hydrates and calcium and sodium aluminosilicate hydrates [11].

Nowadays, geopolymers are recognised as a subset of the broadest category of alkali-activated materials. According to State-of-the-Art Reports of the RILEM Technical Committee 224 (TC-224-AMM) [6], the group of alkali-activated materials (AAMs) encompasses any binder system derived by the reaction of an alkali metal source (solid or dissolved) with a solid silicate powder. This solid source can be a calcium silicate as in alkali-activation of more conventional clinkers, or a more aluminosilicate-rich precursor such as a metallurgical slag, natural pozzolan, fly ash or bottom ash. Geopolymers are identified as low-calcium or calcium-free systems where the binding phase is almost exclusively aluminosilicate and highly coordinated. This definition is often

considered misleading, according to the inventor of the term geopolymer. However, the term geopolymer is widely diffused and accepted in the scientific community to describe a low-calcium alkali activated system and this will be the meaning given to this term all through the thesis.

2.2   Geopolymer reaction model

The two main constituents used in preparing geopolymers are alkaline liquids and source materials rich in silica and alumina. Considering the atomic and nanoscale, the alkali activation mainly consists of three stages that overlap: dissolution, polycondensation, and reorganization [12]. Figure 2.1 describes in a schematic way the process and reaction products of the alkaline activation of a solid aluminosilicate precursor [13].
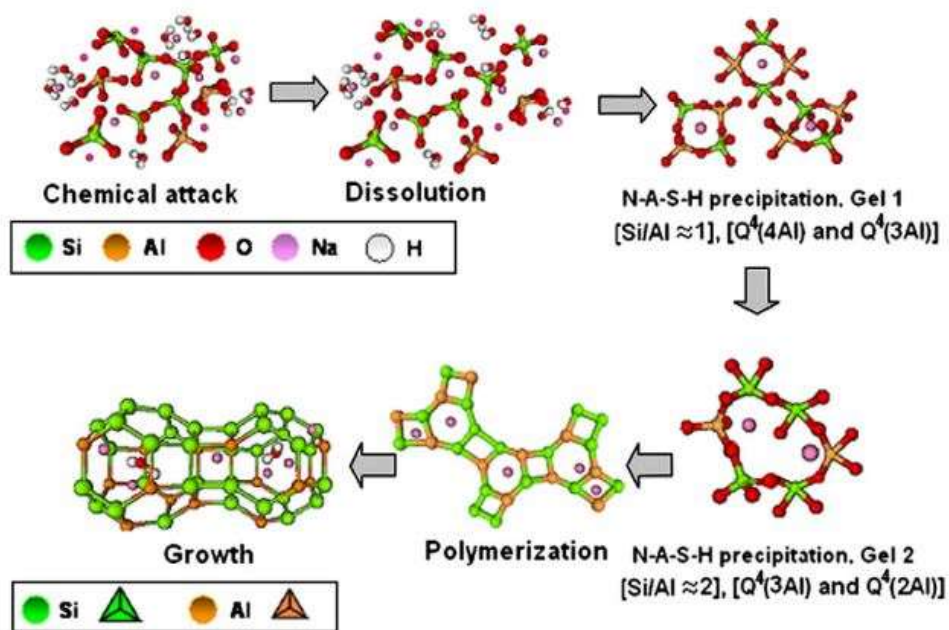
Figure 2.1: Descriptive model of alkali activation of aluminosilicates [13].

At the beginning, a dissolution of the solid aluminosilicate source by the alkaline hydrolysis occurs and silicate and aluminate species are released, most likely in the monomeric form. Due to the high pH, the dissolution phase is rapid and quickly creates a supersaturated aluminosilicate solution. At this point, silicate and aluminate species undergo condensation resulting in the formation of a gel (denoted "gel 1"). This process releases the water that plays the role of a reaction medium, but resides within pores in the gel. This initial aluminosilicate network continues to rearrange and reorganize up to the formation of a more interconnected aluminosilicate network (denoted "gel 2") [12,14,15]. The time for the supersaturated aluminosilicate solution to form the gel is dependent on raw materials, composition of the alkaline solutions, and synthesis conditions [16]. The alkali aluminosilicate gel is characterized by a highly disordered and cross-linked three-dimensional structure in which the Si^{4+} and Al^{3+} cations (often referred to as "T atoms") are tetrahedrally coordinated and joined by oxygen bonds. The negative charge of the AlO_4^- group is charge-balanced by the presence of alkaline

cations (often referred to as "M+", typically Na+ and/or K+). K cations are more rapidly and tightly included into the gel structure than Na at early age [17].

The notation used to indicate aluminosilicate gel is $Q^n(m\text{Al})$ [18], where:

  - n is the coordinator number of the silicon centre;
  - m is the number of Al neighbours and depends on the Si/Al ratio of the gel;
  - $0 \leq m \leq n \leq 4$.

The molecular structure of geopolymers has been deeply investigated during years. The use of ^{29}Si, ^{27}Al and ^{23}Na MAS NMR (i.e. nuclear magnetic resonance) allowed investigating the chemical ordering of silicon and aluminium in geopolymers and the relative extent of incorporation of each type of T-atom into the geopolymer gel framework. It was found that the structure of the gel is significantly influenced by raw material and reaction conditions, as well as by the nature of the alkali cations present [16,18,19]. In particular, the role of reactive alumina in the raw material has been highlighted. When the aluminosilicate source is in contact with the alkaline environment, the Al-O bonds are more readily broken than Si-O bonds. Therefore, for short reaction times, the gel will be constituted by an Al-rich phase. As the reaction progresses, the gel will evolve in a more stable Si-rich phases. However, a certain minimum amount of reactive Al is always necessary to favour the formation of the gels [19].

A distinction in the type of gel that dominates the structure can be made based on the calcium content in the system.
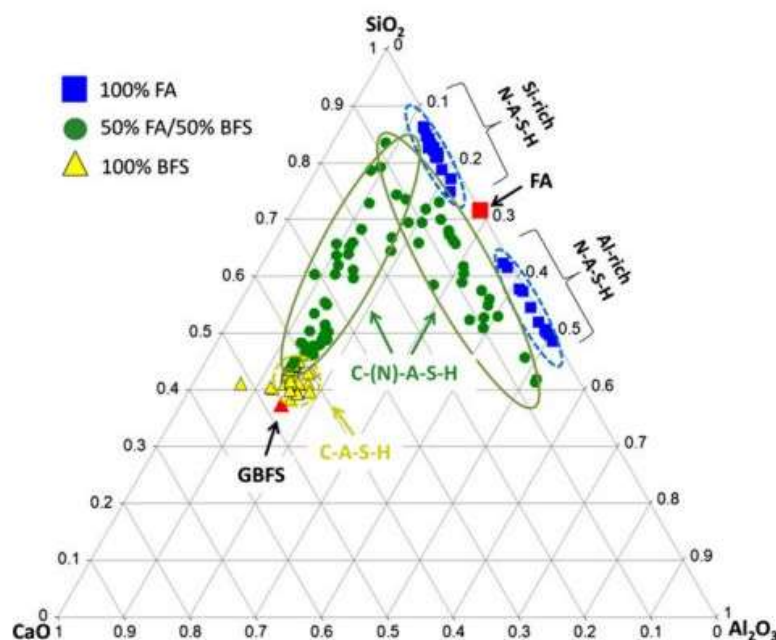
Figure 2.2: Pseudo-ternary plot of alkali-activated binder gel composition. Binders are synthesized by sodium metasilicate activation of fly ash (FA), slag (BFS), and a 1:1 mixture of these two precursors [20].

In the case of systems rich in calcium, a calcium-alumina-silicate hydrate (C-A-S-H) type gel is formed. Conversely, systems poor in calcium tends to form N-A-S-(H) gel. Depending on the cases, the substitution of potassium for sodium up to 100% replacement can be found and in this case a K-A-S-(H) gel is formed. Figure 2.2 shows how the composition of the precursor (i.e. 100% low-Ca precursor (fly ash-FA), 100% High-Ca precursor (blast furnace slags- BFS) and a mix of the previous (50 wt% FA + 50 wt% BFS) affect the obtained alkali-activated binder gel compositions.

Recently, coarse-grained Monte Carlo (CGMC) modelling technique was used to simulate the reaction of an aluminosilicate particle in a highly alkaline solution [12]; information on the structural changes that occur during the formation of geopolymer gel at the mesoscale were obtained. It was found that Si/Al ratio has major influence on the structural evolution of the gel, regardless the precursor particle morphology that was found irrelevant in terms of the nature of the gel growth. Increasing the Si/Al ratio of the system, the percentage of clusters (i.e. nonmonometric species: small oligomers such as dimers and trimers) at the end of the alkali-activation process decreases, leading to an increased amount of silicate and aluminate monomers in the pore solution of the hardened gel. In addition, the Si/Al resulted to influence also the T-O-T linkages in the final gel. For increasing Si/Al ratio of the system, a linear increase in the percentage of Si-O-Si linkage and a linear decrease of Si-O-Al linkages was found. Furthermore, almost no Al-O-Al linkages were found. This is in agreement with the "Loewenstein rule" [21], which states that Al-O-Al bonds are strongly disfavoured in tetrahedral structures [17]. However, the structure is not completely determined as a function of Si/Al ratio but also the cation type has influence on the molecular structure of geopolymer gels. In particular, when potassium is present, aluminium is preferentially incorporated into the framework of the geopolymer gel. In addition, sodium affects geopolymerization by increasing the dissolution rate and promoting a greater short-range ordering and crystallinity of systems than potassium-based system that instead, shows a more disordered structure with higher presence of Al-O-Al linkages. In addition, potassium accelerates the polycondensation reactions leading to a faster setting [18].

Geopolymers are often described as 'X-ray amorphous', since they present an amorphous hump at approximately 27–29 ° 2θ when analysed by X-ray diffraction (XRD). Indeed, geopolymers have a highly disordered structure beyond a length scale of approximately 10 Å. However, similarities between geopolymer gel (N,K-A-S-(H)) structure and structure of zeolites can be found. In particular, X-ray and neutron pair distribution function analysis of metakaolin-based geopolymers, showed that in length scales of up to 5-8 Å, the local structures of the geopolymer binder shows significant structural ordering, similar to the local structure of crystalline zeolitic structures with corresponding Si/Al ratio [14,22]. This information is important for structural modelling of nanostructural properties of these materials. Crystalline zeolites and related phases are the most common secondary phase found in geopolymer systems, often present when high temperature or steam curing is applied [6,14,17].

2.3   Designing a geopolymer: raw materials

The most common precursors used in geopolymers (i.e. low-calcium alkali activated materials) are metakaolin and coal fly ash. Both these sources have been already widely investigated as supplementary cementitious material in Portland cement-based systems.

Metakaolin (MK) originates from the calcination of kaolinite clays at temperatures of around 500–800 °C. The kaolinite is a hydrous aluminium silicate of approximate composition $2H_2O \cdot Al_2O_3 \cdot 2SiO_2$. Generally, kaolin is mined directly as a pure mineral but it can be also sourced in less-pure form from mine tailings or paper industry wastes [14]. The calcination of kaolinite at temperature between 500-800 °C induces a process of dehydroxilation and leads to the breaking down or partial break down of the structure forming a transition phase which is responsible for the reactivity of metakaolin under alkaline conditions. MK typically contains 50–55% SiO_2, 40–45% Al_2O_3 and other oxides present in small amounts including Fe_2O_3, TiO_2, CaO and MgO. MK particles are generally one-half to five microns in diameter [23]. Due to the controlled nature of the processing MK powders are very consistent in appearance and performance [23]. For this reason, metakaolin is often used to obtain geopolymers for "ceramic-like" applications and for laboratory test because of its relatively pure composition compared to other precursors [6,24,25].

Fly ash is a by-product of coal-fired electricity generation. Coal is the world's most abundant and widely distributed fossil fuel and it is the second source of primary energy (roughly 30%), mostly used for power generation. As a result, the global coal industry produces approximately 1090 Mt per year [26] of by-products, mainly in form of coal fly ash. More in details, fly ash is the fine particle residue transported by flue gas through the boiler furnace and collected in the chimneys by electrostatic precipitators. Fly ash consists of powdery particles predominantly spherical in shape and usually characterized by 40-80 wt% amorphous phase [27]. The morphology of fly ash particles depends on the combustion temperature and subsequent cooling rate. Generally, fly ash consists of solid spheres or hollow spheres (cenospheres), and irregular unburned carbon as reported in Figure 2.3. Fly ash is characterized by fine particles with an average size of < 20 μm and has low to medium bulk density (0.54–0.86 g/cm^3) and high surface area (300–500 m^2/kg) [28].

The principal components of coal fly ash are silica, alumina, iron and calcium oxide, with varying amounts of carbon measured by the loss on ignition (LOI). The chemical composition of the fly ash depends on the initial coal composition, and the mineralogical composition depends on the power station design and the power station operating conditions. According to ASTM C618 [30], fly ash can be classified as Class F and Class C based on their calcium oxide contents:

– Class F fly ash has a low calcium content and total SiO_2, Al_2O_3 and Fe_2O_3 content over 70 wt%, and are produced from the burning of bituminous coals or anthracites;

– Class C has total SiO_2, Al_2O_3 and Fe_2O_3 content between 50 and 70 wt% and high in CaO, normally produced from the burning of lignites or sub-bituminous coals.

Similarly, the EN 450-1:2012 European standard [31] classifies fly ash as siliceous and calcareous. Siliceous fly ash contains not more than 10 wt% of CaO and not less than 25 wt% of SiO_2. Because of its pozzolanic

properties, Class F fly ash is commonly used as supplementary cementitious material (SCM) in concrete mix to lower permeability and reduce initial heat evolution [32]. However, the world average reuse of fly ash amounts to only 16% of the total [33], whereas the remaining part is generally dumped in landfills, thus making the disposal of fly ash a serious environmental problem and consequently a very strong candidate as raw material in the production of sustainable materials.
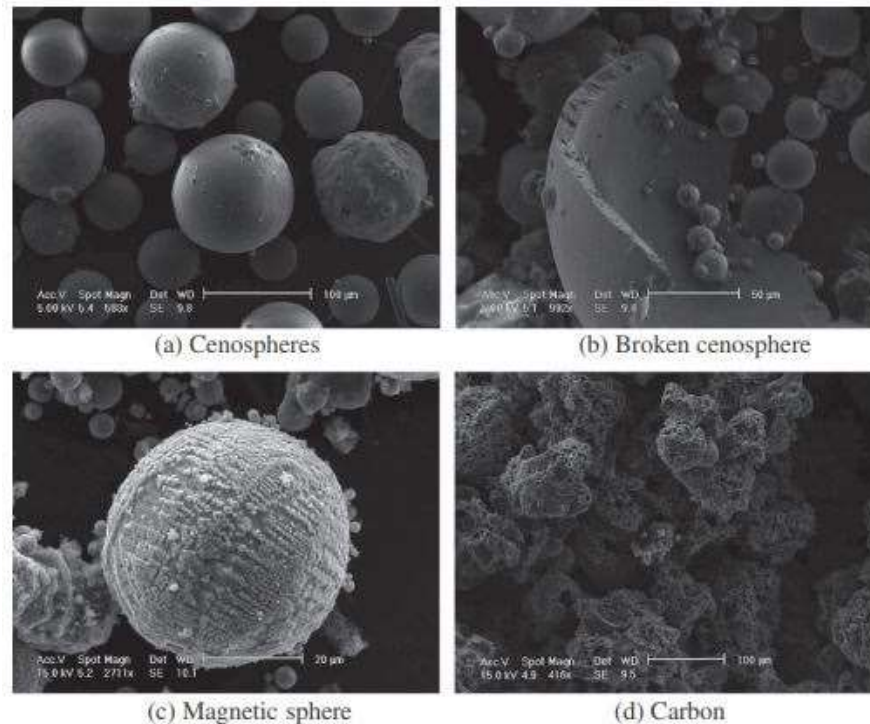

Figure 2.3: SEM micrographs of fly ash [29].

In addition to a reactive aluminosilicate source, the alkali activation requires an alkaline component that in the majority of the cases is in aqueous form. The most used alkali activators are a mixture of sodium or potassium hydroxide (NaOH or KOH) solutions and sodium or potassium silicate solutions (a combination of Na_2O or K_2O, SiO_2 and water). Alternatively, lithium, rubidium and caesium hydroxides can be also used with limitation for large-scale application due to their costs and scarcity. Analogously, the high costs and currently limited production volumes of rubidium and caesium silicates restrict their usage in geopolymers production. Concentration of the hydroxide solution is one of the determining factors for geopolymer synthesis, since higher concentration of NaOH favours the dissolution rate of the aluminosilicate precursor [34]. At the same time, the use of highly concentrated alkali hydroxide solutions can cause efflorescence (i.e. formation of white carbonate or bicarbonate crystals that deposit on the surface of the samples). Efflorescence is generally more marked in the presence of sodium than potassium in hydroxide activated binders [6]. The use of silicate solutions increases the viscosity of the geopolymer. Viscosities of a silicate solution increase dramatically at higher silica content and generally potassium silicate solutions show a much lower viscosity than sodium silicates of comparable composition [6].

2.4   Fly ash–based geopolymers

Fernández-Jiménez et al. [35] proposed a model describing the formation of fly ash-based geopolymer binder (Figure 2.4a). The activator attacks the fly ash particle and a part of the glassy shell is dissolved (a). The external dissolution continues, while the alkaline solution penetrated into the particle begins to dissolve the sphere from the inside out (b). At this point, the reaction products (aluminosilicate gel) form on both the inside and the outside of the sphere. The dissolution process is not always uniform and the reaction of smaller particles (e) can be hindered by the reaction products that block the alkaline liquid from reacting with them. As a result, in fly ash-based geopolymers is often found a coexistence of the geopolymer gel and partially or completely unreacted fly ash particles bound together by the gel (d) [35]. SEM micrograph showing the microstructure of a fly ash-based geopolymer sample is reported in Figure 2.4b. It can be clearly distinguished the presence of both unreacted fly ashes and geopolymer gel, as described in the model.

(a)   (b)
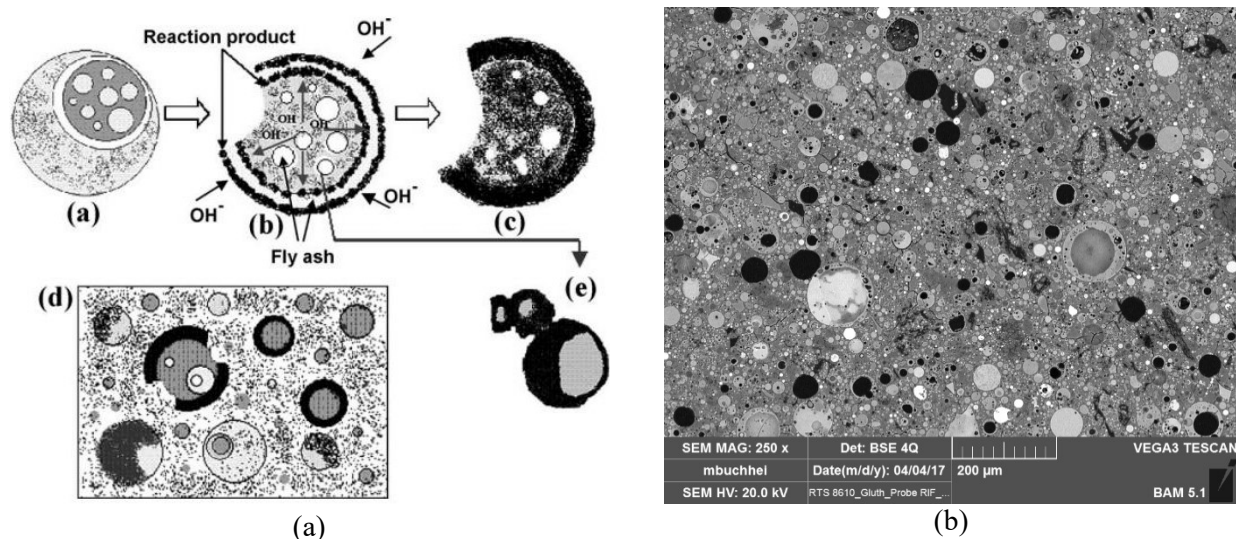
Figure 2.4: Descriptive model of the formation of fly ash-based geopolymer binder (a) [35]; Back-scattered electron image of geopolymer sample produced by the reaction of fly ashes (b).

When fly ash is used as raw material, it has to be considered that the reactive component in the alkali activation process is the amorphous part of fly ash. For this reason, the quantification of the amorphous component of the precursor is of primary importance. When geopolymers are formulated using the amorphous composition, the control on the geopolymerization processes and on the final properties of the material is higher. However, this procedure is challenging and implies the use of different techniques (X-ray fluorescence and quantitative X-ray diffraction) and a rigorous refinement with XRD data [27], and therefore it is not always performed. In addition to the amorphous content, other important compositional parameters to take into account are:

- the amount of aluminium that affects both fresh and hardened properties of the product, among those mechanical strength and strength development profile, setting time, and acid resistance [36];
- the unburned content of the fly ash that comprises of porous and rough not reactive particles whose high specific surface increases the liquid demand necessary to prepare a workable mixture [37].

- The alkali content and calcium content that influence the nature of the gel formed through alkaline activation. Indeed, all alkali metal and alkali earth cations can act as network modifiers in aluminosilicate glasses. Duxson and Provis [36], proposed a simplified pseudoternary classification for fly ashes, correlating the bulk composition of fly ash with three classes of strength development. It can be seen that generally, the strength increases for increasing network modifiers and alumina content.

- Calcium and iron contained in fly ashes can be considered as impurities in geopolymer systems. Their presence has the effect of adding reaction pathways during geopolymerization, thus affecting the properties of the material such as setting time, workability, strength and shrinkage [16].

Because of the large variation of physical, crystallographic and chemical characteristics of fly ashes, their suitability as precursor for geopolymer production is often a matter of debate. In this regard, Zhang et al. [38], proposed the adoption of "reactivity index" to evaluate the suitability of fly ashes for the production of high-strength geopolymer concrete. In particular, they correlate the index of mechanical strength to some of the general parameters of the fly ash: their specific surface area, the inter-particle volume (IPV) defined as gaps between packed particles, the total charge of network modifiers (i.e. Na, K, Ca, Mg, Fe), and the molar number of network formers (i.e. Si, Al, Fe, Ti). In this way, an accurate characterization of the precursor allows to predict the final mechanical properties of the geopolymer obtained from it. The development of indexes based on approaches similar to the one herein briefly described could be helpful for increasing the acceptance of geopolymers as building materials, since it allows to verify the suitability of the local fly ash for the production of a geopolymer with pre-determined properties.

The complexity of the alkali activation process, increased by the large variety of the precursors, is evident and it is impossible to define a unique optimal geopolymer composition. However, some significant parameters for designing geopolymers can be identified. The compositional parameters that mainly influence the nature and the development of the gel generally are Si/Al, M^+/Si and M^+/Al ratio. Furthermore, water content and curing conditions have relevant influence on the physical and mechanical properties of the geopolymers.

Ma et al. [39] deeply investigated the pore structure and the permeability of fly ash-based geopolymers. They concluded that geopolymers generally present pore sizes with diameter in the range of several nm to 0.02 μm corresponding to the gel pores, and pore size ranges of 0.1–1 μm (or larger) representing the capillary pores. The presence of large cavities (in the range of several microns to larger than 10 μm in diameter) owed to the dissolved fly ash particles, were also observed. The compositional parameters such as alkali and silica content largely affect the pore structure of the hardened material. Generally, increased alkali and silica content leads to a less porous systems with finer gel pore and a denser microstructure [39,40]. In addition, increasing the curing temperature reduces the pore sizes [40,41]. Geopolymers synthesized at low temperature (i.e. room temperature curing) are more prone to present pore larger than 0.2 μm [41,42]. The humidity of curing also plays an important role in the pore structure of geopolymers. Indeed, even if a thermal curing is performed,

curing at low relative humidity leads to a granular, porous material. On the contrary, curing at high relative humidity yields a compact material, whose mechanical strength significantly increases over time [43].

The development of the mechanical strength is related to the evolution of the reaction process. In particular, during the dissolution stage, no mechanical strength is observed. During the formation of "gel 1" a big part of the reactive aluminium is incorporated in the gel, but not all the silicon. Therefore, certain mechanical strength is developed but it is not considered significant. The most important phase in terms of strength development is represented by the period in which "gel 1" is transforms in "gel 2" that is a Si-rich gel. When the content of "gel 2" is higher than "gel 1", the obtainable mechanical strength increases to 80 MPa [19]. This is the reason why Si/Al ratio has a strong influence on the mechanical properties of the geopolymer. In particular higher Si/Al leads to a more likely development of high strength [44]. The development of high strength is also promoted by an increase in the concentration of the hydroxide solution used and by the joint use of hydroxide and silicates solutions [45–47].

2.5   Fly ash-based geopolymers as binder for the production of mortars and concrete

As discussed in the previous paragraph, a geopolymer binder is composed of a low-calcium aluminosilicate precursor and generally one or more activators containing alkali metal ions (e.g. alkali silicates and hydroxides). Water, sand, aggregates and other components can be used to obtain a mortar or concrete. As in OPC concrete, usually the aggregates occupy about 80 wt% of geopolymer concrete. It is important to note that geopolymer mortar and concrete can be manufactured by adopting the conventional techniques used in the manufacture of Portland cement concrete.

For the production of mortars and concrete in civil engineering fields, fly ash-based geopolymers often resulted more suitable than metakaolin-based ones. Although the use of metakaolin as precursor allows a better control on final properties, because of its plate-shaped particles metakaolin-based geopolymers are more water demanding and present increased possibility of rheological problems. In addition, the relatively high cost of metakaolin compared to fly ash can be a driving consideration when large amounts of material has to be produced, as in the case of construction materials.

In the last years, many studies conducted on fly ash-based geopolymer mortar and concrete proved their strong potential as building materials; with a tailored mix design high mechanical strengths and good durability performances can be achieved [45,48]. Hardjito et al. [49], conducted a parametric study on the development of compressive strength in fly ash-based geopolymer concrete. They concluded that the compressive strength is positively influenced by a higher concentration of sodium hydroxide solution, higher sodium silicate/sodium hydroxide liquid ratio by mass, and high temperature curing. Heat curing is generally recommended for low calcium-based geopolymer systems to accelerate the hardening of the mixtures and to increase the final mechanical properties [50]. The need of a thermal curing can put limitation on the industrial-scale applicability of this technology, limiting the fields of application to pre-cast components. However, the need for this treatment is related to the reactivity of the precursor and to the mix design [4,42]. In addition, to obtain good

results in terms of strength development also at room temperature, a high control is required on the choice of the activator concentration and composition according to the chemistry of the precursor. Furthermore, attention has to be put on curing which must be conducted under sealed conditions to prevent drying or microcracking, and on water/binder ratio, which must be as low as possible [20].

The water/binder ratio represents a fundamental parameter also in Portland cement-based systems and the necessity to reduce the mix-water without decreasing the workability and mechanical strength of the material led, in the past years, to the development of superplasticizers (SP). The introduction of superplasticizers is considered as one of the key developments in the chemistry of Portland cement-based concretes. These admixtures hinder flocculation of cement particles by electrostatic or steric repulsion. Therefore, adding a small amount of SP can reduce the water/cement (w/c) ratio without influencing workability of concrete and thus ensuring its mechanical and durability performances. Because the commercially available superplasticizers have been specifically tailored to be compatible with the chemistry of Portland cement, their effectiveness in alkali activated binders has to be demonstrated. In most cases, SP seem to degrade in the high alkaline environment and hence found to be not very effective in geopolymer mortars and pastes [6,51]. However, some SP have demonstrated to work also in geopolymer systems. In a previous study on fly ash based geopolymers [52] it was investigated the rheological behaviour of fly-ash geopolymer activated with a mix of sodium hydroxide (12M NaOH) and of sodium silicate solution. It was found that polycarboxylates based superplasticizer was the most effective one, causing an increase in workability and a decrease in yield stress and plastic viscosity of fly-ash systems. Other authors [53] investigated the rheological behaviour of alkali-activated fly-ash concrete containing superplasticizers. The authors indicated a critical value of concentration of the sodium hydroxide solution equal to 4 M, below which SP tested improved workability of concrete. In particular, lignin-based plasticizer was the most effective. Moreover, a good correlation between rheological parameters and slump test results was found. It is clear that results obtained so far in the academic community are not yet conclusive and further research is essential on this topic.

Investigating the suitability of using geopolymer concrete in civil engineering also means investigating its durability performance. Durability is considered by some authors as the factor that overrides all other technological drivers in determining the success or failure of geopolymer technology in the construction industry [54]. In the thesis, it is investigated in depth the durability in terms of thermal resistance of fly ash-based geopolymers, and the state of the art on that will be reported in dedicated paragraphs. Therefore, only a short overview is presented on the other aspects related to durability of alkali activated materials. Among all the geopolymers features, geopolymers result excellent in terms of resistance to chemical attack by chloride (including sea water), various acids, alkali and sulphate [54]. Large part of the research on the durability issue, focuses on the study of corrosion of embedded steel reinforcing bars in geopolymer mortars or concrete [20,55–57]. When a rebar is embedded in concrete, it is essential that the pore solution pH is sufficiently high (above approximately pH 10–12) to passivate it and this condition has to be maintained throughout the service life of the material. Considering the alkaline solutions used for producing geopolymers, this should not be considered as an issue. However, what is missing in geopolymers is a pH-buffering solid hydroxide phase (i.e. $Ca(OH)_2$

in Portland cement based concrete) [20]. Generally, the mass transport properties of the hardened binder material are essential in determining the durability of a concrete because the loss of passivation usually takes place due to the ingress of aggressive species such as chloride, and/or the loss of alkalinity by processes such as carbonation [6]. Once again, the durability of alkali activated materials is strongly dependent on several parameters such as the type of precursor and the nature and concentration of the activator which impact on the nano and microstructure of the reaction products forming in these systems and the chemistry of the pore solution [20]. The importance of the investigation of alkali activated materials durability is also highlighted by the establishment in 2012 of a RILEM Technical Committee (TC 247– DTA - Durability testing of alkali activated materials - https://www.rilem.net/groupe/247-dta-durability-testing-of-alkali-activated-materials-290). The main objective of the TC 247-DTA is to provide recommendations regarding appropriate test methodologies and protocols for the analysis of the durability of alkali-activated binders, mortars and concretes, with particular reference to resistance to frost, carbonation, penetration of chlorides and other aggressive media.

2.6   Fly ash-based geopolymers: thermal properties

Geopolymers can be considered intrinsically resistant at high temperature due to their ceramic-like structure that retains its structural integrity at elevated temperatures [58]. A large number of studies investigated the thermal properties of geopolymers, such as thermal induced microstructural modification, thermal shrinkage, thermal conductivity, mechanical strength retention. Results proved that geopolymers exhibit remarkable thermal resistance compared to the conventional materials. These advantages can be summarized in mechanical strength retain [59] and dimensional stability [60]. Even if it is generally recognised that geopolymers are resistant to high temperature, also the thermal properties are largely influenced by the raw materials, Si/Al compositional ratio, the alkali cation, and impurities, especially when by-products are used for geopolymers production.

The majority of the research on thermal behaviour of low-calcium geopolymers focuses on metakaolin (MK)-based systems because of the relatively pure oxide composition of this precursor. Results obtained so far show that the thermal behaviour of geopolymers is sensitive to the Si/Al ratio and to the alkali activator chosen for the process [61,62]. When properly designed and cured, MK-geopolymers withstand up to 1300°C without significant changes in their structure [63].

Duxson et al [64] investigated the effect of Si/Al on thermal shrinkage and weight loss of MK-based geopolymers activated by sodium silicate solution. They found in all cases a minimal shrinkage up to 100 °C while large amount of free water evaporated. Furthermore, 80% of all weight loss was observed below the temperature of 300 °C, suggesting that the bulk water in the structure of geopolymer material is present as freely evaporable water. For increasing temperature, a rapid shrinkage occurred which was correlated to the Si/Al compositional ratio. The onset temperature of this region of shrinkage was lower for low Si/Al ratio. Finally, a second rapid shrinkage was found only for sample with Si/Al > 1.65 and related to densification and

sintering processes. Both the rate of weight loss and the onset temperature of shrinkage decreased with increasing Si/Al ratio. Rahier et al. [65] indicate the change in slope of the expansion curve as the glass transition temperature (T_g) for aluminosilicates. They also specify that changes in Na_2O/Al_2O_3 ratio and/or in water content have large effects on T_g. Indeed, considering the geopolymeric gel, SiO_2 is a network former, whereas Na_2O or K_2O are network modifiers and lowers T_g and viscosity in the melt.

An extensive study on the thermal behaviour of fly ash-based geopolymer was presented by Rickard et al. [60,66,67]. They suggested a descriptive model of the dimensional changes induced by high temperature exposure of fly ash based geopolymer (Figure 2.5). In particular, although the temperature ranges can be variable and dependent on sample composition and heating rates, six different regions were found in the temperature range from room temperature up to 1000°C. As soon as the geopolymer is heated up, a slight expansion of the solid gel is verified up to 150°C. As the temperature increases, the water contained in the material, either as adsorbed water in the pores or as chemically bond water in the structure, starts to evaporate. This dehydration and further dehydroxilation cause shrinkage, the amplitude and the extension of which is proportional to the water content in the sample. More in details, between 100°C and 300 °C a significant shrinkage is related to dehydration of water whereas between 250°C and 600 °C minimal shrinkage is due to dehydroxilation. A further thermal shrinkage is usually found between 550 °C and 900 °C and it is connected to the sintering of the gel and the subsequent densification of the sample. Beyond the densification region, no consistent trend in thermal expansion has been reported. The observed differences can be related to the differences in the composition. When an expansion is observed, it can be related to the swelling of partially depolymerized silicate gels and/or to the crack formation and to increase in porosity [60,66,68] .The final region is usually identified by a rapid shrinkage due to a continued densification or melting of the sample and/or to a collapse of the pore structure
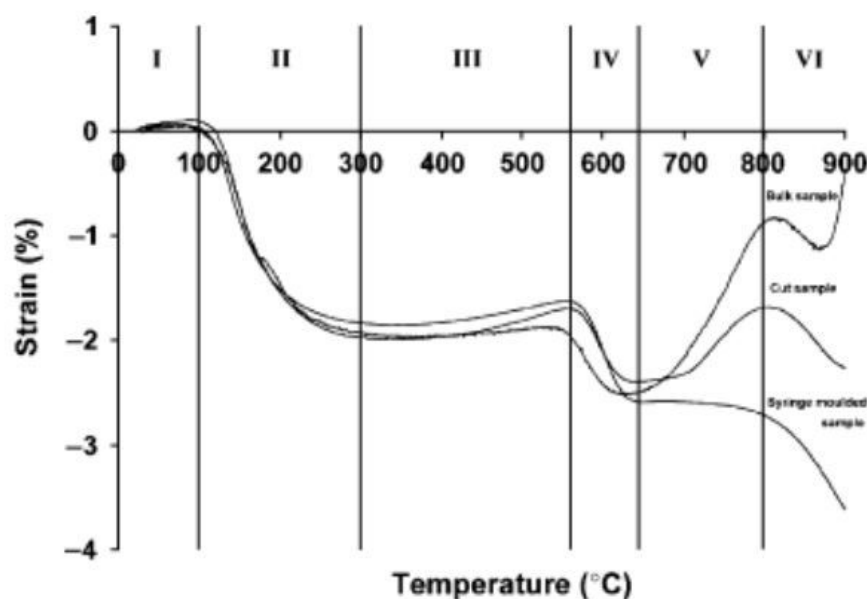
Figure 2.5: Descriptive model of the dimensional changes induced by high temperature exposure of fly ash based geopolymer fly ash geopolymers. Si/Al = 2.3, H_2O/SiO_2 = 2.0 [67].

An important difference between geopolymer and OPC occurs at temperatures greater than 500 °C and is due to the different nature of the water contained in the material. Indeed, in hardened cement approximately 90 % of the water is chemically bound to cement precursors in the form of hydrates. The dehydroxilation of this water causes the destruction of the binding phase, failure of the material and an associated large shrinkage [69]. Conversely, water is not a major structural component of geopolymer gel [14] and is mainly found as free water in large pores, available for evaporation. Water is also present in small percentage (approximately <5%) either physically bound in small pores or chemically bound as hydroxyl groups attached to the Si–Al framework structure [64,65,70]. For this reason the dehydroxilation does not provoke significant shrinkage generated by the rupture of the binding phase [71].

Pan et al. [72], studied the effect of the alkali cation on the softening temperature of fly ash-based geopolymers. They found that the use of potassium instead of sodium as the alkaline cation, leads to an increase of the softening temperature from 610 to 800 °C. However, when mixed alkali cation (Na/K based geopolymers) are used the softening temperature dropped to 570 °C. Bakharev [73] investigated the influence of the alkali cation on thermal stability up to 1200 °C of fly ash-based geopolymer .The Na-based geopolymer developed cracking when exposed to 800 °C, with increasing cracking for increasing water content. In addition, an increased compressive strength was found after heating to 800°C followed by a rapid deterioration for higher temperature. From the mineralogical point of view, the initially amorphous structure of Na-geopolymer crystallized to form nepheline $AlNaSiO_4$ after 800°C, Na-feldspars $NaAlSi_2O_6$ after 1000°C, and albite $NaAlSi_3O_8$ after 1200°C. The crystallization of Na-feldspar on firing was related to the presence of unreacted sodium and was assumed responsible for the loss of the strength at 1000°C. The use of potassium instead of sodium favoured a strength retention also after exposure to temperature exceeding 800°C and no significant modification of the amorphous gel occurred up to 1200°C; after this temperature, traces of crystalline kalsilite and leucite were observed.

Because of the large variety in fly ashes composition and in fly ash-based geopolymer formulations, the mix design of FA-geopolymers often needs to be optimized in order to obtain a high thermal dimensional stability.

2.7   Fly ash-based geopolymers as fire resistant materials

Geopolymers are substantially inorganic based and are considered incombustible, emitting no toxic fumes or smoke when exposed to fire, and therefore considered a highly competitive material when resistance to fire is required. One of the main problems of cement-based material exposed to fire is the spalling phenomena. During fire, steam pressure build-up in the concrete pores; when the internal pore pressure exceeds the tensile strength of the material it causes spalling [74]. Explosive spalling is characterised by large or small pieces of concrete being violently expelled from the surface, thus leading to disintegration of concrete structure in an accidental fire [74].

Conversely, geopolymers retain a high structural stability after exposure to fire and the rapid dehydration of the weakly bound water does not cause significant damages to the binding structure. This aspect is particularly advantageous compared to ordinary Portland cement (OPC).

Kong et al.[75], compared the performance of fly ash- and metakaolin based-geopolymers exposed up to 800°C. FA-based geopolymers showed an increased residual strength (+ 6%), whereas the heat exposure had a detrimental effect on the mechanical properties of metakaolin-based geopolymers (-34%). They related this behaviour to the different permeability of the materials, which in case of fly-ash-based geopolymers was higher, thus providing reduced damage to the matrix caused by the escaping of moisture in the matrix. Zaho et al. [74] compared the spalling behaviour of geopolymer and OPC concretes with the same strength class. None of the geopolymer specimens exhibited spalling when exposed to simulated fire conditions. On the contrary, OPC specimens underwent increasing damages for increasing strength level. The authors also valuated the permeability of both concretes by sorptivity tests. Results highlighted that the more porous structure of geopolymer concrete specimens than the Portland cement concrete specimens facilitates the release of the internal steam pressure during heating, and therefore is responsible for the absence of spalling.

Rickard et al. [59] analysed the mechanical and microstructural properties of high temperature exposure of two different geopolymer concrete containing quartz aggregate and expanded clay, respectively before, during and after high temperature exposure. Significant compressive strength loss in both concrete types between 100 °C and 300 °C, was observed and related to the dehydration. However, for temperature of exposure up to 700°C geopolymer concrete demonstrated good hot strength and strength retention after cooling, considered higher than the one of OPC concrete. Masi et al. [76], tested the fire resistance of fly ash-based geopolymers foamed panels (50 mm thickness) reinforced with either organic (PVA) or inorganic (basalt) short fibres. Both panels exhibited comparable density values and although the PVA foamed fibre showed slightly higher performance under cellulosic fire conditions, it was concluded that the nature of the fibres added did not significantly influence the performance of geopolymers under simulated fire conditions.

Due to the remarkable performance at high temperature, geopolymers have been also investigated as passive fire protection system [5,6,71,77]. Attempts have been made in investigating the feasibility of geopolymer as intumescent coatings, mainly using metakaolin as starting material [78,79]. Sakkas et al. [80–82], extensively studied the possibility of using geopolymer from ferronickel slags activated with either sodium or potassium hydroxide as passive fire protection of concrete substrates. They found that the Na-based geopolymer is a good passive fire protection system for cellulosic fire (ISO 834-1 standard [83]). When more aggressive fire condition is tested (RWS-curve) the Na-based geopolymer failed the test and disintegrated during test. Conversely, the K-based geopolymer showed excellent resistant also in the most harsh fire test conditions.

Studies focused on the use of fly ash based geopolymer as passive fire protection system for the protection of metal substrates [84,85], highlighted the strong influence of the compositional Si/Al ratio on the compatibility of the coating with the steel substrates in terms of adhesive strength and thermal deformations. In addition, they investigated the possibility of using a lightweight aggregate (i.e. vermiculite) for producing a

spray coating. The use of lightweight aggregate (i.e. perlite, vermiculite, pumice, etc.) is largely diffused for the production of commercially available insulation and fire resistant materials based on OPC [86]. Indeed, fireproofing materials, besides their intrinsic thermal stability, must also exhibit good thermal insulation and low weight load. Both these characteristics can be implemented by introducing air in the material structure. One of the most effective foaming agent already successfully experimented in geopolymers is hydrogen peroxide (H_2O_2) [87–89].

It has to be noted that almost in all the reported investigations, a thermal curing was carried out, thus limiting the *in-situ* application.

2.8 The sustainability issue

Geopolymers have been widely advertised as 'green' and sustainable materials because of the possibility of using by-product as starting material that is very attractive when an alternative to Portland cement is researched. Imbabi et al. [2] reviewed the available alternatives to Portland cement and stated that the production of geopolymers emits 95% less CO_2 than OPC, considering the NaOH and KOH solutions as carbon free. However, there is an open-debate on the real sustainability of geopolymers compared to OPC, generated by a large variety of the results presented by the scientific community.

McLellan et al. [3], analysed the lifecycle cost and carbon impacts of geopolymers in an Australian context, estimating an improvement in greenhouse emissions over OPC in the range of 44-64% and highlighting the strong impact of the transportation on the calculation. Reduced benefits in terms of sustainability were found by Turner et al. [90]. They compared the CO_2-e emitted due to the activities necessary for producing $1m^3$ of fly ash-based geopolymer concrete and $1m^3$ of OPC concrete, including energy expending activities associated with mining and transport of raw materials, manufacturing and concrete construction. A thermal curing was considered in the case of the geopolymer concrete. A reduction of 9% in terms of CO_2 footprint was found in favour of geopolymer concrete.

As proved by the variety of data reported in the literature, it is impossible to provide a unique and specific value to describe the sustainability of geopolymers compared to conventional cements and concretes because of the large variety of parameters involved in the geopolymers production (e.g. mix design, dosage of activators, transport distances, source of electricity). In addition, baselines are often inconsistently between reports and are largely influenced by local as well as the choice of mix design for assessment.

All the inputs (material and processes) to take into account for the environmental assessment of an alkali-activated concrete based on two-part system are presented in a descriptive diagram recently published by Provis. Independently for the different case studies reported in the literature, all of them clearly show that the alkali activator, especially sodium silicate solution, is the major contributor to the environmental footprint (Figure 2.6).
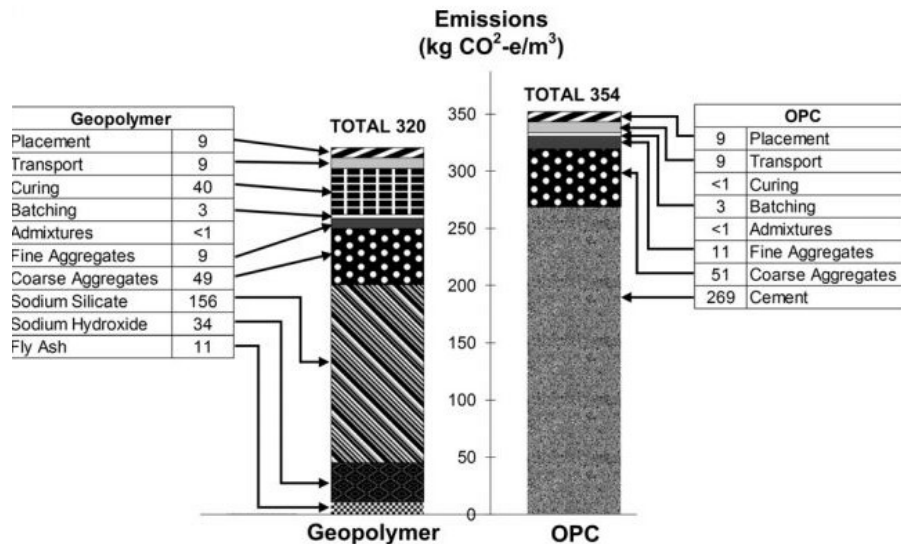
Figure 2.6: CO_2-e concrete mixtures with OPC and geopolymer binders [90].

Although geopolymer always showed low CO_2 footprint in the global warming potential category of LCA, the use of alkali activators adversely affects other categories, among which acidification and eutrophication. It has to be noted that the data available in the databases on the productive process of sodium silicate solutions are not updated to the modern production practices, therefore when included in the life cycle assessment this process results to be extremely unsustainable from the environmental point of view [4].

The best way for increasing the sustainability of geopolymers is to use raw materials recognised as industrial waste. There are ongoing investigations on the possibility of using recycled silica source as activator, instead of chemically produced one [91–94]. In particular, the use of rice husk ash (RHA), if locally available, reduces environmental impacts, including acidification and eutrophication categories, by more than 60%. Thermal curing also increases the impact of geopolymer production. Avoiding the application of heat during the curing, which is the approach adopted in this thesis, is estimated to further increase the sustainability of geopolymers [91,95].

2.9   The standardization issue

A fundamental step towards the commercialisation of alkali-activated materials is represented by standardization. The proposal of the RILEM Technical Committee on Alkali Activated Materials (TC 224-AAM) is to use a performance-based approach for developing recommendations for standards. A performance-based approach means that is suggested not to prescribe the materials to be used, but rather to define the basic performance requirements which must be met by the materials [6]. RILEM TC 224-AAM proposed that the following information about an alkali-activated binder should be provided to the customer:

Raw materials (upon request)

• Origin of material(s)

• Elemental composition, loss on ignition

- Mineral composition, X-ray diffraction analysis
- Density, specific surface, sieve residue (e.g. 45 μm)

Properties before hardening (classification)

- Workability, rheological properties (e.g. flow curve, spread diameter), upon request
- Setting time at a given temperature (some materials set very slowly and need heat treatment)
- Heat of hydration

Properties after hardening (classification)

- Mechanical properties (early, late), definition of mix composition and curing conditions needed
- Compressive strength (early, late)
- Flexural strength, upon request
- Tensile strength, upon request
- (potentially) Shrinkage and/or creep under specified conditions

The worldwide current situation of standardization of alkali activated materials can be summarized as follows [4,6]:

- Europe: In Switzerland, alkali-activated slags are incorporated into national guidelines [96]; in the UK a Publicly Available Specification for alkali-activated cements and concretes has been published [97]; Ukraine (and former USSR) developed and implemented over 60 standards between 1961 and 2007. Most of these standards are technical specifications to prescribe the materials which are suitable to be used in the AAM applications, to regulate various types of concrete made with AAM or to guide manufacturing and application processes.

- Australia: standardization has been driven by specifiers rather than by national regulations. In the state of Victoria are nowadays available specifications for the use of alkali-activated concretes as general concrete paving, drains and pipes, drainage pits, and safety barriers.

- USA: the ASTM standardization regime includes the ASTM C1157 [98] which gives performance requirement on hydraulic cements for both general and special applications, without giving restrictions on the composition of the cement or its constituents. Therefore, AAM can be classified under this standard, as long as the required performance is met. However, ASTM C 1157 [98] acceptance is currently limited to only in five states in the US.

- China: the use of AAMs for chemical resistance applications is described in GB/T2923-2012 [99].

Chapter 3:

Experimental methods

This Chapter reports details of the source materials used in this study as well as the mix design and the mixture procedures used for synthesizing the geopolymers. The techniques adopted for the characterization of the fresh and hardened properties of the obtained materials are also reported.
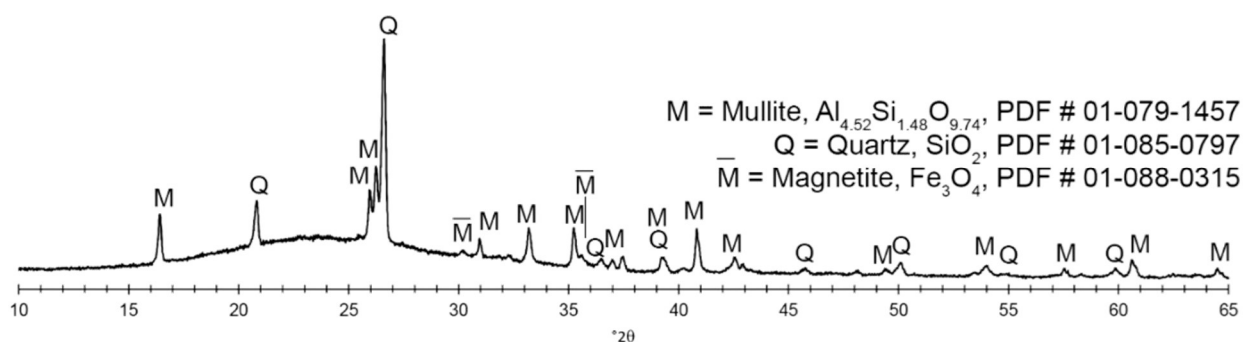
3.1   Materials

3.1.1   Aluminosilicate precursor

Coal fly ash (FA) was used as precursor for the synthesis. The FA was sourced by the Italian coal-fired power station of Torrevaldaliga Nord (Rome) and supplied by Imola Cooperativa Trasporti (Bologna, Italy). This FA complies with EN 450-1 standard [31] and it is approved for the use in the cement and concrete industry. Previous studies carried out in our research group deeply investigated the nature and the suitability of this FA for the geopolymerization process [42,100]. The chemical composition of the investigated FA, composed of spherical shaped particles with an average diameter of 22.1 μm, is reported in Table 3.1. A low content of calcium and iron oxides is observed, while the silicon and aluminium oxides constitute nearly 80% by mass of the precursor.

Table 3.1: Chemical composition of the fly ash.

Oxide	SiO_2	Al_2O_3	Fe_2O_3	CaO	TiO_2	MgO	K_2O	SO_3	Na_2O	BaO	Cr_2O_3	LOI	Insoluble residue
(wt%)	49.37	29.23	2.71	6.63	1.59	1.05	0.60	0.33	0.05	0.07	0.02	3.28	5.07

XRD analysis of FA are reported in Figure 3.1: it is clearly visible the presence of the typical amorphous hump for 2θ values between 20 and 30° and of some crystalline phases, such as quartz, mullite and magnetite. The amorphous phases content, identified by using a Rietveld refinement, is equal to 65.3 ± 0.7 wt%, composed of SiO_2 (35.1 wt%), Al_2O_3 (13.5 wt%), CaO (6.6 wt%), Fe_2O_3 (1.3 wt%) and other oxides (8.8 wt%) [42].

M = Mullite, $Al_{4.52}Si_{1.48}O_{9.74}$, PDF # 01-079-1457
Q = Quartz, SiO_2, PDF # 01-085-0797
$\overline{M}$ = Magnetite, Fe_3O_4, PDF # 01-088-0315

Figure 3.1: XRD pattern of the fly ash.

3.1.2   Alkaline activators

Geopolymers studied in this thesis can be classified as two part geopolymers, since a solid source plus a liquid alkaline activator are involved in the process.

Aqueous solutions of sodium silicate (SiO_2 = 29.86%, Na_2O = 14.43%, H_2O = 55.71%, SiO_2/ Na_2O ratio = 2.07, ρ at 20°C = 1.53 g/cm^3, kindly supplied by Ingessil Srl, Verona, Italy) was always used in combination with either sodium hydroxide solution (NaOH) or potassium hydroxide solution (KOH). If not differently specified, a 8 M sodium or potassium hydroxide solution was used. In some cases, the concentration of the sodium hydroxide solution was modified to obtain 6 M or 4 M NaOH solution, according to the research aim. The hydroxide solution was prepared by dissolving solid sodium (or potassium) hydroxide pellets in deionized water according to the desired concentration.

3.1.3   Fine aggregate

Two different geopolymer mortars (GMs) were produced which differ in amount and maximum size of the quartz fine aggregate used, as follows:

- GM: fly ash-based geopolymer mortar containing 56.2 wt% of commercial quartz sand with maximum diameter d_{max} = 1 mm.
- GM_2: fly ash-based geopolymer mortar containing 65.7 wt% of EN 196-1 [101] sand with the maximum diameter d_{max} = 2 mm.

The particle size distributions of the two sands are reported in Figure 3.2.
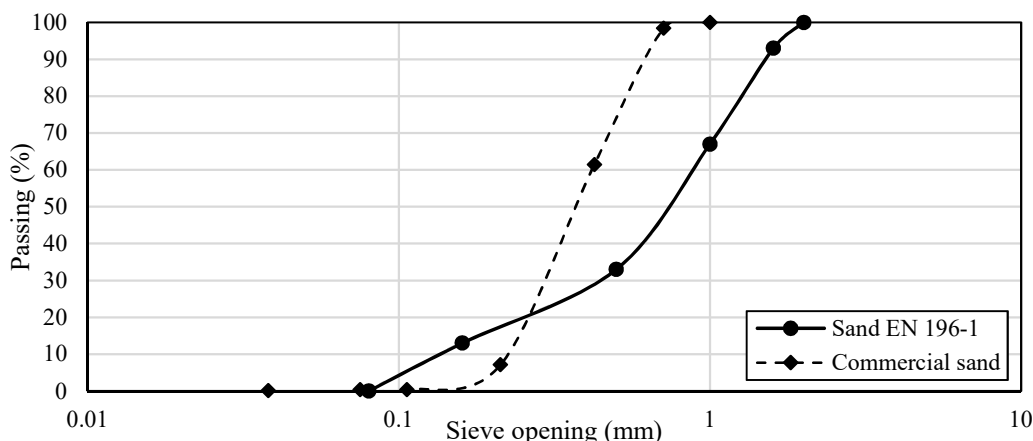
Figure 3.2: Particle size distributions of sands used for producing GM and GM_2.

3.1.4   Refractory particles

Geopolymer composites (GCs) were produced by adding recycled aluminosilicate refractory particles (RRP) (d_{max} = 2 mm, kindly supplied by Keratech, Gorizia, Italy) obtained by milling industrial scraps of refractory roller production. The chemical composition, provided by the producer, is reported in Table 3.2.

Table 3.2: Chemical composition of the investigated recycled refractory particles (RRP).

Oxide	SiO_2	Al_2O_3	ZrO_2	CaO
(wt%)	17	78	4.7	≤ 0.3

By XRD analysis, RRP show a crystalline nature comprised of mullite, corundum and baddeleyite (Figure 3.3) which is consistent with the chemical composition reported in Table 3.2.
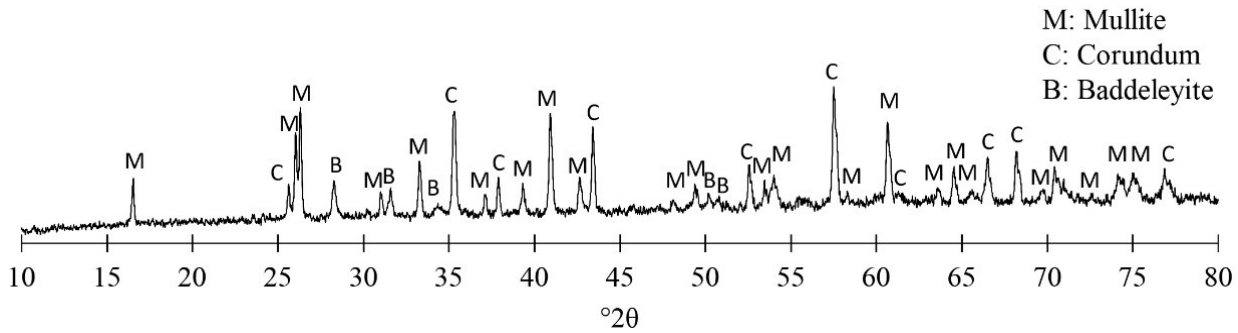
Figure 3.3: XRD pattern of the recycled refractory particles (RRP) [176].

3.1.5 Lightweight fine aggregate

Lightweight geopolymer mortars (LWGs) were produced using expanded perlite (EP) as fine lightweight aggregate. As the name states, expanded perlite is obtained by the thermal treatment of perlite, an amorphous volcanic silicate/alumina rock, which can be expanded from 5 to 20 times its original volume when rapidly heated at 900–1200 °C. Italy is one of the main six countries in terms of perlite production. Expanded perlite is very attractive in building materials industry because of its interesting properties such as low bulk density, high surface area, low sound transmission, low thermal conductivity, high heat resistance and chemical inertness [102]. In this study, Peralit 20 sourced by Perlite Italiana, Corsico (Milan, Italy), was used. The expanded perlite used has a maximum diameter of 2 mm, the chemical composition reported in Table 3.3 and the properties listed in Table 3.4.

Table 3.3: Chemical composition of the expanded perlite (data supplied by the technical data sheet [103]).

Oxide	SiO_2	Al_2O_3	Fe_2O_3	CaO	MgO	K_2O	Na_2O
(wt%)	74-78	11-14	0.5-1.5	1-2	0-0.5	2-4	3-6

Table 3.4: Physical properties of the expanded perlite (data supplied by the technical data sheet [103]).

| Properties of the expanded perlite	
Aspect and colour	The particles are white, hollow, and porous with many shapes
Density (g/cm³)	0.09 - 0.10 ± 15%
Thermal conductivity (W/mK)	0.02
Specific heat (J/kg K)	837

3.1.6   Superplasticizers

Seven types of commercially available superplasticizers (SP), commonly used in OPC concrete industry, were used. Their chemical structure and main physical characteristics are reported in Table 3.5 together with the identification labels. The SP were added in the mixture as supplied with the only exception of LGa and LGb which were diluted with water before use, according to the technical data sheet. Two different amounts were tested expressed as a weight percent by mass of fly ash (i.e. 0.6 and 1.0 wt%).

Table 3.5: Chemical and physical properties of the investigated superplasticizers (data supplied by the technical data sheets).

Label	Chemical structure	Solid content (wt%)	Appearance color	Density (g/cm³)
LGa	Lignosulphonate	48	Brown liquid	1.20
LGb	Sodium lignosulphonate	50	Brown liquid	1.27
SNF	Polynaphthalenmethan sulphonate	100	White powder	0.55
SMF	Sulphonated melamine	100	Brown powder	0.80
PCE	Polycarboxylic ether	17	Brown liquid	1.04
ACRa	Modified acrylic	31	Yellow liquid	1.09
ACRb	Acrylic acid copolymer	21	Yellow liquid	1.08

3.1.7   Foaming agent

Hydrogen peroxide solution (H_2O_2, 30 wt /wt in H_2O) was used as foaming agent. Previous studies already assessed the effectiveness of H_2O_2 as foaming agent for the production of low density geopolymers [88]. Indeed, hydrogen peroxide is thermodynamically unstable and can be easily decomposed to water and oxygen gas according to the following reactions:

$$H_2O_2 + OH^- \longrightarrow HO_2^- + H_2O$$

$$HO_2^- + H_2O_2 \longrightarrow H_2O + O_2 + OH^-$$
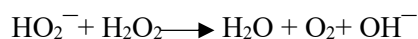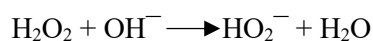
If added during geopolymer mixing, the bubbles of O_2 produced by the reaction are trapped within the matrix producing closed porosities.

3.1.8   Steel textile

Steel textile was used for the investigation of geopolymer mortar as external strengthening system of existing structures. The steel textile employed in this study was supplied by Kerakoll spa. Additional information on the fibres are reported in Table 3.6, according to the technical data sheet.

Table 3.6: Description and main mechanical properties of the steel textile employed in the realization of fibre reinforced geopolymer matrix composites (data supplied by the technical data sheet [104]).

GeoSteel G600			
Actual area of a cord 3x2 (5 wires)	mm^2	0.538	
Equivalent thickness of the textile	mm	0.084	
Tensile strength by unit of width	kN/cm	> 2.35	
Elastic modulus of the textile	GPa	> 190	
Tensile strength of the textile	MPa	> 2800	
Strain at failure	%	>1.50	

3.2 Synthesis

3.2.1 Mix design

Two different formulations of geopolymer matrices were used for the realization of the majority of the mixtures investigated in this study. The formulations are listed in Table 3.7 and are identified by the label G (geopolymer) followed by either the letter A (G_A) or B (G_B). Both formulations have the same activators/precursor ratio equal to 0.45 (wt/wt). However, the ratio between the sodium silicate and sodium hydroxide solutions used as activators was adjusted in order to modify the compositional parameters as presented in the Table 3.7.

Table 3.7: Mix design and significant parameters of the investigated geopolymer matrices.

	Mix design (wt%)			Significant compositional parameters				
label	Fly ash	8 M NaOH	Sodium silicate solution	$\dfrac{\text{Activators}}{\text{Precursor}}$	$n\dfrac{\text{bulk } SiO_2}{Al_2O_3}$	$n\dfrac{\text{bulk } NaO_2}{SiO_2}$	$n\dfrac{\text{amorphous Si}}{Al}$	$n\dfrac{\text{amorphous Na}}{Al}$
G_A	69	5	26	0.45	3.52	0.12	2.91	0.88
G_B	69	20	11	0.45	3.14	0.17	2.51	1.16

If not differently specified, the mixtures were realized using either the G_A or the G_B formulation. When a subscript is present in the label, it refers to a change in the sodium hydroxide solution component. In particular, the following subscripts can be found:

- K (i.e. G_A$_K$): indicates the use of 8 M KOH solution;

- 4 M or 6 M (i.e. G_A$_{4M}$): indicates the use of 4 M or 6 M NaOH solution, respectively.

Starting from the geopolymer matrix produced using either G_A or G_B formulation, as a function of the final application, different fine aggregates/particles were used and the amount of extra-water added during the mixing procedure was adjusted. In Table 3.8 are summarized all the mixtures studied in this thesis; the total water content, calculated as the sum of extra water and the water coming from the solutions (i.e. NaOH solution, sodium silicate solution) is also reported.

In particular, mixtures can be classified in four categories:

- **G**: Geopolymer Paste without aggregates;

- **GM**: Geopolymer Mortars containing quartz fine aggregate;

- **GC**: Geopolymer Composites containing recycled refractory particles (RRP);

- **LWG**: Lightweight Geopolymer mortar containing lightweight fine aggregate (expanded perlite).

Table 3.8: Mix design of the investigated geopolymers. Values are reported a weight percent by the total mass.

	Label	Additional components	Extra water (wt%)	Total water (wt%)	Other additions
Chapter 4	G_A	-	4.6	21.8	Either 0.6 or 1.0 wt% of superplasticizers
	GM$_2$_A	65.7 wt% of fine quartz aggregate (d_{max} = 2 mm)	1.1	7.3	
Chapter 5	GM_A			10.3	
	GM_A$_{6M}$	56.2 wt% of fine quartz aggregate (d_{max} = 1 mm)	3.0	10.5	
	GM_A$_{4M}$			10.7	
Chapter 6	G_A	-	-	18.0	
	G_A$_K$	-	-	17.3	
	GC_A_10	10 wt% of RRP	0.6	16.5	
	GC_A_20	20 wt% of RRP	2.8	16.5	
	GC_A_30	30 wt% of RRP	4.9	16.5	
	GC_A_40	40 wt% of RRP	7.1	16.5	
Chapter 7	G_A	-	8.8	25.2	
	G_B	-	6.6	25.1	
	LWG_A_10	10 wt% expanded perlite	10.9	25.1	
	LWG_B_10	10 wt% expanded perlite	9.0	25.0	
	LWG_A_10_HP	10 wt% expanded perlite	10.7	25.1	0.3 wt% of H_2O_2
	LWG_B_10_HP	10 wt% expanded perlite	8.7	25.0	0.3 wt% of H_2O_2
	LWG_A_13	13 wt% expanded perlite	11.6	25.1	
	LWG_B_13	13 wt% expanded perlite	9.8	25.1	
	LWG_A_13_HP	13 wt% expanded perlite	11.3	25.1	0.3 wt% of H_2O_2
	LWG_B_13_HP	13 wt% expanded perlite	9.5	25.1	0.3 wt% of H_2O_2
	LWG_A$_K$_13	13 wt% expanded perlite	11.6	24.6	
	LWG_B$_K$_13	13 wt% expanded perlite	9.8	23.1	

3.2.2 Mixing procedure and curing conditions

All mixtures were prepared using a Hobart mixer. The mixing procedures were modified according to the specific case and are summarized as follows:

- **G**: Geopolymers were prepared by mixing fly ash with alkaline solutions for 90 s after which water, when present, was gradually added. The mixing was performed for further 150 s, stopped for 90 s, and resumed for additional 60 s. Superplasticizers, when present, were added in the last minute of the mixing process.

- **GM**: Geopolymer mortars were prepared by mixing fly ash with alkaline solutions and water. The compound was mixed for 5 minutes after which sand was gradually added for the next 30 s. Afterward, mixing was performed for 30 s, then paused for 90 s, and resumed for additional 60 s.

- **GM$_2$**: Geopolymer mortars (type 2) were prepared by mixing fly ash with alkaline solutions and water. Mixing was operated for 30 s after which sand was gradually added during the following 30 s. Afterward, water was introduced, followed by the superplasticizer, when present. The mixing was paused for 90 s and resumed for additional 60 s.

- **GC**: Fly ash and refractory particles were pre-mixed and then poured in the Hobart mixer where alkaline solutions were added together with extra water. After 6 minutes of mixing, the mixer was paused for 60 s and then resumed for further 3 minutes.

- **LWG**: Fly ash and perlite were manually pre-mixed and then poured in the Hobart mixer where alkaline solutions and sodium silicate solutions were successively added. After mixing for 90 s, water was gradually added and mixed for additional 150 s. After a pause of 60 s, hydrogen peroxide, when present, was added and mixed for further 60 s.

The fresh properties of the materials were assessed immediately after mixing as described in paragraph 3.3.1. The mixtures were poured in different size moulds (which varied according to the test procedure), vibrated, and cured sealed in plastic bags to prevent the fast evaporation of the water at laboratory conditions (T=21±2 °C). After at least 24 hours and no more than 72 hours, the hardened specimens were demoulded and cured at the aforementioned conditions until the day of the test, which if not differently specified, corresponded to 7 and/or 28 days.

Only for GC specimens a heat curing (T = 70 ± 1 °C) for the first 24 h was also performed. After the first 24 h in the oven at 70 ± 1 °C, all the specimens were demoulded and cured sealed in plastic bags at room temperature for further 6 days.

For tests that involve the use of specific specimens (i.e. fire test, bond tests) a detailed description of the specimens preparation and curing is reported in the dedicated paragraphs, together with the test procedure.

3.3   Methods

3.3.1   Fresh properties

Workability of geopolymers was evaluated through the minislump test [105]. After mixing, geopolymer mixture was poured into a truncated conical mould (dmin = 19 mm, dmax = 38 mm, h = 57 mm). The mould was lifted up and the mean diameter of spread paste was measured after one minute. This test was performed immediately after mixing (t=0'). When superplasticizers are investigated, the test was repeated after 5, 15 and 30 minutes on the same mixture, in order to evaluate the variations of workability during time.

Workability of the geopolymer mortars was measured by means of the conventional flow table test, in accordance with the EN 1015-3 [106]. The workability, expressed in terms of consistency %, was determined as the percentage of the difference between the average diameter of the spread mixture and the diameter of the conical ring (100 mm) divided by the diameter of the conical ring (100 mm).

In order to evaluate the influence of SP on the **air entrainment** in the fresh mixture, the air content of the fresh geopolymer mortars was determined according to EN 1015-7 [107] using a 1L porosimeter.

3.3.2   Microstructure and physical properties

Scanning electron microscope was used to investigate the adhesion between steel fibres and geopolymer mortars (see Chapter 5) using a SEM, EVO 40XVP-M, Carl Zeiss Microscopy GmbH. In addition, to analyse the microstructural changes due to the high temperature exposure (see Chapter 6), SEM analysis of representative samples regions were obtained in backscattered electrons of polished sections. In the latter case, SEM observations were carried out by a Tescan Vega 3 microscope.

X-ray diffraction analysis were conducted on powdered samples with a Rigaku Ultima IV device. Data were collected in the angular range of 10-65° 2θ with a step size of 0.02° and a scanning speed of 0.5° 2θ min^{-1}. The analysis of quantitative mineralogical compositions of the samples studied in Chapter 6, were determined by PW3830 X-ray diffractometer. Powdered specimens, diluted with 10 wt% of rutile as internal standard, were side loaded to minimize preferred orientation. Data were collected in the angular range 10-80° 2θ with steps of 0.02° and 5 s/step and the Rietveld refinements were performed using GSAS27 [108].

Fourier transform infrared spectroscopy (FT-IR) for the admixtures characterization were carried out by means of PerkinElmer Spectrum Two instrument. The spectra were recorded by Attenuated Total Reflection (ATR) sampling technique on samples of PCE and ACRa admixtures, previously dried in a vacuum dryer. In order to test the chemical stability of PCE and ACRa in the alkaline solution media, the superplasticizers were also mixed with an 8M NaOH solution (weight ratio 1:1). After 30 min stirring, the solution was dried in a vacuum dryer and the sample spectra was registered.

The **bulk density** (ρ_{bulk}) of specimens was obtained as dry mass divided by the geometric volume. Drying was performed in oven at T = 105 ± 2 °C for 24 hours or until the specimens reached constant mass ± 0.1 %.

The **water absorption** (WA%) of specimens was obtained by soaking dried samples in water for at least 24 h or until the specimens reached constant mass ± 0.1 %. Results are expressed as percentage of the difference of saturated surface dry mass (m_{ssa}) and dry mas (m_d) divided by the dry mass, according to the equation:

$$WA\% = \frac{m_{ssa} - m_d}{m_d}$$

In some cases (see Chapter 7), water absorption test was also conducted under vacuum conditions ($WA_{uv}\%$).

The pore size distribution of samples was investigated by **mercury intrusion porosimetry** (MIP) (Carlo Erba 2000) equipped with a macropore unit (Model 120, Fison Instruments). This technique is based on the intrusion of a non-wetting fluid (mercury) into the pore structure under increasing pressure. A wide range of pores (pore radius in the range of 0.004 – 70 μm) can be explored and a pore size distribution can be obtained. The Washburn equation [109] is used to relate the pressure to pore size:

$$r = \frac{-4\gamma\cos\theta}{P}$$

Where:

r = pore radius;

γ = surface tension of the liquid (0.48 N/m);

θ = contact angle of intrusion liquid of 141.3°

P = pressure of liquid.

Low magnification imaging was performed using the Olympus SZX10 optical microscope. In some cases, the **optical microscopy analysis** was used in combination with the image analysis software LAS V3.8 for obtaining information on the porosity of the hardened specimens.

Capillary water absorption tests were performed according to EN 15801 [110] (results in Chapter 4) or EN 13057 [111] (results in Chapter 5) in order to evaluate the interconnectivity of the pores. As required by the standard, the amount of water absorbed per unit area at the time t_i was expressed by the capillary water absorption curve.

Drying shrinkage was investigated according to EN 12617-4 [112] using 40 × 40 × 160 mm prisms. The length of the prisms was measured at the age of 1, 3, 7, 14, 21, 28 and 56 days. Shrinkage was determined as the specific length variation, i.e. the change in length over the initial specimen length. The average of the specific length of three prisms for each age was used to study shrinkage for each matrix type.

3.3.3   Mechanical tests

The **mechanical characterization** of geopolymer mortars was carried out by performing compressive and flexural strength test according to EN 196-1 [101] on prisms (40 × 40 × 160 mm). Flexural and compressive strengths were determined by a Wolpert machine (maximum load: 100 kN) at a constant displacement rate of 50 mm/min.

Dynamic modulus of elasticity (E_d) was determined using a commercial ultrasonic testing instrument (Matest) composed of a pulse generator and two transducers (55 kHz) that were positioned at opposite ends of 160 mm long sample. The dynamic modulus of elasticity is calculated as:

$$E_d = v^2 \rho \ \frac{(1+ \upsilon)(1- 2\upsilon)}{(1- \upsilon)}$$

Where:

v = ultrasonic pulse velocity (m/s)

ρ = bulk density (kg/m^3)

υ = Poisson's ratio (assumed equal to 0.25)

3.3.4   Bond tests

Single-lap direct-shear tests were performed on specific specimens in order to analyse the bond behaviour of the composite-concrete joints. In order to produce the specimens for the test, geopolymer mortar (GM) prepared as described in 3.2.2 was used as matrix for embedding high strength textiles on concrete or masonry substrates. The textile used for this study are described in more detail in paragraph 3.2.5. The matrix was used only in the bonded area to embed the textiles and bond the composite to the substrate. Two different substrates were considered for the experimental investigation:

   – a concrete prism (150 × 150 × 600 mm) characterized by a compressive strength equal to 23.5 MPa
     (CoV = 0.06). The surface of application of the concrete prism was previously sandblasted to favour
     the adhesion between the composite and the substrate. The bonded length was equal to 450 mm and
     the bonded width was equal to 50 mm (Figure 3.4). The fibres were left bare outside the bonded area,
     which started 50 mm from the top edge of the prism.
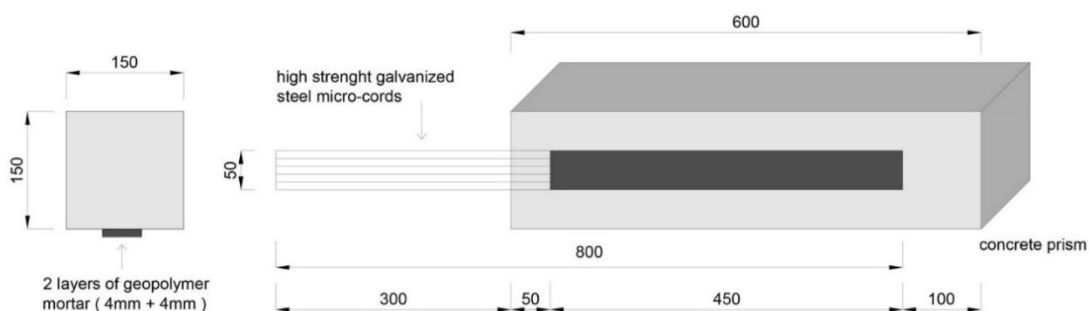
Figure 3.4: Schematic representation of the FRGM-composite bonded to concrete blocks (dimensions in mm).

– A masonry prisms ($125 \times 125 \times 380$ mm) made of six $125 \times 125 \times 55$ mm clay bricks (having 20.3 N/mm^2 (CoV 0.17) compressive strength, 3.16 N/mm^2 (CoV 0.12) tensile strength and 7.3 GPa (CoV 0.29) Young's modulus) and five mortars joints. The bonded length was equal to 300 mm and the bonded width was equal to 50 mm (Figure 3.5). The fibres were left bare outside the bonded area, which started 35 mm from the top edge of the prism.
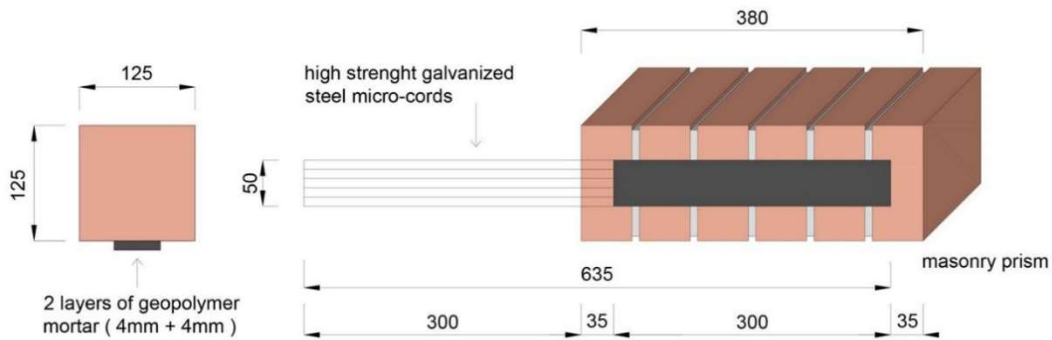
Figure 3.5: Schematic representation of the FRGM-composite bonded to masonry blocks (dimensions in mm).

In both cases, a 4 mm layer of mortar was applied on one face of the substrate; fibres were applied on the first layer of mortar and covered by a second layer (4 mm) of mortar. Specimens were cured at room temperature covered by a PVC film until the day of the test (Figure 3.6).

(a)   (b)

Figure 3.6: Curing of the FRGM composites bonded to concrete (a) and masonry (b) substrates.

After at least 7 days of curing, single-lap direct-shear tests were performed on these specimens. Before testing, a 75 mm-long epoxy tab was constructed with a thermosetting epoxy at the end of the fibre sheet and used to improve gripping during testing. The classical push-pull configuration was adopted for the direct shear test, where fibres were pulled while the prism was restrained. Direct shear tests were conducted under displacement control using a close-loop servo-hydraulic universal testing machine. Two Linear Variable Displacement Transducers (i.e. LVDTs named LVDTa and LVDTb) were mounted on the concrete surface, close to the top edge of the bonded region. The LVDTs reacted off of thin aluminium Ω-shaped plate that was attached to the bare fibre surface adjacent to the beginning of the bonded area (Figure 3.7). The average of the

two LVDT measurements was defined as the global slip. The global slip was increased at a constant rate equal to 0.00084 mm/s. A detailed description of the test setup is reported elsewhere [40].
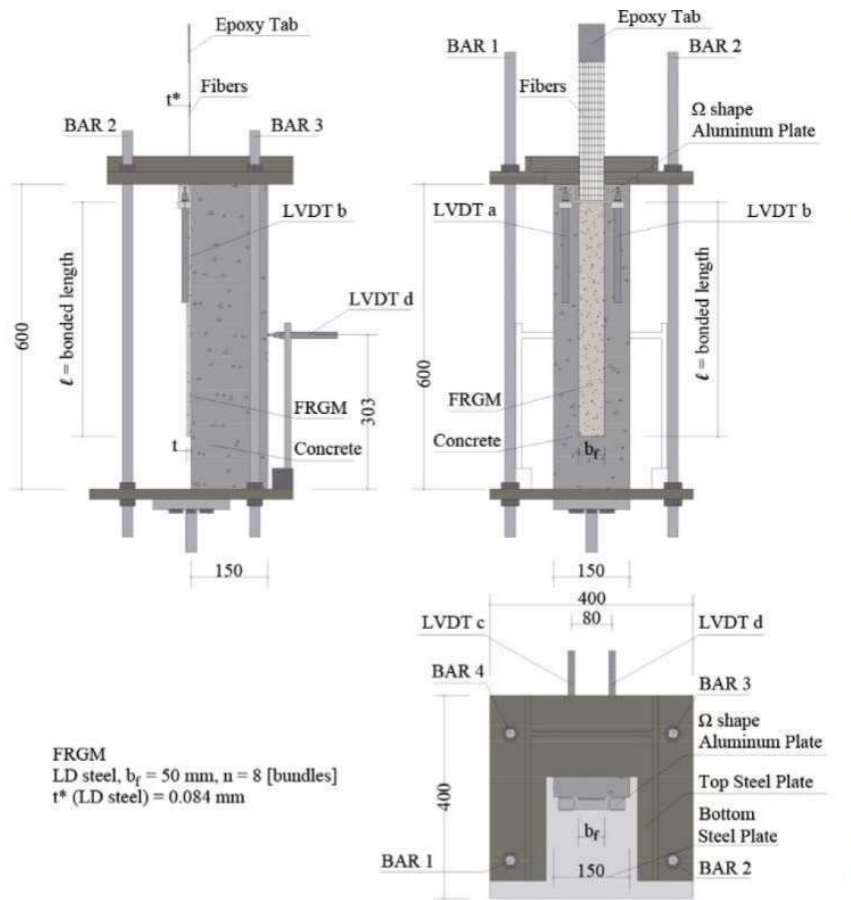
(a)

(b)   (c)

Figure 3.7: Single lap direct shear test setup-dimensions in mm (a) [113]; Photos of direct shear tests (b,c).

Pull-off tests were performed to obtain insight into the adhesion between the mortar and the substrate and between the mortar and the fibre. To perform this test, specific specimens were produced. A 4 mm layer of mortar (GM_A$_{4M}$) was applied on one face of the substrate, the steel-fibre textile was applied on the first layer of mortar and covered by a second layer (4 mm) of mortar. Specimens were cured at room temperature covered by a PVC film for 28 days.

| (a) | (b) |

| (c) | (d) |
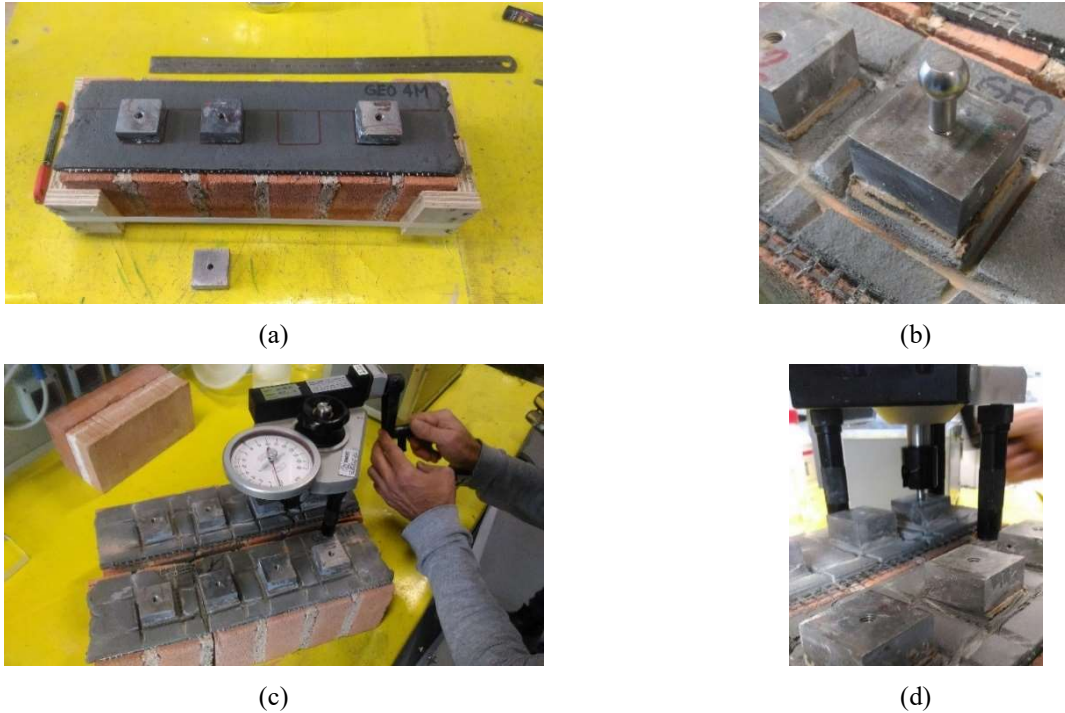
Figure 3.8: Pull off test procedure.

The test was performed following the guidelines of EN 1542 [114]. The method of test is by direct dolly pull-off using a dolly bonded to the surface of the repair product or system, with the test area having been defined by coring through the surface (Figure 3.8 a and b). The test was performed by means of a DYNATEST measurement device (load cell of 16 kN) that displays the exerted force by an analogue system test (Figure 3.8 c and d).

The outputs of the test are:

– the tensile bond strength, obtained dividing the failure load by the area of the test specimen;

– the failure mode, determined from a visual assessment.

3.3.5 Thermal analysis

The weight loss during high temperature exposure was measured using **thermogravimetric analysis** (TGA). Results presented in Chapter 6 were obtained through a STA 449 C Jupiter instrument, heating at constant rate of 10°C/min in nitrogen atmosphere up to 1000 °C. To remove the initial moisture equilibrium at 40°C was performed for 30 minutes. Results presented in Chapter 7 were obtained by a TGA Q500 instrument heating at a constant rate of 10°C/min in air up to 900°C. In this case, the sample was pre-dried at 105°C before starting the test.

Thermodynamic processes were measured using **differential scanning calorimetry** (DSC). DSC was performed with a DSC Q10, TA Instrument, under nitrogen flow. Sample was placed in an aluminium pan and heated up to 280 °C with a constant heating rate of 20°C/min. From DSC measurements it was possible to calculate the **specific heat** (c_p) of the material in the temperature range 30 - 200 °C, according to the EN 821-3 [115]. In order to calibrate this output, the test piece was replaced by α-alumina to use as calibrant of known specific heat and the baseline behaviour was determined by a test with an empty test piece cell. The specific heat of the test piece at any temperature T was calculated as follows:

$$c_{ps} = \frac{(S_s - S_e) \cdot m_c \cdot c_{pc}}{(S_c - S_e) \cdot m_s}$$

Where:

c_{ps}: specific heat of the test piece

c_{pc} : specific heat of the calibrant

S_s : output signal of the test piece;

S_e : output signal of the empty cell;

S_c : output signal of the cell plus calibrant (α-alumina);

m_s : mass of the test piece;

m_c : mass of the calibrant.

Thermal conductivity was analysed by a Transient Plane Source (TPS) method. The method is based on the use of a transiently heated plane sensor consisting of an electrically conducting pattern in the shape of a double spiral. This spiral is sandwiched between two thin sheets of an insulating material (e.g. Kapton, Mica, etc.). TPS1500S from Hot Disk® AB equipped with kapton-insulated sensors (room temperature tests) and mica-insulated sensors (150°C-700°C tests) was used. The system applies the transient plane source technique described in ISO 22007-2 [116] and is applicable over a wide range of temperatures. The plane Hot Disk sensor is fitted between two pieces of the sample, each one with a plane surface facing the sensor. By passing an electrical current, high enough to increase the temperature of the sensor between a fraction of a degree up to several degrees, and at the same time recording the resistance (temperature) increase as a function of time, the Hot Disk sensor is used both as a heat source and as a dynamic temperature sensor [117]. The Hot Disk technique provides a direct measure of the thermal conductivity (k) of the material.

Sensors with 9.719 mm radius were used; the power provided to the sensor in the test was between 35 -75 mW, depending of temperatures conditions, the measuring time was 160 s. Two rectangular slabs of material (80 × 80 × 30 mm) were used as tested samples. Sample and sensor assembly was setup as described from ISO 22007-2 [116] (Figure 3.9). The thermal conductivity is sensitive to the moisture content of a material. Therefore, all the specimens used for this test were pre-dried in oven with the aim to avoid errors during the measure owed to differences in the initial moisture content. For the high temperature measurements, the sample assembly was located in a Chamber Furnace (LF2 SP from Vecstar Ltd). The furnace chamber was conditioned, before the start of each test, by removing the air from the system by a vacuum pump, filling with

nitrogen and repeating this cycle more times. During the experimental runs, the furnace chamber was purged by pure nitrogen with a flowrate of 7.5 mL/min. Each measurement is the mean of five individual measurements, with variation of $\pm$ 0.01 Wm^{-1} K^{-1}.
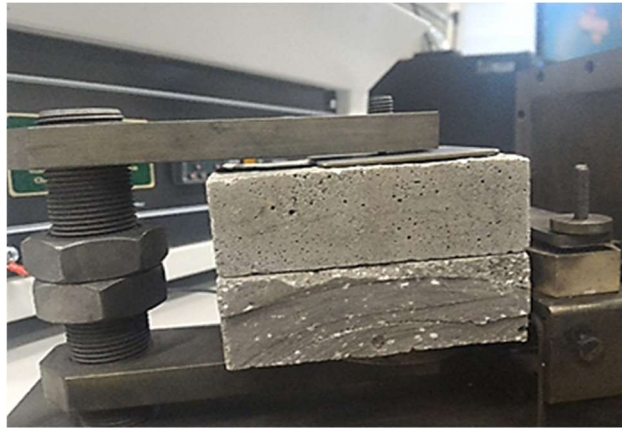
Figure 3.9: Test setup: sensor assembled in between two slabs of specimens.

The linear dimensional variations were measured by a **dilatometer** 402 E, Netzsch GmbH. Prismatic samples of 5 × 9 × 25 mm were heated from ambient temperature up to 1000°C at a constant rate of 10 °C/min.

A **heating optical microscope** (HSM, Expert System) was used with the aim to follow up the behaviour of the product during heating. Samples of 3 × 3 × 5 mm were heated at a constant rate of 5°C/min until the complete melting of the sample was achieved.

Acoustic Emissions were measured during the thermal treatment in a muffle furnace to study the cracking mechanism occurring during a high temperature exposure. Cracking and crack growth in brittle materials is accompanied by the emission of elastic waves. Detection and analysis of these transient signals ('hits') therefore gives insight into the processes taking place at different times during the experiments. Both the heating and cooling period were investigated. For this test, specimens were heated at 2°C/min up to several set temperatures (i.e. T = 500, 550, 600, 650, 800 °C), maintained for 1 h at the set temperature and then allowed to cool naturally back to room temperature. Photos of the test setup are reported in Figure 3.10. Three samples (40 × 40 × 50 mm) were tested for each run. Two of them were in contact with waveguides on their top surface and equipped with acoustic emission (AE) sensors. A third sample was drilled in its lateral surface in order to obtain a hole (3 mm diameter and 20 mm length) where a thermocouple was arranged for measuring the temperature inside the sample during the test. In this way, it was possible to obtain temperature-time curve to correlate with the hits-time curve resulting from the acoustic emission measurements.
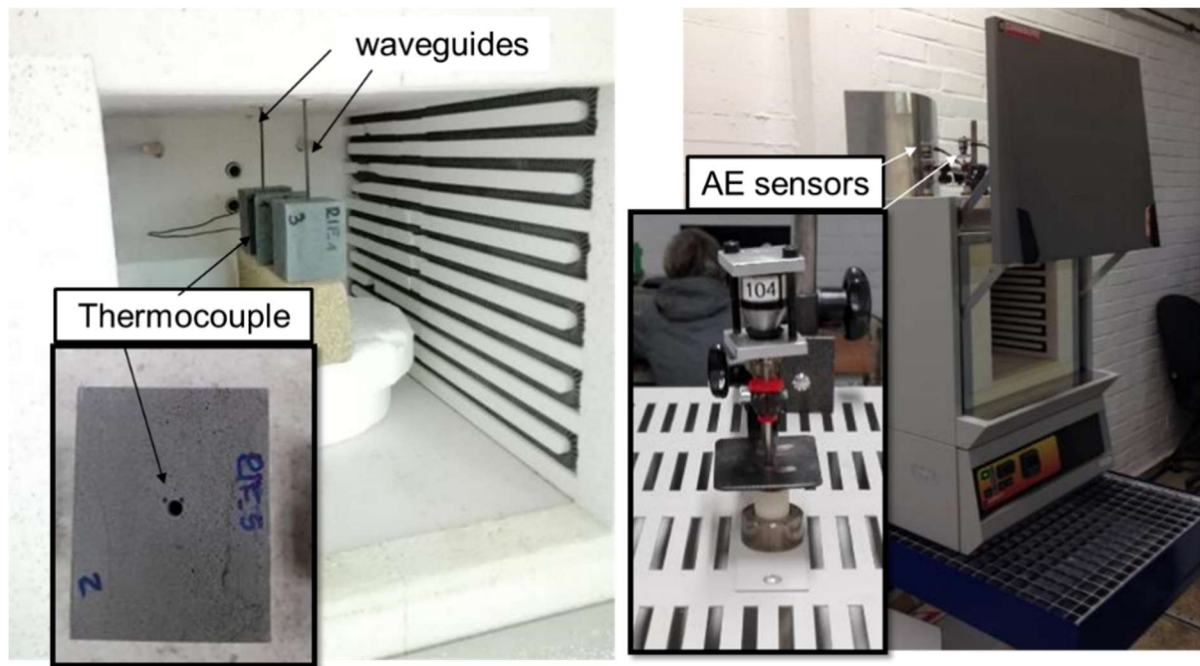
Figure 3.10: Setup for measuring acoustic emissions during thermal treatments in the muffle furnace.

Different **thermal treatments using a muffle furnace** were performed to obtain insight into the thermal behaviour of the geopolymer composites (GC series - paragraph 6.3). For this test, the as cured specimens were heated at 5°C/min up to the two different set temperatures of 800 and 1000°C. The set temperature was maintained for 2 hours and then the samples were left inside the oven and allowed to cool naturally back to room temperature. Specimens before and after the thermal exposure were characterized.

3.3.6   Fire tests

In order to test the fire resistance of various elements of construction, standard heating conditions have been established by standards. In particular, the heating conditions reported in standards define a temperature-time relationships simulating those occurring in real fire. The most commonly adopted fire curves are the so called cellulosic and hydrocarbon fire curves (Figure 3.11). The former is the most appropriate for testing the fire resistance of fire protection systems in ordinary buildings since is based on the burning rate of general combustible building materials and building contents [58].

The temperature development of the cellulosic fire curve is defined in several standards (e.g., ISO 834 – 1 [83], EN 1363 – 1 [118]) and it has to follow the relationship:

$$T = 345 \log (8t+1) + 20$$

Where:

T is the average furnace temperature, in degree Celsius;

t is the time from the start of the test in minutes.

The hydrocarbon (HC) fire curve simulates harsher conditions than the cellulosic one, where small petroleum fires might occur; higher temperatures and a rapid rate of growth characterize such fires. According to EN 1363-2 [119], a temperature-time curve to be designed as the hydrocarbon curve shall be defined by the following expression:

$$T = 1080 \left[1 - 0.325 \, e^{-0.167t} - 0.675 \, e^{-2.5t} \right] + 20$$

Where:

T is the average furnace temperature, in degree Celsius;

t is the time from the start of the test in minutes.
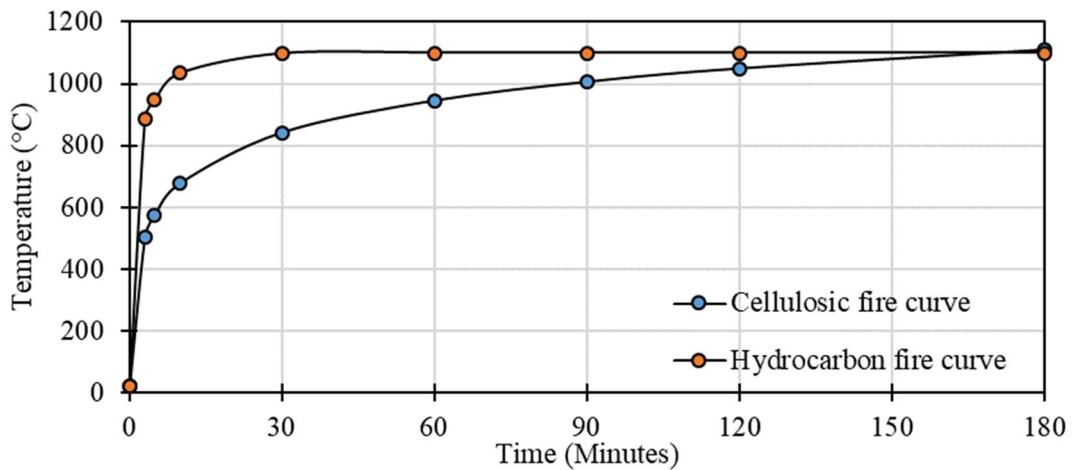
Figure 3.11: Standardized temperature-time fire curves.

Fire tests were conducted using a medium-scale (i.e. furnace with an internal volume of approximately 1m³ – Figure 3.13 a) testing set-up. Specific specimens were realized for this test: the mixture was poured in a silicon mold (80 × 80 × 50 mm) containing a stainless steel plate (75 × 75 × 2 mm) on the bottom. The steel plate was arranged in order to have the sandblasted surface in contact with the mortar. The specimens (Figure 3.12 a,b) were cured in sealed conditions at room temperature (T = 21 ± 2 °C). After 24 h, the specimens were demoulded and cured in the aforementioned conditions for further 27 days. After the 28th day of curing the specimens were allowed to dry in a climate chamber (T = 23 ± 2 °C, RH = 50 ± 5 %) for at least one week and until the day of the test (Figure 3.12 c). In this way, the moisture content of the test specimens approximated to those expected in normal service. Before testing, two thermocouples (type K) were spot-welded onto the backside of each specimen to continuously record the temperature of the cold side of the steel plate during the fire exposure. In addition, a steel waveguide (Figure 3.12 d) was also welded on the backside of the steel to couple the acoustic emission sensor (type VS 150). An AMSY 6 acoustic emission system was used to process and store the detected signals. One specimen for each formulation and a bare steel plate were positioned in a vermiculite sample holder containing nine square openings (side 80 mm – Figure 3.13 b). For each fire test, two sample holders were prepared in order to obtain an average measurement for each formulation. The sample holders were attached to the opening in the sides of the furnace (Figure 3.13 c). Afterwards, the waveguides were equipped with pre-amplifiers and frequency filters to increase signal amplitudes and to minimize noise

(Figure 3.13 d,e). Both the so arranged waveguides and the thermocouples were connected to the data-recording systems.

Three fire tests (Figure 3.14 f) were performed according to the experimental program reported in Table 3.9.

Table 3.9: Fire tests. Experimental program.

Test	Fire curve- Standard	Thickness of the mortar layer	Time of firing	Recorded data	
				Temperature-time curve	Acoustic emissions
1	Cellulosic fire - ISO 834-1	15 mm	45 min	x	x
2	Cellulosic fire - ISO 834-1	20 mm	60 min	x	-
3	Hydrocarbon fire – EN 1363-2	20 mm	35 min	x	x

The temperature-time curves were recorded to identify the time after which the temperature of the cold side of the steel plate exceed 500°C which is identified as the critical threshold for the properties of steel, since steel loses about one-half of the strength at 500 °C [120]. The fire was stopped 20 minutes after the achievement of 500°C by all the specimens. In addition, acoustic emissions were recorded during both heating and during cooling for one more hours, to have insights into the mechanism of cracking related to the thermal exposure.
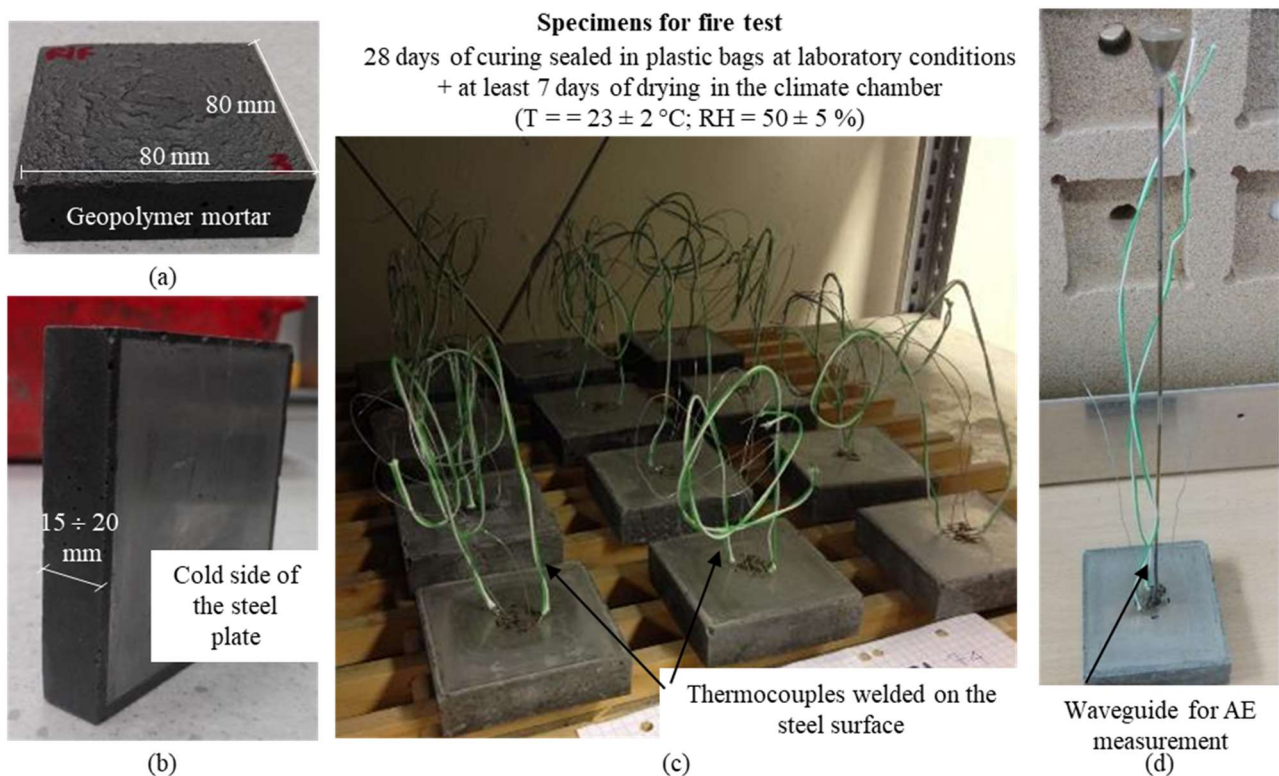
Figure 3.12: Photos of the specimens produced for the fire tests.
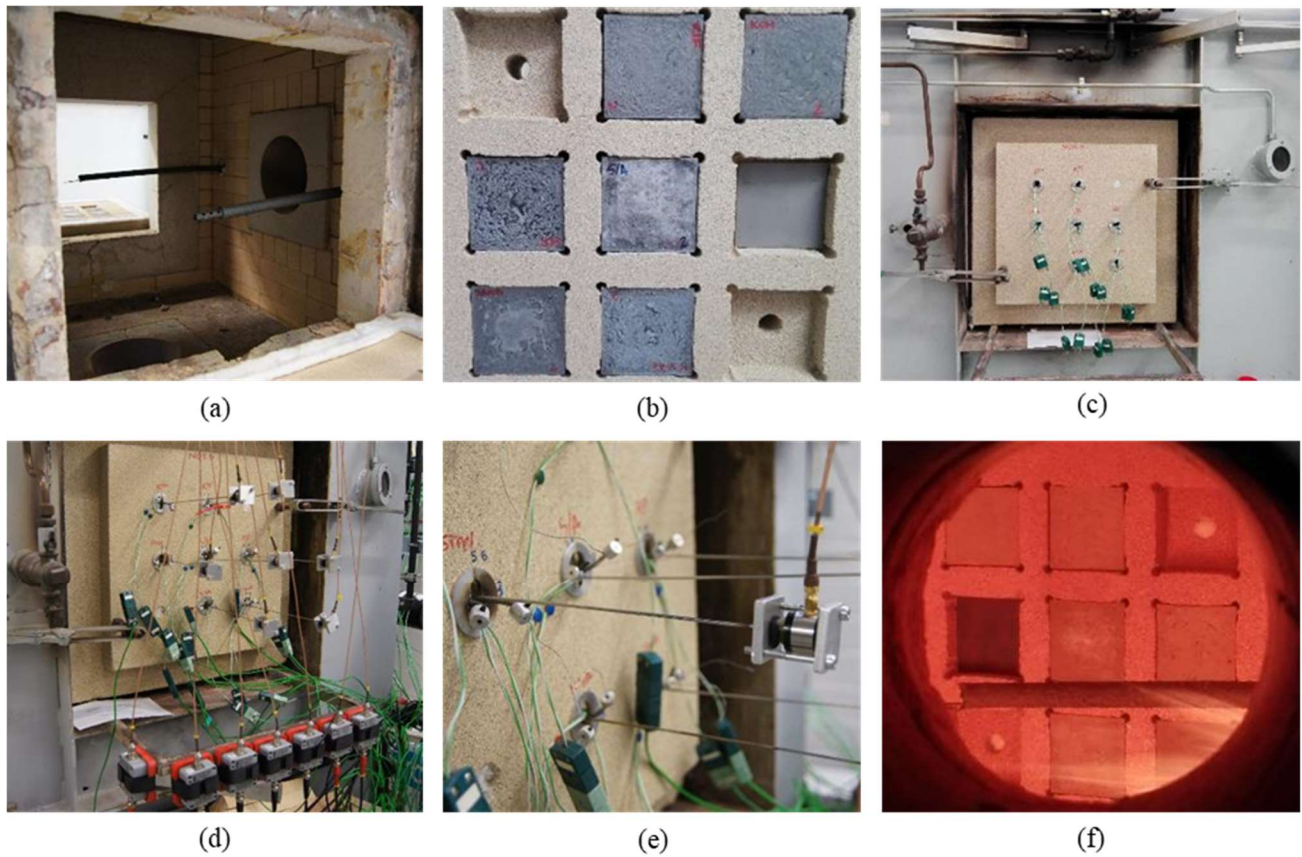
Figure 3.13: Photos of the medium-scale fire test setup.

3.3.7   Test campaign

An overview of the performed tests is reported in Table 3.10.

Table 3.10: Test campaign.

	Mixture	Characterization test
	Superplasticizers	Fourier transform infrared spectroscopy (FT-IR) on PCE and ACRa
	G_A	Workability - minislump test
Chapter 4	**GM₂_A**	Workability - flow table test - EN 1015-3 [106] Air entrainment in the fresh mixture - EN 1015-7 [107] Bulk density Optical microscopy analysis in combination with the image analysis Mercury intrusion porosimetry Capillary water absorption - EN 15801 [110] Mechanical characterization - EN 196-1 [101] Determination of E_d
Chapter 5	**GM_A** **GM_A₆ₘ** **GM_A₄ₘ**	SEM analysis Workability - flow table test - EN 1015-3 [106] Bulk density Water absorption Mercury intrusion porosimetry Capillary water absorption - EN 13057 [111] Mechanical characterization - EN 196-1 [101] Determination of E_d Drying shrinkage - EN 12617-4 [112] Single-lap direct-shear test on FRGM composites Pull-off test on FRGM composites

Chapter 6	**G_A**	Acoustic emissions measurements during heat treatment X-ray diffraction analysis SEM analysis in backscattered electrons of the polished sections Thermogravimetric analysis – TGA in nitrogen atmosphere Quantitative XRD analysis Thermal treatments using a muffle furnace Optical microscopy analysis Bulk density Water absorption Heating optical microscope Dilatometer
	G_A$_K$	Acoustic emissions measurements during heat treatment X-ray diffraction analysis
	GC_A_10 GC_A_20 GC_A_30 GC_A_40	Thermal treatments using a muffle furnace Optical microscopy analysis Bulk density Water absorption Heating optical microscope Dilatometer Quantitative XRD analysis (only on samples GC_A_30 and GC_A_40) Determination of the compressive strength (GC_A_40)
Chapter 7	**G_A G_B LWG_A_10 LWG_B_10 LWG_A_10_HP LWG_B_10_HP LWG_A_13 LWG_B_13 LWG_B_13_HP LWG_A_13_HP**	Bulk density Water absorption Water absorption under vacuum Mercury intrusion porosimetry Thermogravimetric analysis – TGA in air Differential scanning calorimetry - DSC Determination of specific heat (c_p) - EN 821-3 [115] Thermal conductivity at T = 20 °C Determination of R_c Determination of E_d Optical microscopy analysis was used in combination with the image analysis (only on samples LWG_B_13_HP and LWG_A_13_HP) Thermal conductivity up to 700 °C (only on samples G_B, LWG_B_13_HP, and LWG_A_13_HP)
		Additional test
	LWG_A_13 LWG_B_13 LWG_A_13_HP LWG_A$_K$_13 LWG_B$_K$_13 GM_A	Medium-scale fire tests

Chapter 4:

Implementing geopolymers fresh properties:
the use of superplasticizers

4.1   Background and research aims

Superplasticizers (SP) are widely used in concrete technology. These admixtures can be used as water reducer maintaining a fixed workability or as plasticizers increasing workability without modifying the mix design. First applications of chemical admixtures as water reducers date back to the 1940s with the adoption of lignosulfonate (LS) followed by the development in the 1960s of high water reducer based on sulphonated naphthalene formaldehyde (SNF) and sulphonated melamine formaldehyde (SMF). Finally, in the early 1980s, a new generation of superplasticizers based on polyacrylate polymers was designed [121]. Several studies [122–126] have been conducted on the chemistry and the operating principle of superplasticizers in cement matrix, confirming that their use allows to enhance mechanical and microstructural properties and durability performances of concrete. Therefore, the adoption of SP can be considered one of the most important improvements in concrete technology that contributed to its worldwide diffusion [121,126].

As happened for OPC concrete, understanding the effectiveness and influence of superplasticizers in geopolymer systems is one of the essential requirements for its large-scale acceptance as building material. The superplasticizers currently available have been specifically designed to work with the chemistry of Portland cement. Despite the fact that in terms of performances geopolymer and OPC based materials can be comparable, it has to be highlighted that the reaction mechanism and products of these two systems are completely different [14,15].

However, in the absence of specific superplasticizers designed for alkali activated systems, it is useful to understand if the available SP can be successfully adopted for the production of geopolymers. Research conducted on this topic are often contradictory on establishing which is the chemical structure of the admixtures that can promote a significant plasticizing effect [52,53,127–130]. In addition, it is well known that in the case of traditional OPC concrete the use of SP can increase the air-entrainment during the mix or can affect porosity and pore size distribution of the hardened material [131,132]. For this reason, research focused on this topic is necessary, being porosity strictly connected to the durability issues of final products.

In this chapter, the influence of commercially available superplasticizers designed for OPC concrete on properties of geopolymers (G_A) and geopolymer mortars (GM$_2$_A) are investigated. Seven types of commercially available superplasticizers (see paragraph 3.2.3), commonly used in OPC concrete industry were used. Both geopolymers and geopolymers mortar were labelled according to the chemical structure of the admixture (Table 3.5), followed by its amount expressed in percentage by mass of precursor (i.e., PCE_06 refers to a mixture containing 0.6 wt% of polycarboxylic ether by mass of fly ash). Furthermore, a reference mixture without superplasticizer was prepared and named either G_A or GM$_2$_A. Fresh and hardened properties were analysed with a special focus on porosity and its distribution in order to get a more comprehensive overview of the influence of superplasticizers in geopolymer materials.

4.2   Effect of superplasticizers on fresh properties

<u>Workability</u>

Workability test on fly ash-based geopolymer was carried out in order to evaluate the effectiveness of the investigated SP and it has been expressed as relative spread for geopolymers and consistency for mortars. The relative spread was defined as the difference, expressed in percentage, between the spread of the tested mixtures containing SP and the spread of G_A mixture divided by G_A spread diameter. Figure 4.1 reports the results of the minislump test as function of time (0, 5, 15, 30 min after mixing).
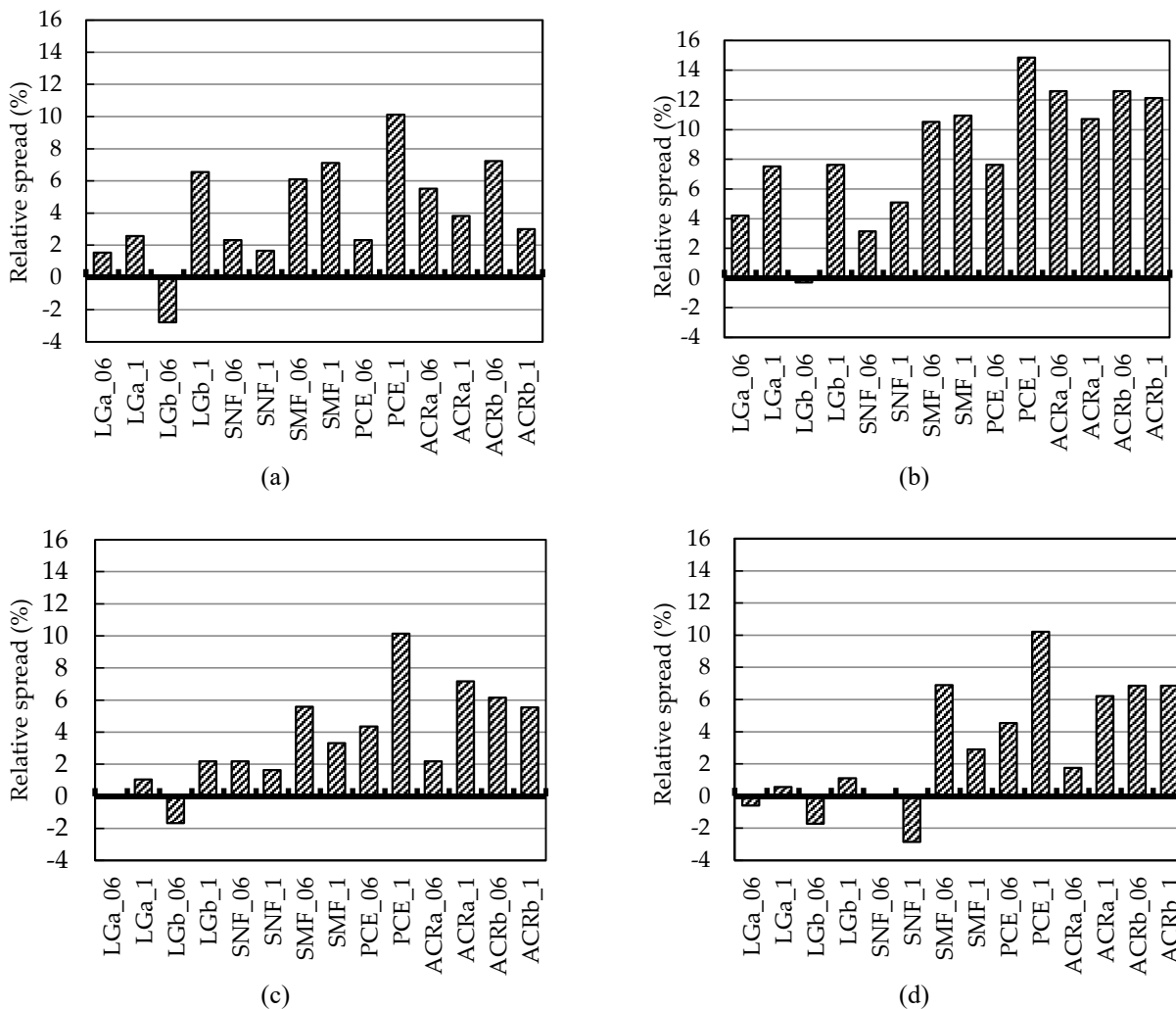
Figure 4.1: Workability of geopolymer expressed as relative spread (increase or decrease in %) of the geopolymer mixtures immediately after mixing (a), after 5 minutes (b), 15 minutes (c) and 30 minutes (d) [133].

Lignosulphonate and naphthalene based admixtures (LGa, LGb, SNF) did not significantly improve workability of geopolymers either in case of the added amount of 0.6 wt% or when 1.0 wt% of SP was used. Moreover, in the cases of LGb_06 and SNF_1 mixtures, the results showed a reduction in spread when compared to G_A. On the contrary, geopolymers containing SMF, PCE, ACRa and ACRb superplasticizers showed a spread higher than G_A during all the tested times (0, 5, 15 and 30 minutes). Increasing the amount of SP from 0.6 to 1.0 wt% was effective only when PCE was used, whereas it did not always correspond to an

increase in workability for SMF, ACRa and ACRb. At t=0', the relative spreads of SMF_06, PCE_1, ACRa_06 and ACRb_06 mixtures were equal to 6.1%, 10.1%, 5.5% and 7.2% respectively, thus highlighting an increase in the flow diameter of these mixtures up to 10.1% compared to G_A. For this reason, these SP were also tested on geopolymer mortar specimens.

Figure 4.2 shows the flow table test results obtained on mortar samples. Consistency was expressed as average of four different tests per mixture. At t=0', PCE_06, PCE_1, ACRa_06 and ACRb_06 showed a consistency in the range of 74 - 87%, which was higher than the reference one (GM$_2$_A). ACRa_06 and PCE_1 mixtures exhibited the highest values and at t=30' they showed consistency equal to 69 ± 2% and 68 ± 4% respectively, thus exhibiting a workability very close to the one of GM$_2$_A at t = 0' (73 ± 4%).

As a general trend, mortar workability decreased with time with a similar rate for all the investigated mixtures and for PCE higher values were always registered for superplasticizer content of 1 wt% rather than 0.6 wt%.
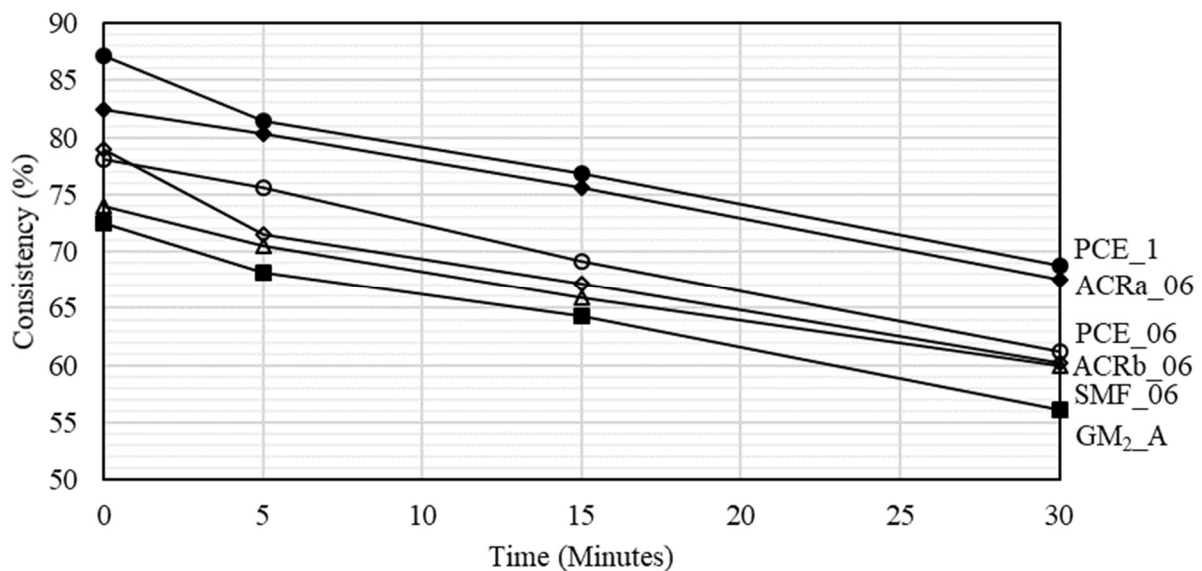
Figure 4.2: Consistency of geopolymer mortars as function of time (average of four measurements, PCE_1 (●), ACRa_06 (◆), PCE_06 (○), ACRb_06 (◇), SMF_06 (△), GM$_2$_A (■)). Standard deviation is not reported in the plot for clarity sake however it is in the range of ±5 [133].

Results concerning the consistency of the geopolymers and mortars show that the latest generation admixtures (PCE and acrylics based types) are more effective in terms of workability improvement than lignosulphonate, naphthalene and melamine based SP. Such differences can be ascribed to the different chemical structure. Indeed, LS, SNF and SMF based superplasticizers rely on an electrostatic repulsion: in the cement based materials, the electrostatic attractive forces among cement particles, which generate agglomeration, are neutralized by the adsorption of anionic polymers negatively charged for the presence of the SO_3^- groups on the surface of cement particles. The dispersion is obtained by the electrostatic repulsion produced by the negatively charged SO_3^- groups on the opposite side of the main polymer chain [134] .

Regarding the latest generation of SP, the dispersion mechanism is more related to a steric hindrance effect generated by the side chains of the polymer, than to the presence of negatively charged anionic COO^- group, which is responsible for the adsorption of the polymers on the surface of cement particles[134].

Although a study [129] related to the efficiency of SP in alkali activated slag systems revealed that the majority of SP used for OPC based binder seems to degrade in the high alkaline environment, the chemical structure of PCE based superplasticizer and the presence on numerous lateral side chains can prevent the tendency of binder particles to agglomerate [52]. Moreover, a recent study [135] on adoption of PCE based superplasticizer in alkali activated slag pastes confirms that by acting on the molecular architecture of the PCE, its performances as superplasticizer are improved. Finally, it has to be mentioned that setting occurred regularly when the different SP were added and no delay was registered in demoulding procedure.

Air content

The determination of air content is essential for understanding if the detected workability improvement is ascribed to an increase of air entrainment due to the use of SP rather than to their plasticizing effect [136]. The air content test was conducted on the reference geopolymer mortar (GM_2_A) and on PCE_1 and ACRa_06, the two mixtures showing the best results on the flow table test.

The consistency of mortars immediately after mixing (t=0') and the relevant air content % are reported in Table 4.1. From the results, no correlation between the workability improvement and air content was found. Indeed, PCE_1 mix exhibited an equal or lower air content than the other tested mixtures, even if it showed the highest consistency.

Table 4.1: Consistency and air content of GM_2_A, PCE_1 and ACRa_06 (average values of four and two measurements, respectively) [133].

	Consistency (%)	Air content (%)
GM_2_A	73±4	4.9±0.5
PCE_1	87±3	4.9±0.1
ACRa_06	83±5	5.1±0.1

4.3   Superplasticizers chemical stability in alkaline environment

Infrared spectroscopy is technique largely used for studying superplasticizers in cement and alkali activated materials [51,129,137,138]. The infrared spectra for PCE and ACRa dried in a vacuum dryer and after mixing with an 8M NaOH solution are reported in Figure 4.3. Comparing the spectrum of the dried admixture (red) with the one where the admixture was treated with NaOH solution (black), for both PCE and ACRa superplasticizers, the band at 3450-3400 cm^{-1} corresponding to OH^- group, slightly increased thus indicating a good chemical stability of PCE and ACRa in the alkaline medium. Indeed, this peak usually strongly increases when polymer degradation occurs according to the increase content of the OH terminal chain group formed during hydrolysis. Moreover, for ACRa spectra (Figure 4.3 a) the band at 1730 cm^{-1}, which corresponds

to C=O carboxylic derivatives, remained almost unchanged when the alkaline treatment is carried out, confirming a good chemical stability. Conversely, for PCE (Figure 4.3 b) the band at 1725 cm^{-1} practically disappeared, but only one (at 1418 cm^{-1}) of the two characteristic bands (1575 and 1418 cm^{-1}) corresponding to carboxylate groups appeared as a shoulder of the peak at 1447 cm^{-1}. Thus, for PCE a certain degree of main chain degradation can be hypothesized, however a large part of the lateral chains comprising ether bond (peak at 1100 cm^{-1}) still remains bound and able to exert its action of steric hindrance [129].

(a)

(b)
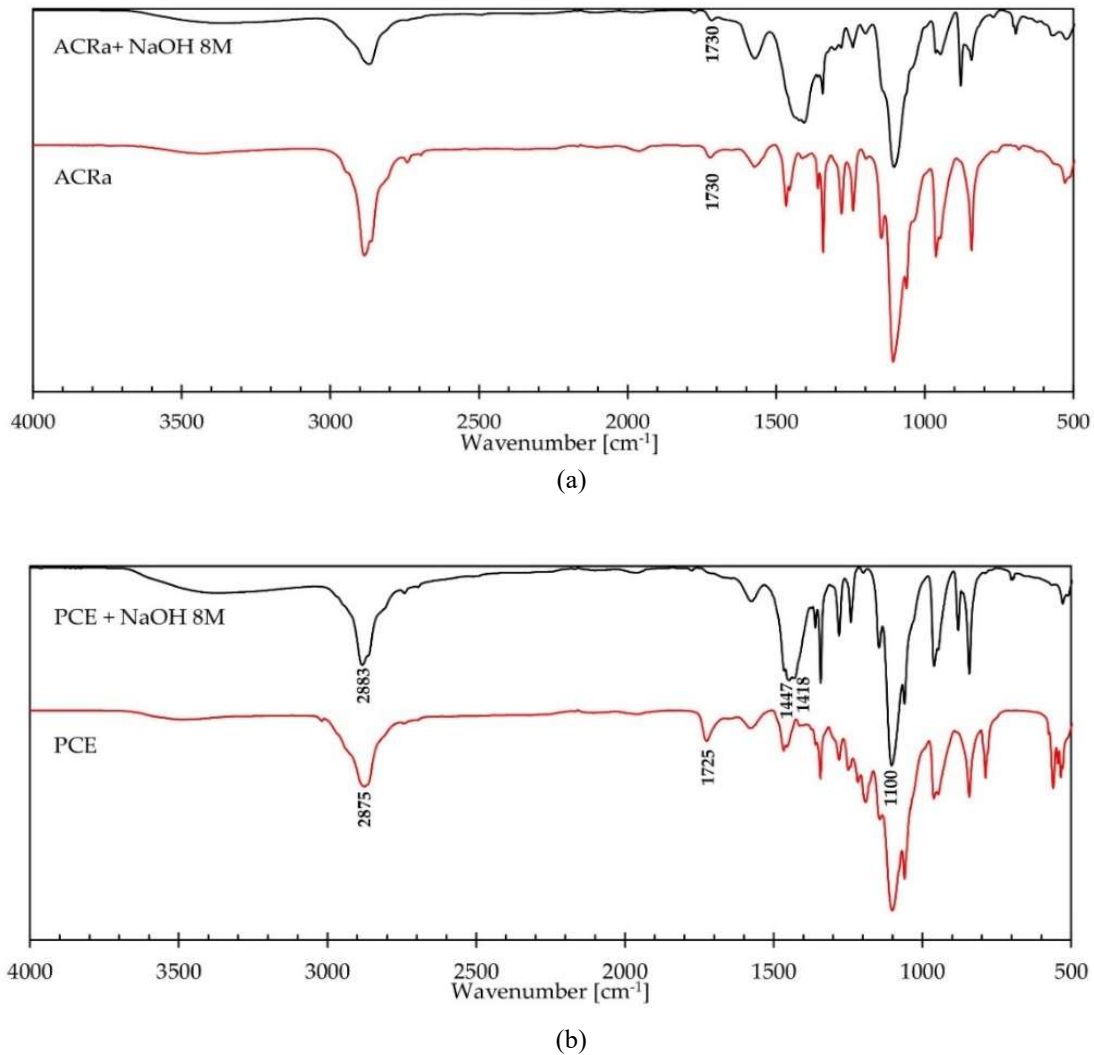
Figure 4.3: FT-IR spectra for ACRa (a) and PCE (b) superplasticizers dried in a vacuum dryer and after mixing with an 8M NaOH solution [133].

4.4   Effect of superplasticizers on microstructure and mechanical properties

Figure 4.4 shows the cross sections of the geopolymer mortar specimens investigated in this study after 28 days of curing. Externally, hardened geopolymer mortars had a dark grey colour and they did not present any efflorescence on the surface.
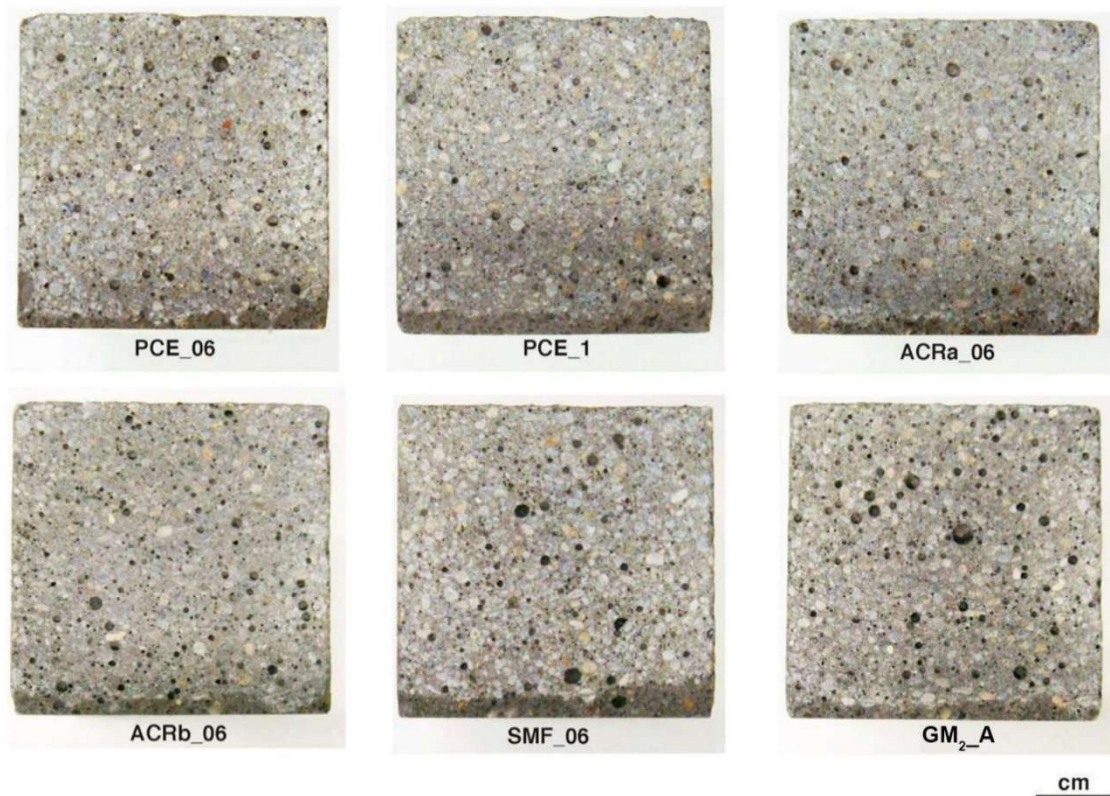
Figure 4.4: Photos of the cross section of hardened geopolymer mortar specimens.

Flexural (R_f) and compressive (R_c) strength were evaluated to determine if the use of SP affects the mechanical properties of the hardened materials. The results are presented in Figure 4.5: the reference sample GM_2_A showed a compressive strength equal to 60.0 ± 1.5 MPa and the relevant values for the samples containing SP were between 60-62 MPa. A similar behaviour is also detected for flexural strength, where GM_2_A exhibited a value of 7.7 ± 1.1 MPa and samples with SP are about 9 MPa. All the ultrasonic pulse velocity measurements are in the range of 3.4-3.7 km/s. During the test, the ultrasonic pulse can be reflected or refracted if discontinuities, voids or cracks are present in the sample. Therefore, all the samples appeared quite similar, indicating that the addition of SP did not affect substantially the final product. This result is confirmed by the bulk density, which was found in the range of 2.1 - 2.2 g/cm^3 for all the investigated specimens. The mechanical properties highlighted that the presence of SP did not interfere with the development of compressive and flexural strength, thus proving that the action of SP was limited to increase the workability of the fresh mixture, as expected. Such a behaviour was particularly evident when PCE was used. In this case, higher workability and very similar mechanical performance were found for increasing amount (from 0.6 to 1.0 wt%) of PCE used. Therefore, their addition did not disturb the geopolymerisation process and promoted the formation of products with performance comparable with those usually determined for a high strength class cement (e.g. 52.5 MPa).
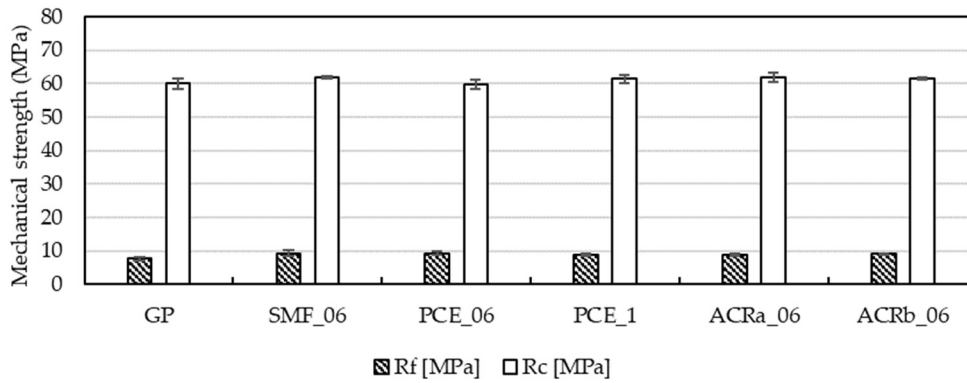
Figure 4.5: Mechanical properties of hardened geopolymer mortars after 28 days of curing at room temperature (values are reported as average of three measurements) [133].

In order to better elucidate the effect of SP on samples microstructure, optical microscopy analysis and mercury intrusion porosimetry were carried out on the reference mix GM₂_A and the best performing mixtures PCE_1 and ACRa_06, after 28 days of curing. Figure 4.6 shows representative optical microscopy images of geopolymer mortars cross section. GM_2_A sample showed a large number of spherical pores of diameter up to 1.57 mm, whereas PCE_1 and ACRa_06 showed pores with a maximum diameter of 0.87 and 1.07 mm, respectively.

(a)

(b)

(c)
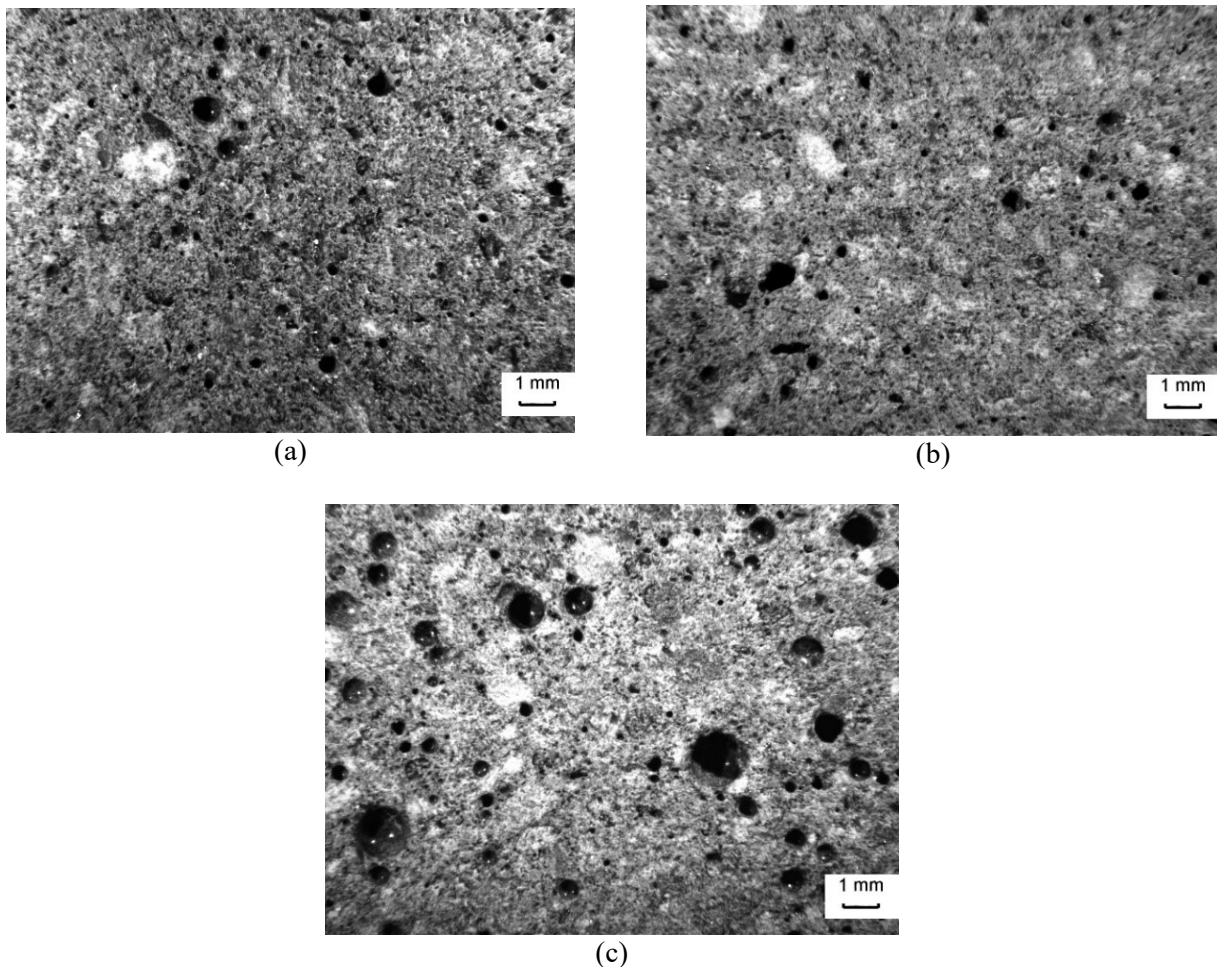
Figure 4.6: Optical images of geopolymer mortars after 28 days of curing: PCE_1 (a), ACRa_06 (b), GM_2_A (c). (Magnification 8x) [133].

In Figure 4.7 is reported the content % of pores arranged per ranges of pore diameters (d) obtained by imaging analysis of two cross sections per sample. Results confirmed that GM_2_A was the sample with the highest amount of pores with $d \geq 0.50$ mm. The content of pores with diameters in the range $0.05 \leq d < 0.25$ mm and $0.02 \leq d < 0.05$ mm was similar for all the formulations. The total porosity (P_t) determined by imaging analysis followed this order $P_t\_GM_2\_A$ (11.7%) > $P_t\_ACRa\_06$ (9.0%) > $P_t\_PCE\_1$ (6.8%), indicating that even if the air content in the mortar at the fresh state was similar, the lowest workability of GM_2_A did not allow the entrapped air to easily escape, thus promoting large pores formation.
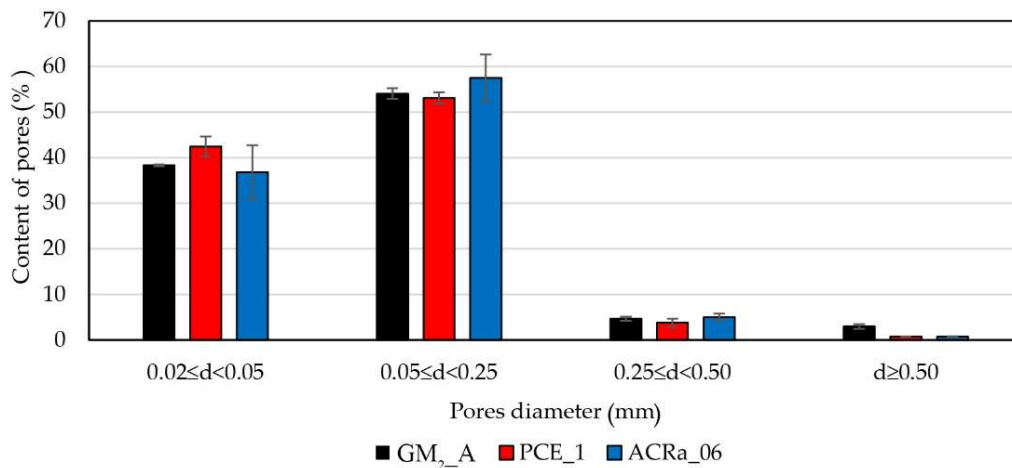
Figure 4.7: Pore distribution obtained via image analysis of two sections of hardened mortar (Investigated area = 145 mm^2) [133].

The results of MIP analysis are plotted in Figure 4.8. Unlike microscopy analysis, MIP allows to investigate open porosity between 0.004-70 μm. Similar pore size distribution curves of GM_2_A, PCE_1 and ACRa_06 (Figure 4.8a) were found, characterized by 40% of pores in the capillary range (0.1–1μm) in accordance with the typical pore size distribution of fly ash- based geopolymer [39]. The addition of PCE_1 and ACRa_06 favoured a pore refinement, slightly decreasing the average pore radius and increasing the pores content with dimension in the range 0.1-0.3 μm (Figure 4.8b). In particular, the detected average pore radius was 0.21, 0.12 and 0.16 μm for GM_2_A, PCE_1 and ACRa_06, respectively.

Capillary water absorption test was also carried out in order to investigate the pores interconnectivity. Results (Figure 4.9) showed that all the three mortars at the end of the test, reached similar values of water absorbed per unit area thus indicating a similar total open porosity. However, GM_2_A sample saturated after 225 min (≈ 4 hours), whereas ACRa_06 and PCEa_1 samples reached the saturation after 700 min (≈ 12 hours) and 900 min (15 hours), respectively. The different distribution in capillary pores as detected by MIP, played an important role in the saturation rate. The highest content of small capillary pores ($0.1 \leq r < 0.3$ μm) found for PCE_01 and ACRa_06 samples slowed down the saturation rate [139] and, consequently, increased the material durability [20,55,56].

a)

b)
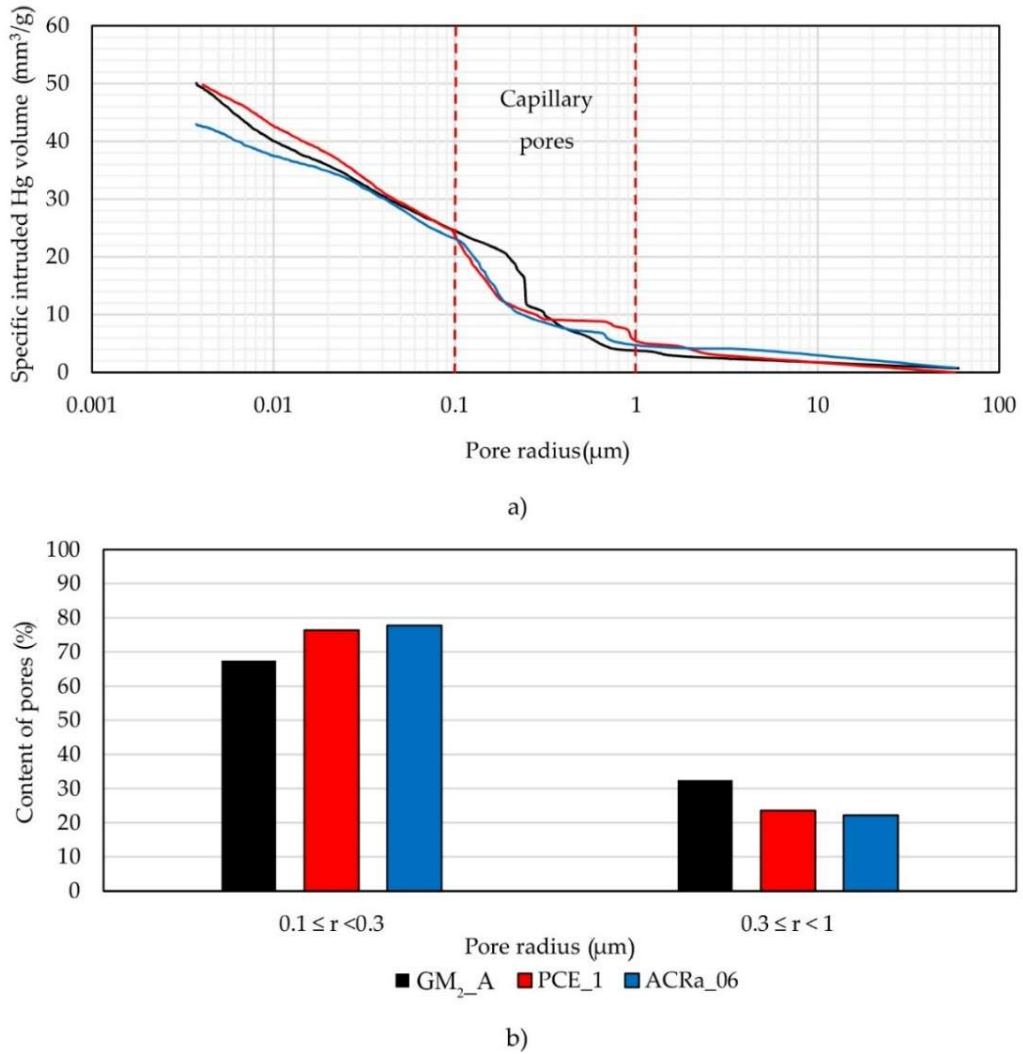
Figure 4.8: Pore size distributions curves of the investigated geopolymer mortar samples (a); Content % of pores arranged per ranges of pore radius (r) within the range of $0.1 \leq r < 1$ μm (b) [133].
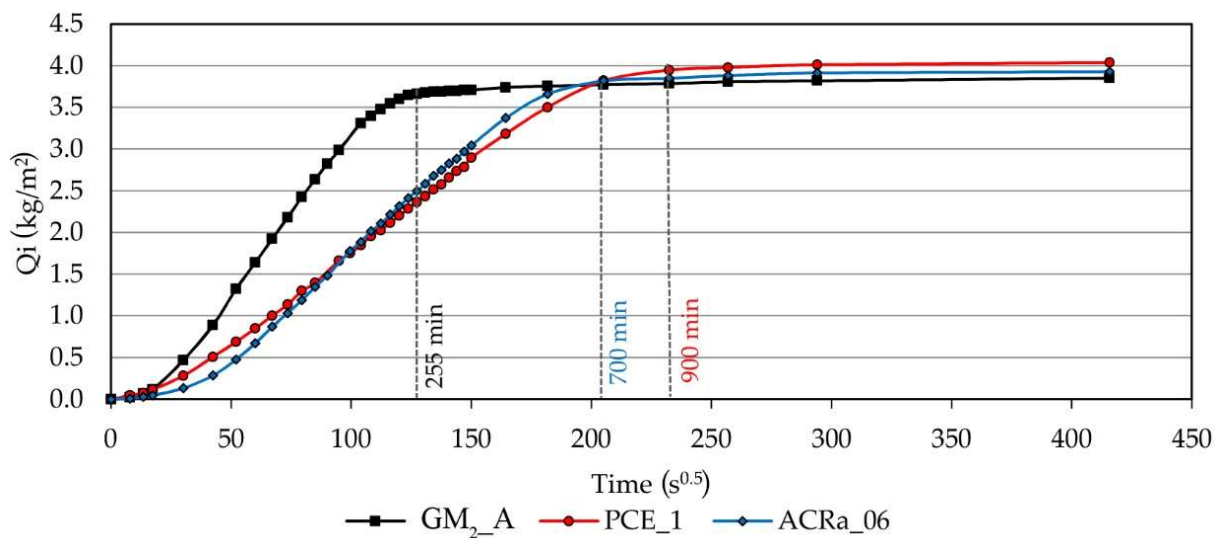
Figure 4.9: Capillary water absorption test results for GM_2_A, PCE_1 and $ACRa\_06$ samples. The time of saturation for each sample is indicated with a vertical line [133].

4.5   Main remarks

The results here discussed allow drawing the following conclusions:

-   among the seven different commercially available superplasticizers investigated in this study, polycarboxylic ether (PCE) and modified acrylic (ACRa) based ones showed the highest efficacy in improving the workability of fly ash-based geopolymer mixtures. Therefore, were considered worthy of further investigation.

-   PCE and ACRa superplasticizers were found stable in the alkaline medium and even when some degradation occurred (for PCE), the steric hindrance due to the side chains was still effective to break fly ash particles agglomeration, thus avoiding workability loss.

-   Both PCE and ACRa, belonging to the last generation of admixtures, provided a satisfying workability improvement in the geopolymer mixtures without increasing the air content at the fresh state and affecting the mechanical properties developed during the room temperature curing.

-   Modified acrylic and polycarboxylic ether based superplasticizers allowed to obtain geopolymer mortars with a more compact microstructure. This can be related to the increased workability that facilitated the entrapped air evacuation during the casting procedure and favoured the refinement of the average pore radius.

Chapter 5:

Investigation of geopolymer mortars
for external strengthening of existing structures

The contents of this chapter formed the basis of the following publications:

Carabba L., Santandrea M., Carloni C., Manzi S., Bignozzi M.C., *Steel fibre reinforced geopolymer matrix (S-FRGM) composites applied to reinforced concrete structures for strengthening applications: a preliminary study*, Composites part B: Engineering, 128, 83 - 90, 2017.

Carabba L., Santandrea M., Manzi S., Carloni C., Bignozzi M.C., *Geopolymer mortars for strengthening existing reinforced concrete structures*, Proceedings of The New Boundaries of Structural Concrete 2016, Capri, Italy, 29th September – 1st October 2016.

5.1   Background and research aims

In this chapter, fibre reinforced geopolymer matrix (FRGM) composites are investigated as a new tool in strengthening and rehabilitation of existing reinforced concrete and masonry structures.

Due to durability issues or damages caused by external events, strengthening or repair interventions of existing structures are often required in order to preserve their load-carrying capacity or to extend their original service life. In the last few decades, externally bonded composite materials have been widely and successfully used to strengthen structures. In particular, the so called fibre reinforced cementitious matrix (FRCM) composites were recently introduced as an alternative to traditional fibre reinforced polymer (FRP) composites [140–144]. FRCMs and FRPs are comprised of continuous high strength fibres embedded within a matrix. FRCM composites employ an inorganic matrix, rather than epoxy as in FRPs, which improves the high temperature and Ultra-Violet (UV) resistance and the vapour permeability with respect to the substrate [145]. Currently, the main applications of FRCM systems involve the restoration of historical buildings and particularly the reinforcement of masonry structures, the improvement of structures in seismic areas with increase of strength and ductility of masonry and reinforced concrete elements and the reinforcement of tunnels and structures which need high fire resistance [141]. When a mortar is considered as a repair material, it is highly recommended the selection of a material with similar features to those of the existing structure in terms of microstructural, physical, and mechanical properties [146]. However, this condition is not always achievable using epoxy or cementitious materials. The possibility of studying alternatives to for repairing and strengthening existing structure is therefore of strong interest.

There is ongoing research focused on geopolymers as a repair material, mainly investigating patch repair applications [147–151]. In particular, a previous study [152] showed an excellent bond behaviour and adequate compatibility with concrete substrates, independently of the roughness of the surface and the curing time. The same study also highlighted the cost efficiency of geopolymer, which resulted 6.9 times less expensive than the commercial repair product considered in the study. Other study reported that the bond capacity of properly designed geopolymers applied to cement mortar substrates is barely affected by the thermal exposure up to 300°C [153]. The use of geopolymer as strengthening system is instead less investigated. Geopolymers have been successfully used as matrix in composites to strengthen concrete elements [154,155]. However, there is a lack of detailed data on geopolymer matrices and, again, in most cases metakaolin was used as precursor [156–158], which reduces the environmental benefit of using geopolymer instead of cementitious matrix.

In this Chapter, an interdisciplinary approach to study newly developed fibre reinforced geopolymer matrix (FRGM) composites for strengthening applications of RC and masonry structures is presented. Three different geopolymer mortars (GM_A) were prepared and used as binding agent to embed and bond different types of fibre sheets to concrete prism surfaces or masonry blocks, thus realizing fibre reinforced geopolymer matrix (FRGM) composites. The molar concentration of the sodium hydroxide solution, used as alkaline activator, was varied (i.e. 4 M, 6 M, and 8 M NaOH solution was used) in order to evaluate the compatibility of the

alkaline environment of the matrix and the galvanized steel fibres used in the composite. Physical, mechanical, and microstructural properties of the geopolymer matrices are measured to characterize completely the material. Finally, FRGM strips are bonded to concrete and masonry prisms and single-lap direct shear tests are performed to study the stress transfer mechanism between the composite and the substrates.

5.2   Characterization of the matrix

Workability of the three fresh matrices was investigated immediately after the compounds were mixed. A slight improvement of workability of the mixtures was found as the molarity of the NaOH solution used decreases. Such a behaviour can be ascribed to an increase of the content of water related to the dilution of the NaOH solution when the molarity decreases. For the three matrices, the workability, which is expressed as consistency %, was determined to be between 55 and 65%, which was proved to be sufficient to cast FRGM composite strips. The effect of NaOH concentration on workability loss agrees with what reported by Singh et al. [159], who found a correlation between activator concentration and the time required for the formation of alkali aluminosilicate gels, i.e. the higher is the concentration, the faster is the workability loss.

At the age of 7 and 28 days, bulk density and water absorption were evaluated for the three hardened geopolymers. Regardless of NaOH molarity used, prisms cured for 7 days showed water absorption and bulk density values between 8.2 and 8.4% and 1.84 - 1.87 g/cm3, respectively. At 28 days, the bulk density and water absorption increased and decreased, respectively, with increasing NaOH molarity (Table 5.1). The GM_A showed the highest value of bulk density and the lowest water absorption among the three matrices.

Table 5.1: Physical and mechanical properties of geopolymer mortars after 7 and 28 days of curing at room temperature [160].

Curing time	MIX	ρ_{bulk} (g/cm^3)	Water absorption (%)
7 days	GM_A	1.87	8.4
	GM$_6$_A	1.87	8.2
	GM$_4$_A	1.84	8.3
28 days	GM_A	1.95	7.2
	GM$_6$_A	1.89	7.5
	GM$_4$_A	1.87	7.9

Porosity of the three geopolymer matrices was investigated through capillary water absorption test and MIP analysis (Figure 5.1). The influence of curing time on the development of the pore structure of the material is evident from capillary water absorption results. For the three matrices, cylinders cured for 7 days saturated after 10 minutes, whereas after 28 days, cylinders reached the saturation after approximately185 minutes. The rate of saturation is similar among the three different matrices, both at 7 and 28 days. However, for cylinders that were cured for 28 days, the amount of water absorbed per unit area decreased when the molar concentration of NaOH increased, which confirms that the GM matrix has a more compact and less porous structure than the GM_A$_{6M}$ and GM_A$_{4M}$ matrices. These results are in agreement with the results of bulk density and water absorption reported in Table 5.1.

Those results were also confirmed by the MIP analysis performed on geopolymers at 28 days. The pore size distributions of samples are reported as a function of the specific volume of mercury intruded in the sample. For the three matrices, 40% of the total porosity corresponded to pores with a diameter in the range $0.1 - 1$ μm, which are classified as capillary pores [39]. Among the three geopolymers, GM_A exhibited the least porous microstructure. Similar pore size distributions were observed for GM_A$_{6M}$ and GM_A$_{4M}$. The total open porosity (Pt (%)) and the average pore radius (r_m (μm)) decreased for the three geopolymers as follows: GM_A$_{4M}$ (20.9%, 0.36 μm) > GM_A$_{6M}$ (17.9%, 0.28 μm) > GM_A (17.2%, 0.21 μm).
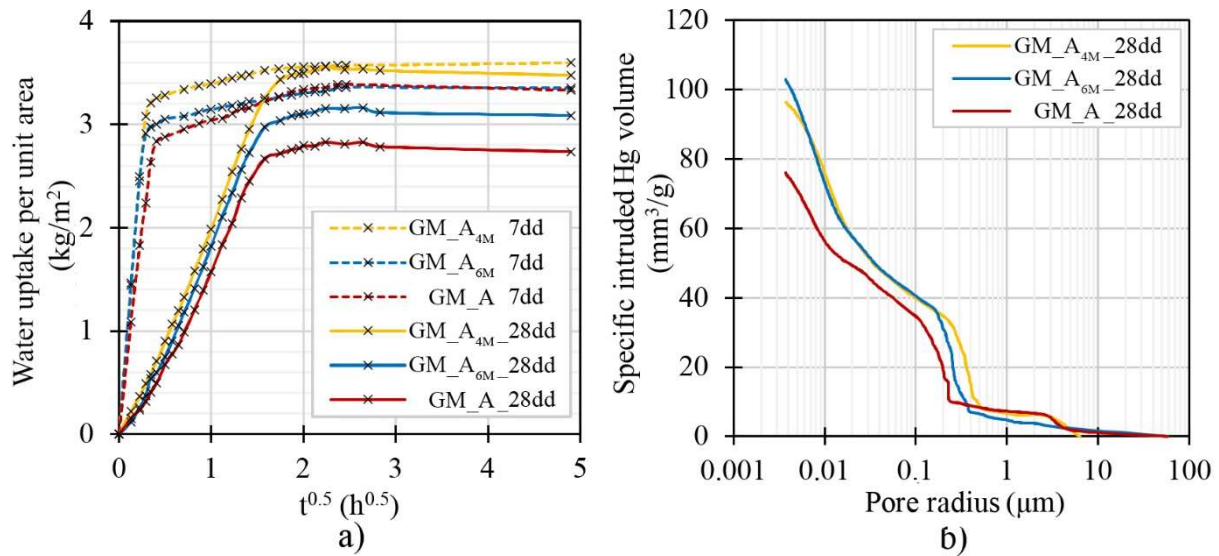
Figure 5.1: Capillary water absorption test results at 7 and 28 days (a); Pore size distributions of geopolymer matrices at 28 days (b) [113].

The influence of both curing time and NaOH molar concentration on the mechanical properties of geopolymer can be observed in Figure 5.2. An increase of the strength was observed as a function of the curing time for all specimens tested. Figure 5.2 reports only the mechanical data at 7 and 28 days as these ages are the ones usually considered for mechanical characterization of cement based materials. At the age of 28 days, GM_A achieved the highest values of both flexural (5.6 MPa) and compressive (33.6 MPa) strength among the three matrices; compressive strength decreased linearly with decreasing NaOH molar concentration. The same trend was obtained when the dynamic modulus of elasticity (E_d) was evaluated, which confirms a more compact and stiff structure of GM_A compared to the GM_A$_{6M}$ and GM_A$_{4M}$. These results were somehow expected since previous studies on fly ash-based geopolymers already assessed the importance of the NaOH concentration on the strength development [34,159]. The NaOH activates the leaching of Si and Al of the fly ash; the higher is the NaOH concentration, the higher results the amount of leaching and the subsequent geopolymerization degree and mechanical properties of the geopolymer [34].

It is important to highlight that even if the physical and mechanical properties indicate that GM_A is the best matrix among the three formulations investigated, the mechanical properties of both the GM_A$_{6M}$ and

GM_A$_{4M}$ matrices are comparable to the properties of commercially available hydraulic binders used for strengthening applications of RC [161].

Shrinkage behaviour of the three geopolymer matrices is reported in Figure 5.3. GM_A$_{6M}$ and GM_A$_{4M}$ exhibit higher shrinkage than GM_A, however the values are in good agreement with data recently reported in the literature for geopolymers [151]. Moreover, when the FGRM strip was applied to concrete, no visual evidence of microcracks/crevices was observed on the hardened matrix, which indicates that shrinkage does not promote superficial damage.
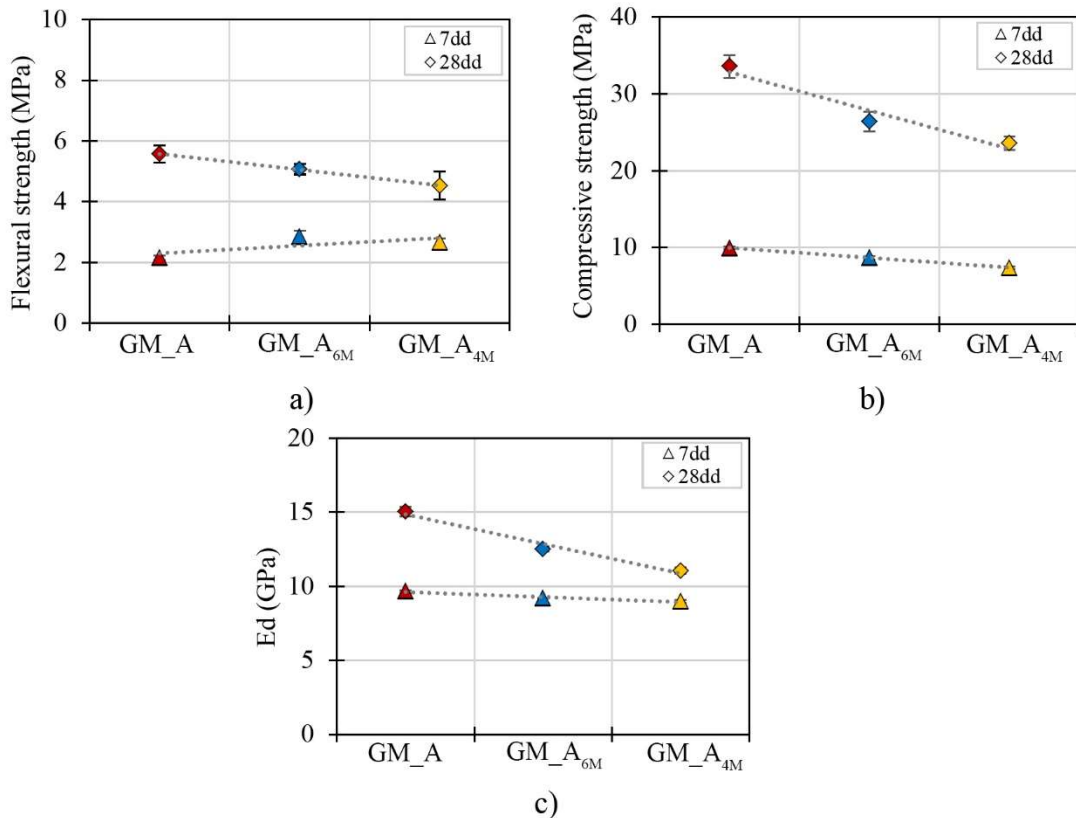
Figure 5.2: Flexural (a) and compressive (b) strength, and dynamic modulus of elasticity (c) of geopolymer matrices at 7 and 28 days (values are reported as average of five measurements for compressive strength and three measurements for flexural strength and E$_d$) [113].
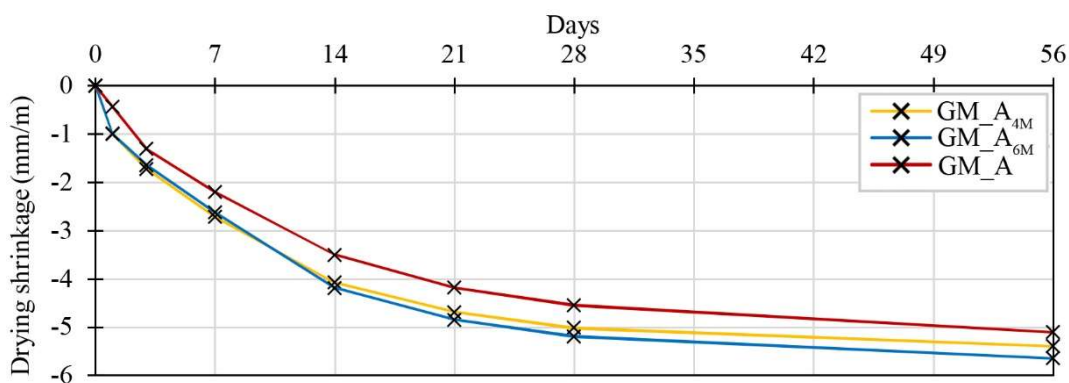
Figure 5.3: Drying shrinkage of geopolymer matrices (values are reported as average of three measurements) [113].

5.3 Bond behaviour of fibre reinforced geopolymer matrix composite-substrate joints

In this section, the results of single-lap direct shear tests are presented to analyse the behaviour of steel FRGM composites bonded to concrete and masonry blocks. Three specimens were used to conduct preliminary direct shear tests to define which geopolymer matrix showed the best bond behaviour. Thus, one direct shear test was performed for each type of geopolymer matrix (the corresponding direct shear specimens were named DS-GM_A_{4M}, DS-GM_A_{6M}, and DS-GM_A). For the preliminary tests, concrete was considered as substrate. The applied load-global slip responses of those three tests are reported in Figure 5.4. For all specimens, failure was associated with the debonding of the external layer of matrix and fibres from the internal layer of matrix (interlaminar failure) that remained bonded to the concrete substrate. For all three specimens, the applied load-global slip response showed an initial linear portion followed by a non-linear branch before the peak load P* was reached. During the linear and non-linear phases, drops in the load, mainly due to micro-damage at the matrix-fibre interface, were observed. Once the peak load was reached, an interfacial longitudinal crack initiated and propagated in the matrix and the load response showed a nominally constant trend up to failure. The peak load, P*, for specimens DS-GM_A_{4M}, DS-GM_A_{6M}, and DS-GM_A is equal to 9.48 kN, 6.97 kN and 7.77 kN, respectively. Specimen DS-GM_A_{4M} showed also a higher value of the global slip g at the peak load (3.21 mm) if compared with DS-GM_A_{6M} (1.99 mm) and DS-GM_A (2.37 mm). Specimens DS-GM_A_{4M} and DS-GM_A exhibited similar values of slip at failure (4.07 mm and 4.30 mm, respectively), which are higher than the one of specimen DS-GM_A_{6M} (2.83 mm).
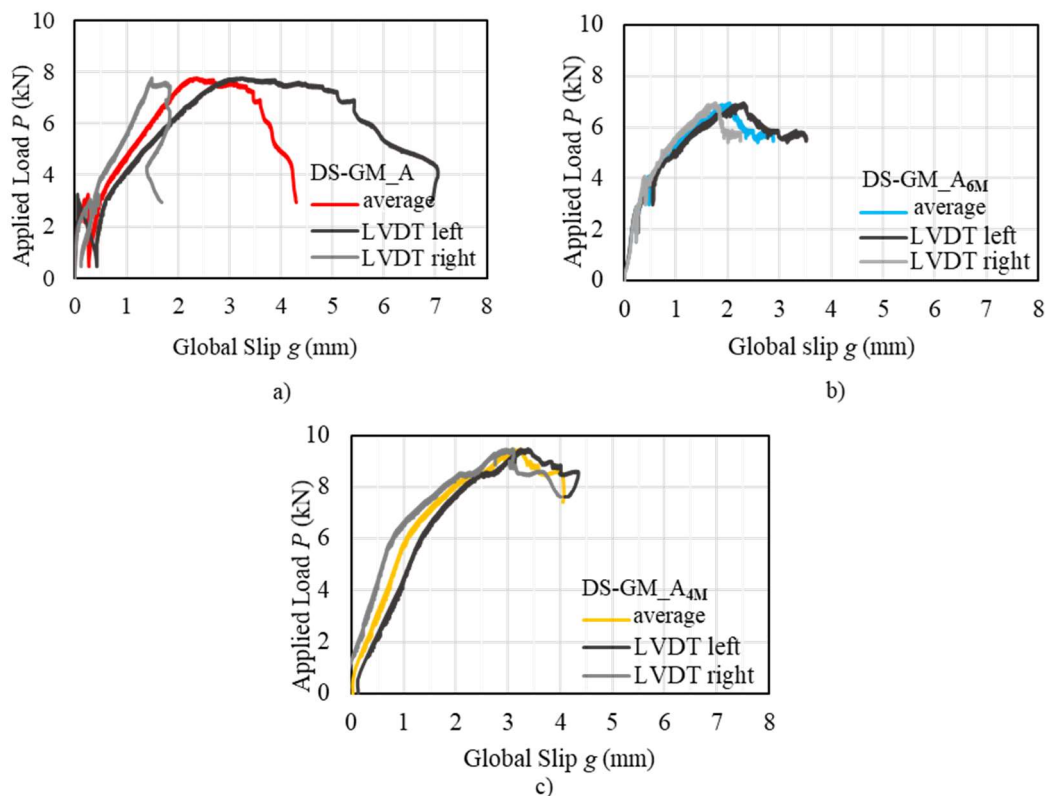
Figure 5.4: Applied load *P* versus global slip *g* plot of DS-GM_A (a), DS-GM_A_{6M} (b), DS-GM_A_{4M} (c). The responses of right and left LVDTs and the average of the two LVDTs measurements are reported [160].

Analysing more in detail the curves, it can be seen that DS-GM_A (Figure 5.4 a) exhibited a remarkable difference between the two LVDT readings, which in turns implied a rigid rotation of the Ω-shaped bent plate. This aspect indicates that a non-uniform load distribution among the longitudinal fibres occurred during testing. This can be ascribed to a loss of bond strength between fibres and matrix due to the local porosities caused by the reaction between the matrix and the zinc coating of the fibres. As a result, the value of peak load and global slip cannot be considered indicative of the real behaviour of the DS-GM_A composite. From the experimental results of the preliminary direct shear tests, it appears that specimen DS-GM_A_{4M} exhibited the best bond behaviour among the three specimens, thus suggesting that a decrease in the molar concentration of NaOH solution promotes an improved interfacial interaction between matrix and fibres.

SEM micrographs of FRGM composites, after direct shear tests (Figure 5.5 and 5.6) were performed help explain why the different matrices behaved differently. According to the results reported above, GM_A is the least porous formulations investigated, which has also the best mechanical and physical properties. Moreover, GM_A_{4M} exhibits a large portion of unreacted fly ash particles (Figure 5.5 a); whereas in GM_A, geopolymer gel is prevalent (Figure 5.5 b) with only few unreacted fly ash particles. The presence of unreacted or partially reacted fly ash particles is common in fly ash-based geopolymers, especially when they are cured at room temperature, and their presence strongly influence the performances of the final product [162,163].
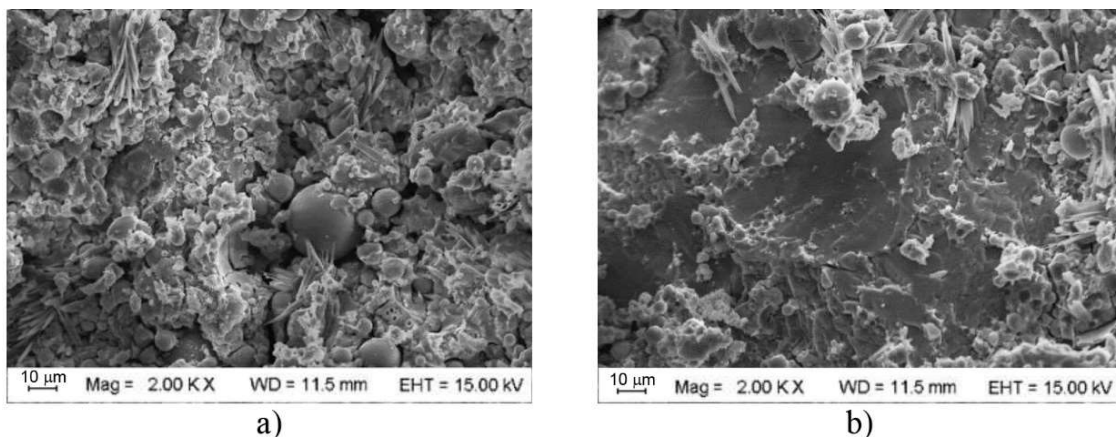
Figure 5.5: SEM micrographs of matrix microstructure: GM_A_{4M} (a) and GM_A (b) [113].

In the case of the GM_A matrix many large pores are localized in the matrix at the interface with the fibres (Figure 5.6 b); whereas, only few pores are visible in the GM_A_{4M} matrix (Figure 5.6 a). The pores localized at the fibre/matrix interface suggest that a chemical reaction between the galvanization layer and the matrix occurred when the composites strips were cast. According to its amphoteric behaviour, Zn dissolution also occurs for pH greater than 12 [164]. Thus, a decrease of the molarity of NaOH solution in the geopolymer mix design implies a degradation of the physical and mechanical properties of the matrix and an improvement of the adhesion between fibres and matrix. The improved interfacial interaction between the fibres and the GM_A_{4M} matrix is also confirmed by the geopolymer fragments that were still attached to the fibres (Figure 5.6 c, Figure 5.7) after the shear test. Fragments are not present at all on the fibres from specimens cast with the GM_A matrix (Figure 5.6 d).
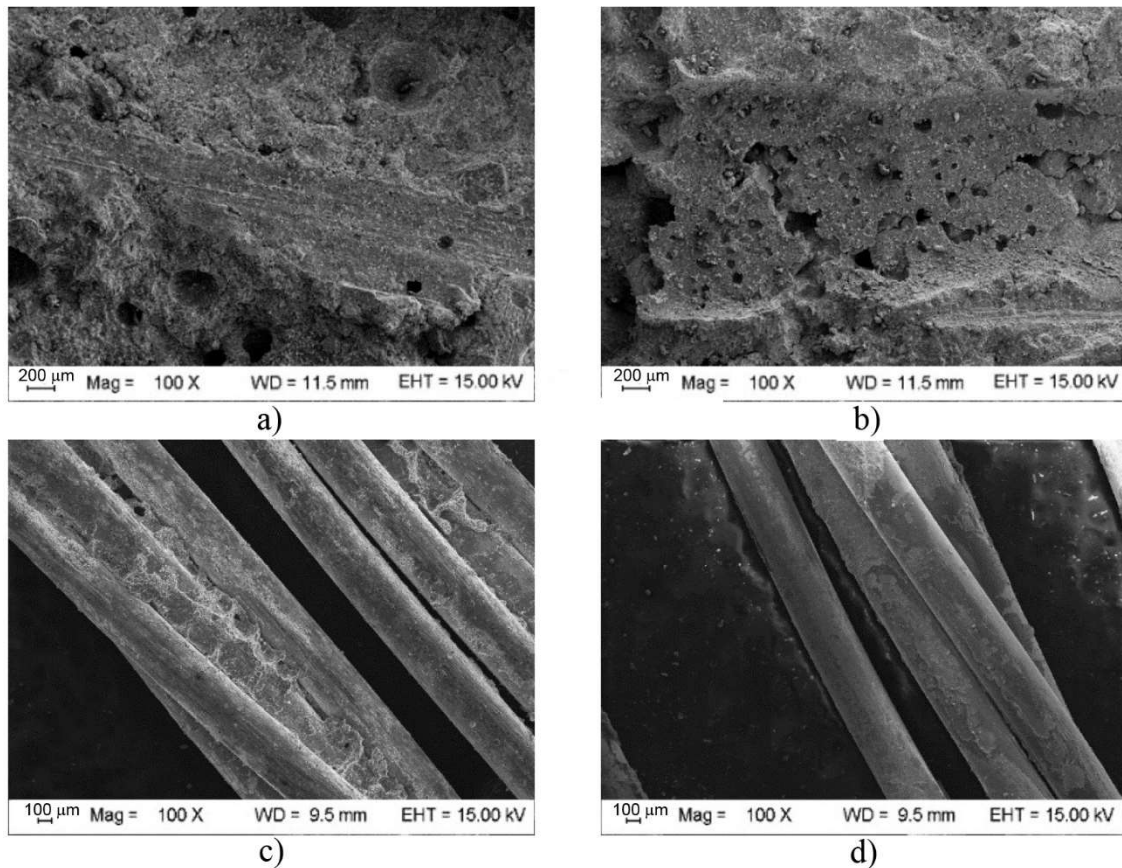
Figure 5.6: SEM micrographs of FRGM composites constructed with GM_A$_{4M}$ (a, c) and GM_A (b, d) after single lap direct shear test. (a, c) = matrix at the interface with galvanized steel fibres after debonding; (b, d) = fibres after debonding [113].
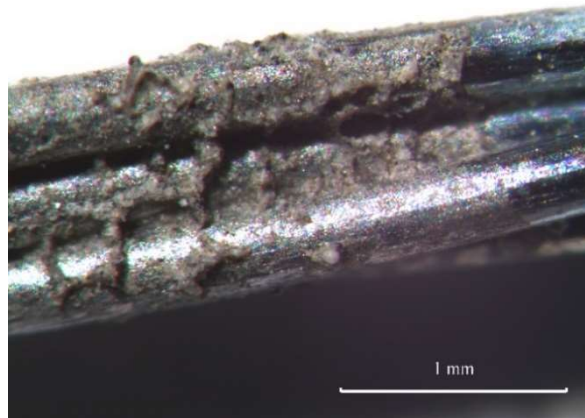
Figure 5.7: Optical images (50X) of fibres embedded in GM_A$_{4M}$ after debonding.

Based on the results of the three preliminary tests, additional tests were performed. The GM_A$_{4M}$ matrix was used to manufacture the strips of five FRGM-concrete joints and of five FRGM-masonry joints, to further investigate its bond behaviour. The FRGM composites bonded to concrete substrate were named **FRGM-C**, whereas the label **FRGM-M** was used to indicate FRGM composites bonded to masonry substrate. Five specimens were tested (DS-**FRGM-C**-1, DS-**FRGM-C**-2, DS-**FRGM-C**-3, DS- **FRGM-C**-4, and DS-**FRGM-C**-5) and their load-global slip responses are reported in Figure 5.8a. The applied load-global slip responses were similar to the responses of the preliminary tests. After the peak was reached, the applied load-

global slip response showed a drop of the load, due to the onset of the interfacial longitudinal crack inside the matrix, followed by an approximately constant branch. For all specimens, interlaminar failure (at the matrix-fibre interface - Figure 5.8b) was observed. After the longitudinal crack started to propagate along the bonded area, high values of the global slip were reached. The average value of the peak load, P*, for the five tests was equal to 8.65 kN (CoV = 0.081). Therefore, the maximum stress in the fibres was equal to 2010 MPa, i.e. the 67% of the tensile strength provided by the manufacturer.
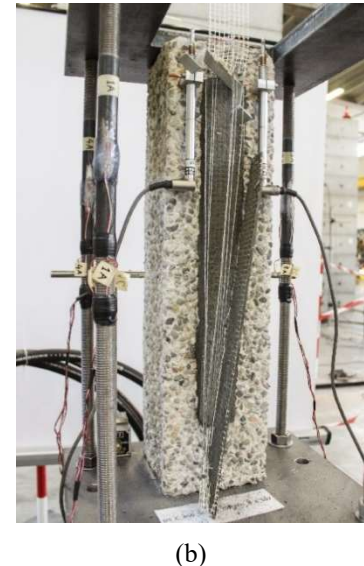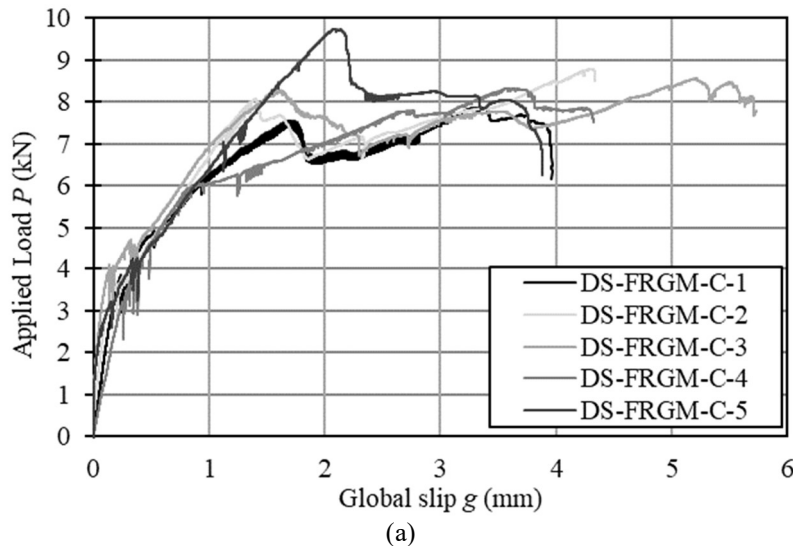
Figure 5.8: Applied load-global slip response of FRGM-C composites: DS-**FRGM-C**-1, DS-**FRGM-C**-2, DS-**FRGM-C**-3, DS-**FRGM-C**-4, and DS-**FRGM-C**-5. For each test, only the average results are plotted (a); failure mode (b) [113].

Figure 5.9a shows the load-global slip responses of five specimens named DS-**FRGM-M**-1, DS-**FRGM-M**-2, DS-**FRGM-M**-3, DS-**FRGM-M**-4, and DS-**FRGM-M**-5. The applied load-global slip responses were consistent with the responses of the FRGM-C composites. The average value of the peak load, P*, for the five tests was equal to 8.76 kN. Therefore, the maximum stress in the fibres was equal to 2035 MPa, i.e. the 68% of the tensile strength provided by the manufacturer. Also in this case, interlaminar failure (at the matrix-fibre interface - Figure 5.9b) was observed. These results are in good agreement with the results recently obtained within a round robin test on FRCM-masonry that included also geopolymer matrices [165].

Figure 5.10 reports the failure mode after performing the pull-off test. In particular, the behaviour of the FRGM-M composite obtained by using the GM_A_{4M} mortar to bond steel fibres to masonry blocks was investigate. As happened during the single lap direct shear test, specimens failed within the composite at the fibre-matrix interface that can be considered as the wick point of the composite. At the same time, GM_A_{4M} mortar exhibited a good adhesion to the masonry substrate. The tensile bond strength resulted to be equal to 0.66 ± 0.07 MPa.

(a)

(b)
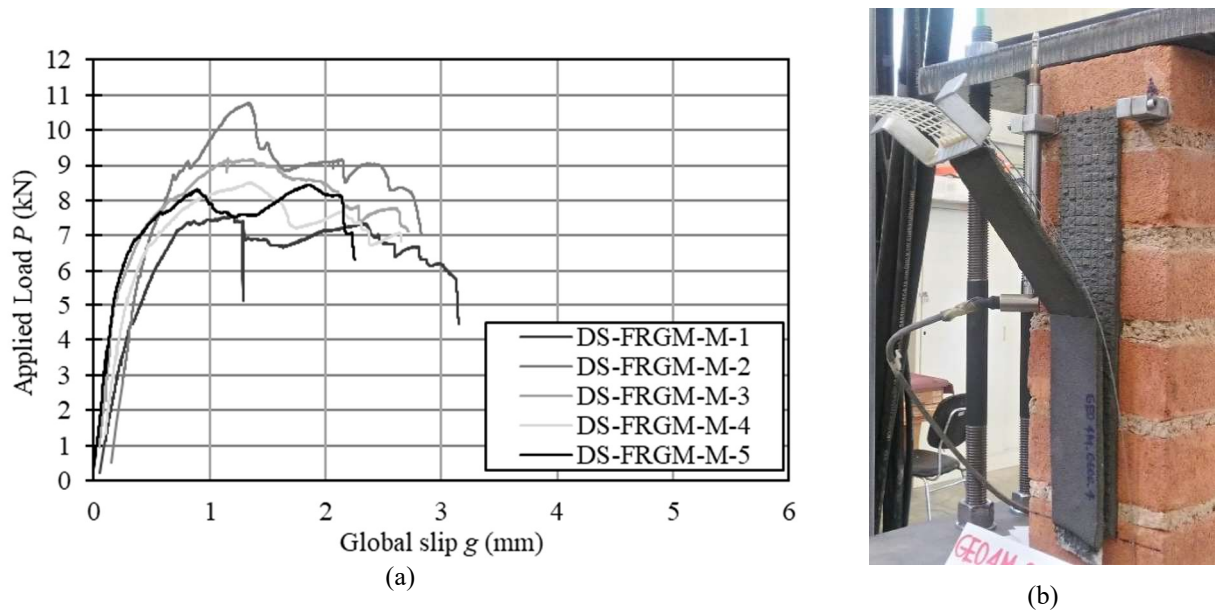
Figure 5.9: Applied load-global slip response of FRGM-M composites: DS-**FRGM-M**-1, DS-**FRGM-M**-2, DS-**FRGM-M**-3, DS-**FRGM-M**-4, and DS-**FRGM-M**-5. For each test, only the average results are plotted (a); failure mode (b).
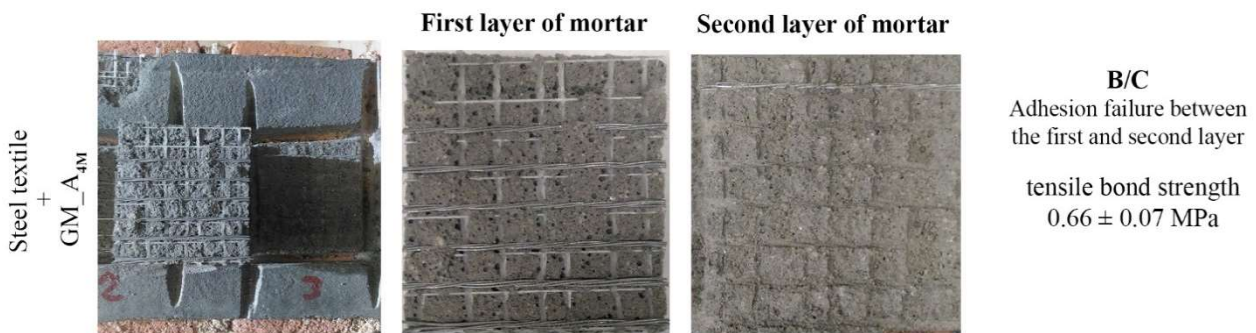
Figure 5.10: Pull-off test failure mode.

5.4   Main remarks

The results here discussed allow drawing the following conclusions:

-   all the geopolymer mixtures showed satisfactory workability at the fresh state and were suitable as matrices for casting FRGM composites. The decrease in molar concentration of NaOH solution (from 8 to 4 M) implied a degradation of the physical and mechanical properties of the matrix. This behaviour is ascribed to the different degree of geopolymerization obtained; however, the physical and mechanical properties of the GM_A$_{4M}$ and GM_A$_{6M}$ matrices were considered satisfactory for their use as matrix in FRGM systems.

- When galvanized steel fibres are used in FRGM composites it is important to limit the reaction between the alkaline environment of the matrix and the zinc coating of the fibres. Therefore, the mix design of the geopolymer matrix has to be tailored in order to avoid a detrimental interaction between the matrix and the fibres. A decrease of the molar concentration of sodium hydroxide activator produced an improvement of the adhesion between the materials, which in turn enhanced the composite performance.

- An adequate compatibility and adhesion of the composite with both concrete and masonry substrates were found. Indeed, for all direct shear test specimens, the failure mode was debonding (interlaminar failure) of the external layer of matrix from the internal layer rather than debonding at the matrix-concrete interface. The same failure mode was observed when pull-off test was performed. In the case of the best performing composite (DS_ GM_A$_{4M}$ series), the average value of the maximum stress in the fibres in direct shear tests resulted equal to 67% of the tensile strength provided by the manufacturer.

Chapter 6:

Investigation of the thermal behaviour of geopolymers and geopolymer composites

This part of the research was implemented in collaboration with:

The contents of this chapter formed the basis of the following publications:

6.1 Background and research aims

One of the most interesting features of geopolymers is the remarkable thermal stability due to the intrinsic thermal resistance of their inorganic structure [63,166,167]. A detailed review on the thermal properties and high temperature performance of geopolymers has been already reported in Chapter 2. However, it is worth to remind that when fly ash are used as precursor, the obtained geopolymers are more complex material than metakaolin-based ones, since coal fly ash originates from waste streams and for this reason its microstructure is much more complex, comprising a mixture of amorphous and crystalline components [38,168]. In addition, fly ash generally contains a significant proportion of impurities such as iron oxides, which have direct influence on the thermal expansion, the phase composition, and the morphology of the material after heating [67]. For this reason, even if thermal expansion in geopolymer is generally isotropic due to their amorphous gel structure, non-uniform expansion can occur because of the local variations in composition [6].

In this Chapter, the behaviour of the fly ash-based geopolymers activated at room temperature and exposed to high temperature is investigated. In the first part, the cracking mechanism of geopolymer matrices (G_A and G_A_K) exposed to high temperature is investigated in detail through acoustic emission measurement during the thermal treatment, and further investigated by SEM and XRD analysis. In the second part, the mix design of the geopolymer was implemented by adding refractory recycled particles, thus obtaining composites (GCs) with enhanced thermal dimensional stability.

6.2 Investigation of cracking mechanism of geopolymers exposed to high temperature

In this section, the thermal behaviour of G_A was investigated with special focus on the study of cracking mechanism owed to high temperature exposure. To do that, thermal treatments at different set-temperatures of 500, 550, 600, 650, and 800 °C where performed in a muffle furnace (see paragraph 3.3.5). All the results discussed in this paragraph refer to specimens after 28 days of curing.

Figure 6.1 reports images of the samples before (a) and after (b) the thermal treatment at the different temperatures. It can be noted the change in colour from dark grey to reddish colour and more intense red as the heating temperature increases. This phenomenon is common in fly ash-based alkali activated materials and it is usually related to the oxidation of the iron species contained in the fly ash [67,169].

(a)   (b)
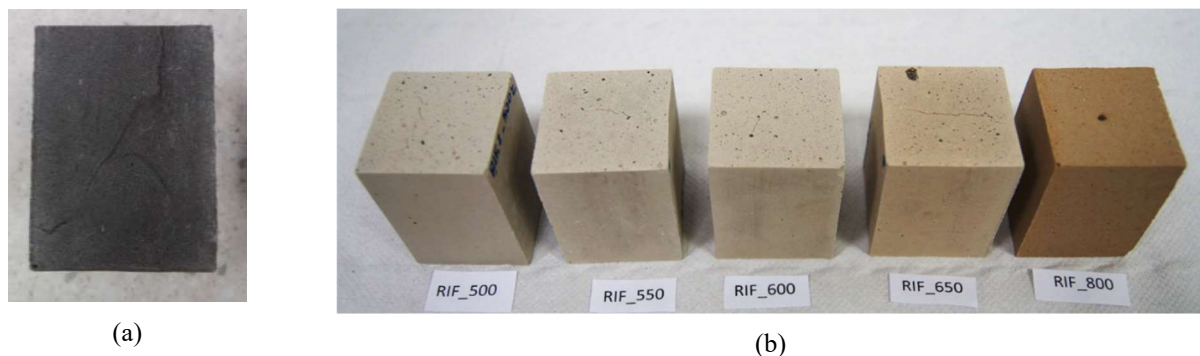
Figure 6.1: Pictures of the G_A specimen as cured (a) and after thermal treatment at 500, 550, 600, 650, and 800°C (b) – specimens dimensions 40 × 40 × 50 mm.

Acoustic emission (AE) measurements during heating and subsequent cooling in a muffle furnace were performed as reported in paragraph 3.3.5 to obtain insight into the cracking phenomena induced by the thermal exposure. Cracking and crack growth in brittle materials is accompanied by the emission of elastic waves. Therefore, the detection and the analysis of these transient signals ('hits') gives insight into the processes taking place at different times during the experiments. In Figure 6.2 are reported the temperature-time curves correlated to the acoustic emission results of G_A specimens for the different temperatures of exposure.
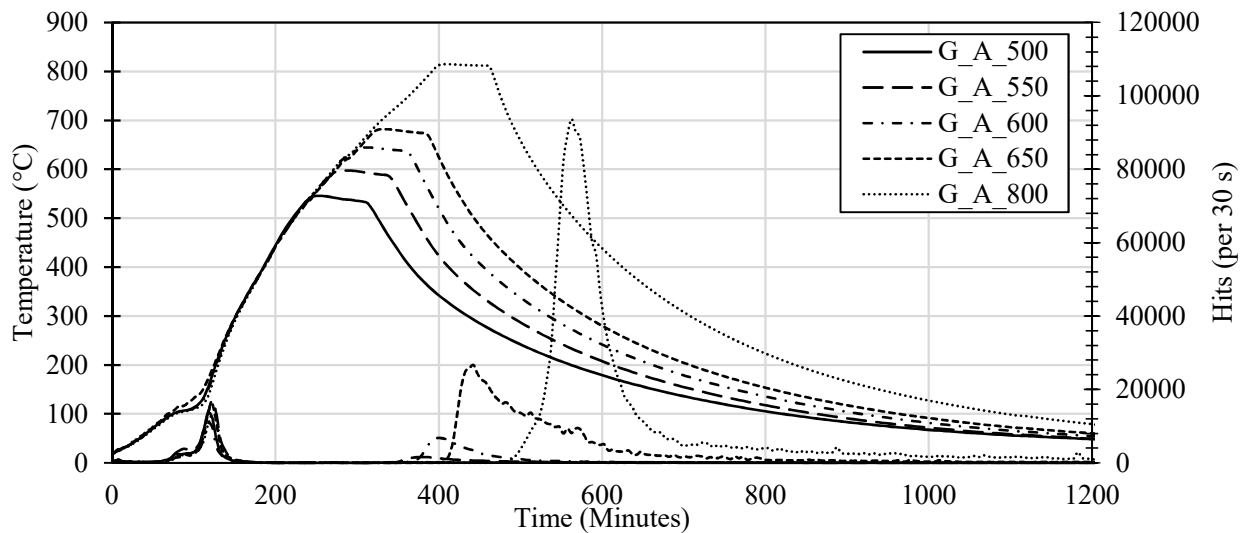
Figure 6.2: Temperature-time curves correlated with hits-time curve of G_A specimens heated up to 500, 550, 600, 650, and 800 °C.

In all cases, cracking during heating was observed after reaching the temperature of 90°C and up to around 360°C. Two different types of acoustic emissions were recorded that can be both related to the dehydration processes (Figure 6.3). Generally, in geopolymers water is mainly in the form of free water at the surface and in large pores and adsorbed and bound water is present in small pores and in the form of Si-OH groups [22,65]. As explained by Rahier et al. [65], the free water evaporates without large influence on the dimensional stability of the material, whereas dehydration of weakly bound and bound water causes the material to shrink by desorption of water out of the small pores and structural changes on a molecular scale. The temperature ranges for which the dehydration is verified vary according to the types of water: generally, free water will evaporate readily and mostly below 100 °C, desorption of the weakly bound water occurs below 250°C and dehydroxilation occurs for temperature higher than 250 °C [65]. The first AEs were identified in correspondence to a plateau of the temperature related to the endothermic dehydration of free or weakly bound water contained in the specimens (Figure 6.3a). When all the free and weakly bound water evaporated (temperature range 90-130 °C), the temperature in the specimens restarted to increase. In the temperature range between 130 and 360 °C higher acoustic emission activity was recorded. This activity was associated to the dehydration of the bound water and to the dehydroxilation, which for systems similar to the investigated one, occurs in the temperature range of 250 - 600° C [67]. Therefore, the higher activity recorded in this temperature range can be likely related to a more severe cracking caused by a stronger capillary pressure during

dehydration. These assumptions were also confirmed by TG analysis presented in Figure 6.3b. The figure shows the weight loss of G_A in nitrogen atmosphere. The weight loss was approximately 9 wt% and the majority of weight (6 wt%) was readily lost in the temperature range of 90 - 130°C. These results also confirm that in geopolymers the physically and chemically bound water is present in small percentage as stated in the literature [64,65,70].

Dehydration of free and weakly bound water

Dehydration of the bound water and dehydroxilation
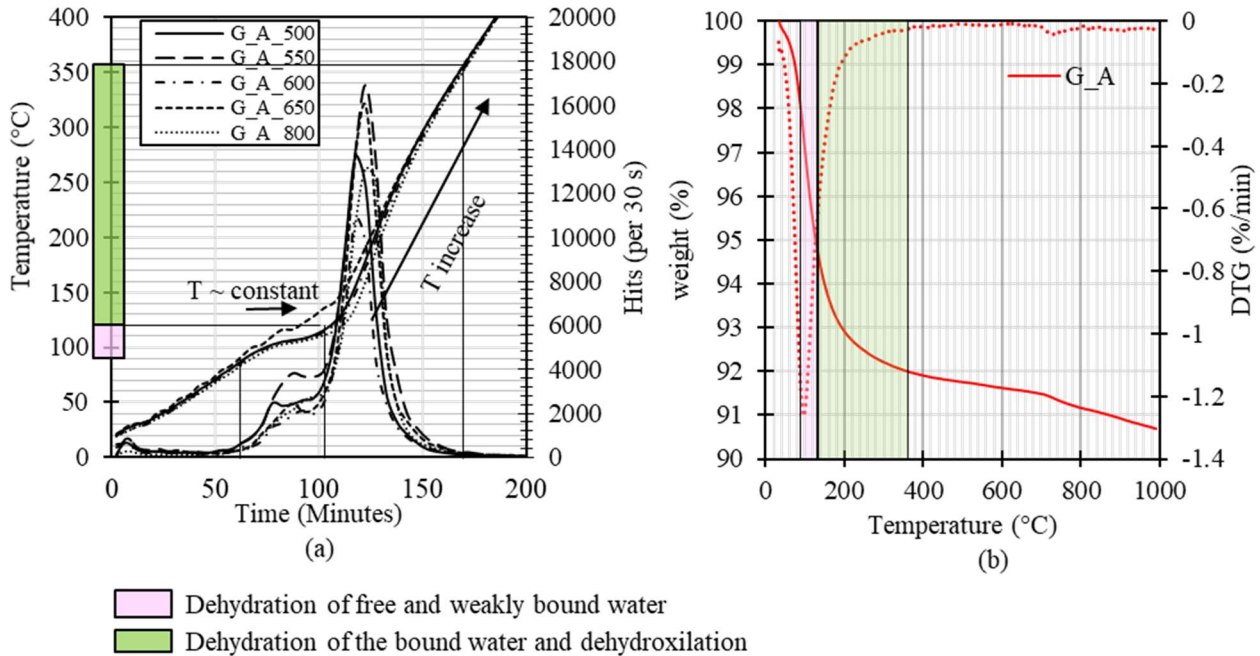
Figure 6.3: Correlation between acoustic emissions measured on heating and temperature (a); TGA and DTG curves for G_A sample (heating rate 10°C/min in nitrogen atmosphere) (b).

Specimens heated up to 500°C showed no further AE emissions during the test (i.e. both heating and cooling periods). As soon as the set-temperature increased to 550°C, a light AE activity appeared on cooling period. The AE activity recorded on cooling increased for increasing set-temperature of the test. This suggests that above 550 °C some modifications in the microstructure occurred which induced some tensions into the material during cooling and therefore the formation of cracks.

To investigate in depth the microstructure of the G_A and to identify the cause of the observed AE on cooling, SEM and XRD analysis were performed on samples before and after the thermal treatments. Mineralogical analysis of the G_A as cured and after heating up to 500, 550, 600, 650, and 800°C are reported in Figure 6.4. XRD patterns of the as cured G_A (bold line) showed a prevalent amorphous nature and small amounts of mullite, quartz, and magnetite as crystalline phases coming from the FA precursor. Heating up to 650°C did not induce modification in the mineralogical composition of the material. A new crystalline phase appeared only after heating up to 800°C. In particular, crystalline nepheline was found in the G_A_800 sample. From these results, appeared that AE emissions detected above 550°C can not be related to the formation of new crystalline phases as no modification of the mineralogical nature of the material was observed between samples heated up to 500 and 550 °C. However, the crystallization of nepheline that occurred at 800 °C may

be responsible for increased stresses during the cooling period, since the AE activity of G_A_800 sample on cooling was significantly higher than other samples.
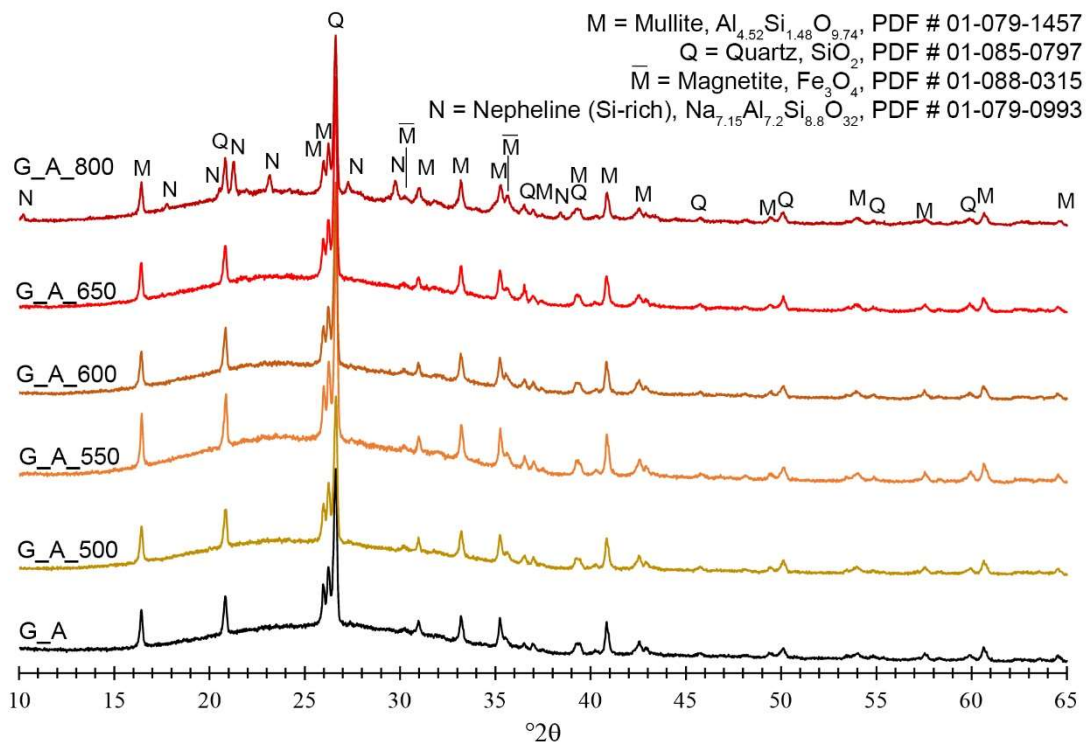
Figure 6.4: XRD patterns of the as cured G_A sample and of G_A sample after the thermal treatments.

More information were found by SEM analysis. In Figure 6.5 are reported SEM micrographs obtained in backscattered electrons of polished sections of representative regions of G_A specimens before and after heating up to 500, 600 and 800°C. The as cured sample showed the typical morphological nature of a fly ash-based geopolymer cured a room temperature where in addition to the geopolymer gel, several unreacted fly ash particles are found [42]. The second row of the Figure 6.5 shows the sample heated up to 500°C. As can be observed, no significant changes were found either in the porosity or in the morphology of the solid part. The last two rows of the Figure 6.5 show the sample heated up to 600 and 800°C. For increasing temperature, a more significant change in the microstructure of the material was found. The sample heated at 600 °C showed an increased cracking and in the majority of the cases, it can be observed a detachment of the geopolymer gel from the unreacted fly ash particles. After the exposure to 800°C, SEM micrographs showed evidence of sintering of the microstructure and a reduction in the amount of unreacted fly ashes which appeared embedded in the sintered phases. In addition, a modification of the pore structure that appeared more irregular and interconnected was found. These results are in good agreement with a previous study where a sintering leading to localized melting was observed starting from the temperature range of 600 – 700 °C, depending on the composition of the geopolymer [66]. The same authors suggest that localized melting not consistent across the sample can induce considerable strain leading to increased macro-cracking [66].
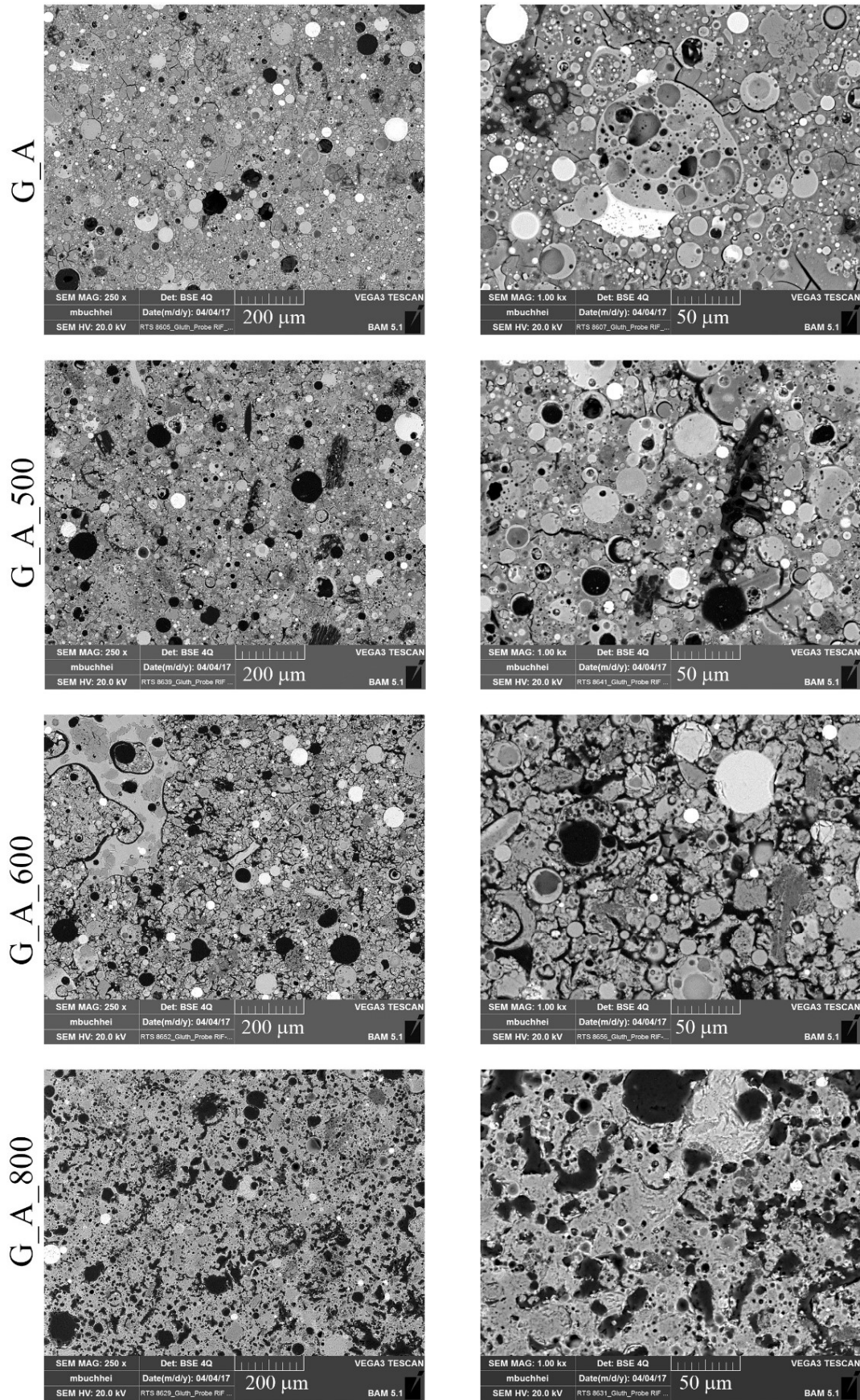
Figure 6.5: SEM micrographs of G_A geopolymer as cured and exposed to elevated temperatures.

The SEM investigation in combination with the XRD and AE measurements suggested that up to 500°C the G_A was thermal stable, besides for some minor cracks occurred during the dehydration process. Above 550°C a partial sintering in localized areas started to occur which involved increasing portions of the material for increasing temperatures. The possibility of a partial sintering occurred above 550 °C is supported by the work of several authors who detected the softening temperature of fly ash-based geopolymers in the temperature range 610 °C (±20 °C) for the Na based geopolymer [60,72,170]. The phases that experienced sintering during heating experienced also a rapid quenching immediately as the temperature in the furnace started to decrease. In the meantime, other regions (e.g. crystalline impurities from the fly ash) remained stable. It is possible that this phenomenon caused stress between stable and sintered phases and therefore may be at the origin of the cracking recorded by AE during the cooling period.

Substitution of Na with K

Previous study proved that the alkali cation used for the geopolymer production has influence on the thermal deformations of the geopolymer during heating. In particular, the use of potassium instead of sodium leads to a reduction of the thermal shrinkage [171]. In addition, the alkali cation has also influence on the softening temperature of aluminosilicate glasses that is lower when Na^+ is used [72].

For these reasons, in order to increase the thermal performance G_A geopolymer, the 8 M NaOH solution was substituted by 8 M KOH solution during the sample preparation, thus obtaining a geopolymer with mixed cation type (Na/K). AE measurements and XRD analysis were repeated on the G_A_K specimens after 28 days of room temperature curing in sealed conditions. In Figure 6.6 are reported the temperature-time curves correlated to the acoustic emission results of G_A_K specimens for the different temperature of exposure. A comparable behaviour to the one previously described for G_A specimens was observed. Focusing on the AE found during the cooling period, again the critical temperature was found to be above 550°C. In fact, after heating the specimens up to 550 °C a light AE activity appeared on cooling period that increased for increasing set-temperature of the test.
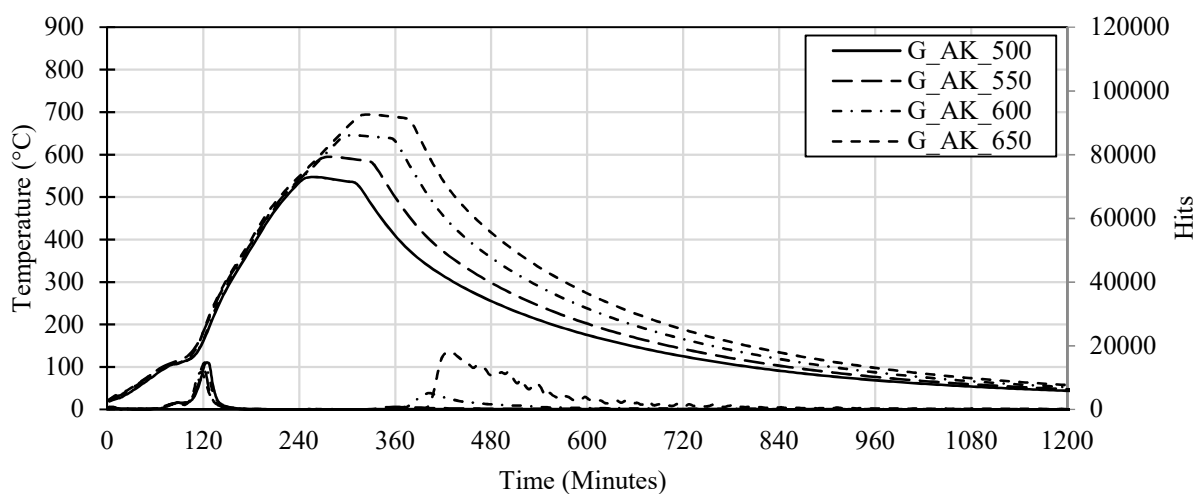
Figure 6.6: Temperature-time curves correlated with hits-time curve of G_A_K specimens heated up to 500, 550, 600, and 650 °C.

The XRD patterns of the as cured G_A$_K$ (bold line) and of the G_A$_K$ heated up to 500, 550, 600, 650 are reported in Figure 6.7. All the XRD patterns showed a prevalent amorphous nature and small amounts of mullite, quartz, and magnetite as crystalline phases coming from the FA precursor. In accordance to what was found for G_A, heating up to 650°C did not induce modifications in the mineralogical composition of the material. From these results, the substitution of 8 M NaOH with 8 M KOH solution in the investigated fly ash-based geopolymer systems, is not effective in diminishing or retarding the crack formation that occurs during cooling.
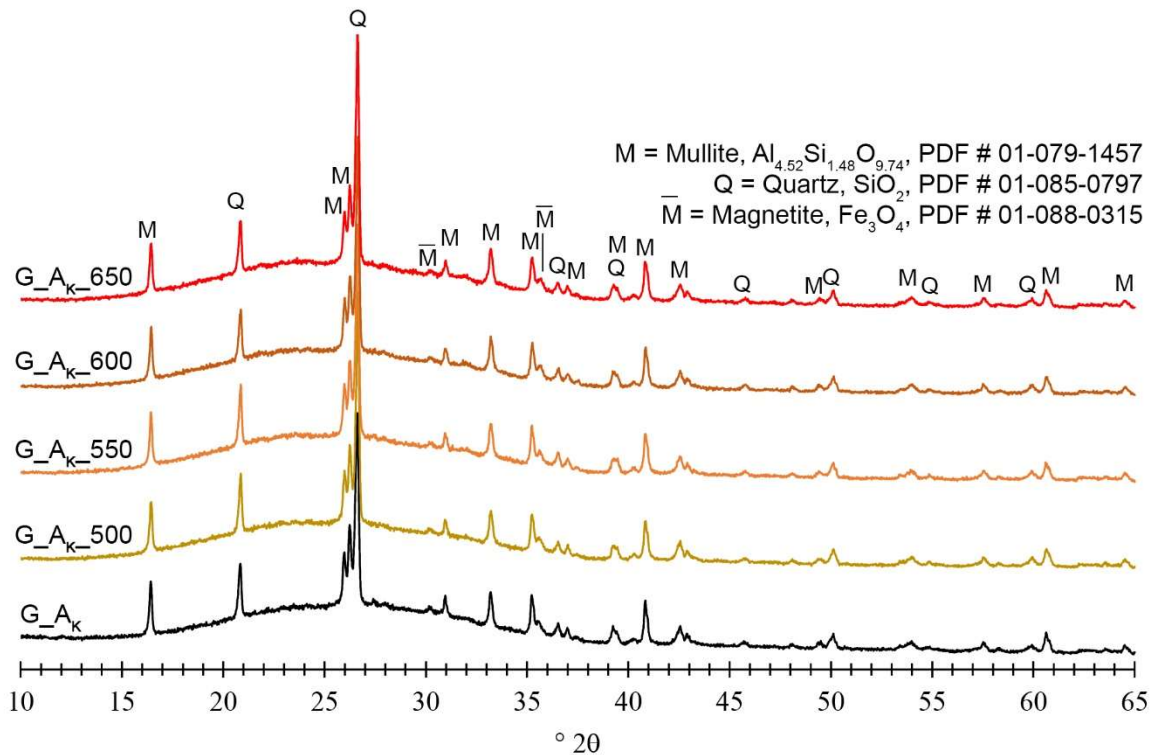
Figure 6.7: XRD patterns of the as cured G_A$_K$ sample and of G_A$_K$ sample after the thermal treatments.

6.3 Enhancement of the thermal dimensional stability by using recycled refractory particles

Previous studies dealing with high temperature exposure of alkali activated materials showed that it is possible to improve their thermal behaviour by adding suitable fillers and/or reinforcing phases in the matrix. In particular, the good compatibility of aluminosilicate, α-alumina, wollastonite, chamotte, PVA, basalt particulates and fibres with alkali activated matrices was assessed [25,76,172–175], confirming the possibility to overcome issues such as high shrinkage and changes in compressive and flexural strength due to the high temperatures exposure.

In this section, the geopolymer matrix (G_A) was implemented by adding recycled refractory particles (RRP), thus obtaining fly ash-based geopolymer composites (GC_A series) with enhanced thermal dimensional stability. The main characteristics of the RRP are reported in paragraph 3.1.4. The possibility of using recycled particles in combination with the use of fly ash as precursor potentially allows reducing the

production costs and promotes a circular economy model. Composites were produced as explained in paragraph 3.2, by adding different content of RRP (10, 20, 30, and 40 wt%) to the G_A matrix. All the results discussed in this paragraph refer to the obtained products after 7 days of curing (Figure 6.8).
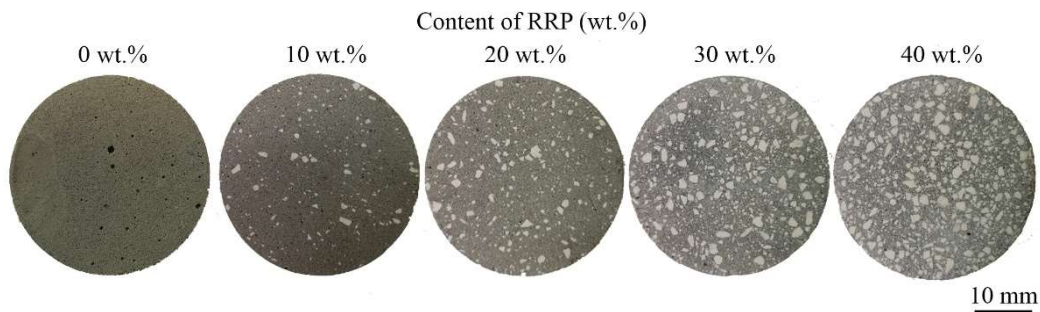
Figure 6.8: Pictures of the cross section of the as cured specimens containing increasing amount of RRP [176].
.

The mineralogical composition of the as cured G_A, GC_A_30 and GC_A_40 specimens was analysed through quantitative XRD analysis. The mineralogical composition of the as cured G_A sample was in agreement with the XRD diffrattogram previously presented in paragraph 6.2 (Figure 6.4). A prevalent amorphous nature (87.3 ± 0.6 wt%) and a small amount of mullite (6.6 ± 0.6 wt%) and quartz (6.1 ± 0.4 wt%) were detected. As for the composites, corundum and traces of baddeleyite were detected as new crystalline phases originating from RRP. Compared to the matrix (G_A), a lower content of amorphous phase and an increased amount of mullite were determined, according to the different content of dispersed RPP. Amorphous phase proportionally decreased with the increase of the RRP content (Figure 6.9), indicating that the RRP was neither reactive during the activation process nor hindered the process itself and can be effectively considered as inert in the process.
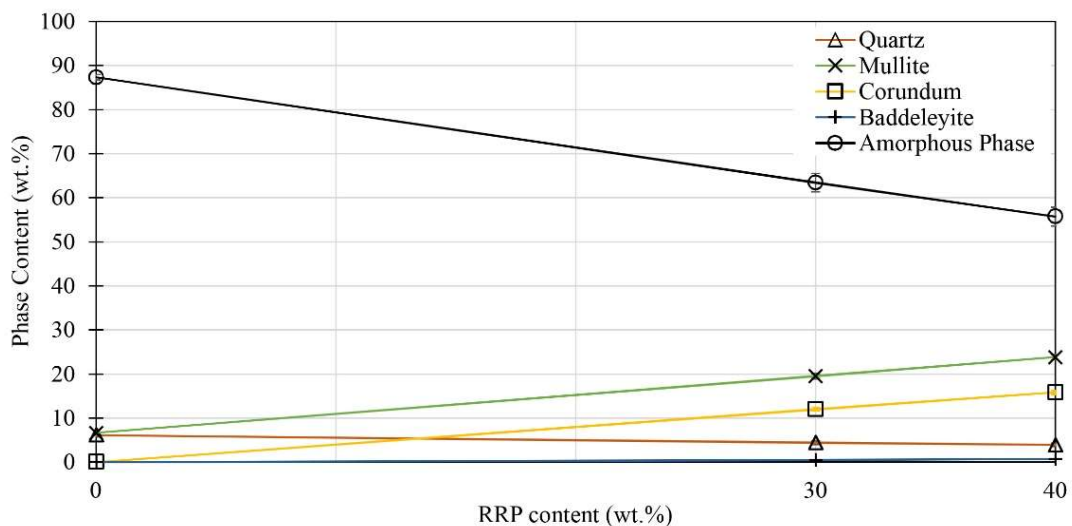
Figure 6.9: Mineralogical phase composition of the as-cured G_A, GC_A_30, and GC_A_40 samples [176].

Quantitative XRD analysis were repeated after the thermal treatment of the specimens at 800 and 1000 °C (performed as described in 3.3.5) and the relevant mineralogical phases are reported in Table 6.1.

Table 6.1: Mineralogical phase composition of G_A, GC_A_30 and GC_A_40 samples after the thermal treatments at 800 and 1000°C [176].

Phase content (wt%)	G_A 800	G_A 1000	GC_A_30 800	GC_A_30 1000	GC_A_40 800	GC_A_40 1000
Quartz	2.3±0.3	2.2±0.2	2.3±0.2	1.9±0.2	2.8±0.3	2.7±0.3
Mullite	5.0±0.8	5.4±0.8	24.2±0.6	24.9±0.5	33.3±0.6	33.2±0.6
Corundum	-	-	16.2±0.5	16.3±0.4	24.1±0.6	24.0±0.5
Baddeleyite	-	-	0.7±0.2	Trace (<1)	Trace (<1)	Trace (<1)
Nepheline	4.5±0.8	4.9±0.6	1.2±0.5	1.2±0.5	Trace (<1)	Trace (<1)
Plagioclase feldspar	33.7±0.5	37.4±0.3	26.2±0.6	28.2±0.6	20.4±0.8	22.4±0.8
Amorphous phase	54.5±3.0	50.1±3.0	29.2±3.0	27.0±3.0	19.0±3.0	17.0±3.0

In all cases, after heating up to 800°C for 2 h, a reduction in the amorphous phase content compared to the as cured materials occurred. Nepheline and plagioclase feldspar were found as predominant new crystalline phases. After the thermal treatment at 1000°C, no other new crystalline phases were formed, but plagioclase feldspar content slightly increased and amorphous phase slightly further decreased. These two findings are correlated since it is highly probable that the new phases are the result of a partial crystallization of the amorphous aluminosilicate gel [66,177]. Even if some authors reported a detrimental effect on geopolymers properties linked to the feldspars crystallization [73], in other cases the presence of these new phases is considered beneficial to their performace [60,178]. To verify this effect, the residual compressive strength of GC_A_40 cubic specimens (40 mm side) after the thermal treatments at 800 and 1000°C was assessed. The obtained results, reported as average of two measurements, confirmed a positive effect of the plagioclase feldspar crystallization. Indeed, the GC_A_40 compressive strength was equal to 44.6 ± 7.8 and 50.7 ± 0.3 MPa in the case of exposure to 800 and 1000°C, respectively. These values represent a six fold compressive strength increase compared to the same composite (GC_A_40) cured at room temperature, which was characterized by a compressive strength of 8.0 ± 0.8 MPa. Therefore, the phase composition changes due to the amorphous into crystalline transition were responsible for the determined improvement in the mechanical performance of the composite.

Figure 6.10 shows the mass loss, density, and water absorption of the specimens after the thermal treatments as a function of the RRP content. The black bars represent the composites mass loss after been dried at 105°C for 24 hours to measure the relevant bulk density and water absorption (also reported in black). Generally, the substantial variation of mass was verified during drying at 105°C. Heating up to 800°C caused a further mass loss connected to the additional dehydration of the bound water and to the dehydroxilation [179], whereas in the temperature range going from 800°C to 1000°C specimens can be considered stable, as variations < 1 % in the mass are observed. Regardless the RRP content, the thermal treatment at 800 °C also causes an increase in density values and a decrease in the measured water absorption compared to the as cured

samples. This behaviour is likely related to a localised sintering process of the matrix gel [66]. The reduction of water absorption values, indicating a modification of the samples open porosity, can also be related to the localised viscous sintering of the gel [64]. Indeed, it is possible that the viscous flow hinders the accessibility of the porosity, creating isolated pores which remain unfilled with water during the test. Both density increase and reduction of porosity validate the increase in compressive strength determined in GC_A_40 specimen after the thermal treatments. In addition, the introduction of RRP was beneficial in terms of mass stability generally leading to a lower mass loss compared to the relevant matrix. Indeed, composite containing 40 wt% of RRP shows a mass loss of 16.0% (GC_A_40) after the exposure to 1000°C, whereas the mass loss of the relevant matrix was equal to 19.3% (G_A) as reported in Figure 6.10.
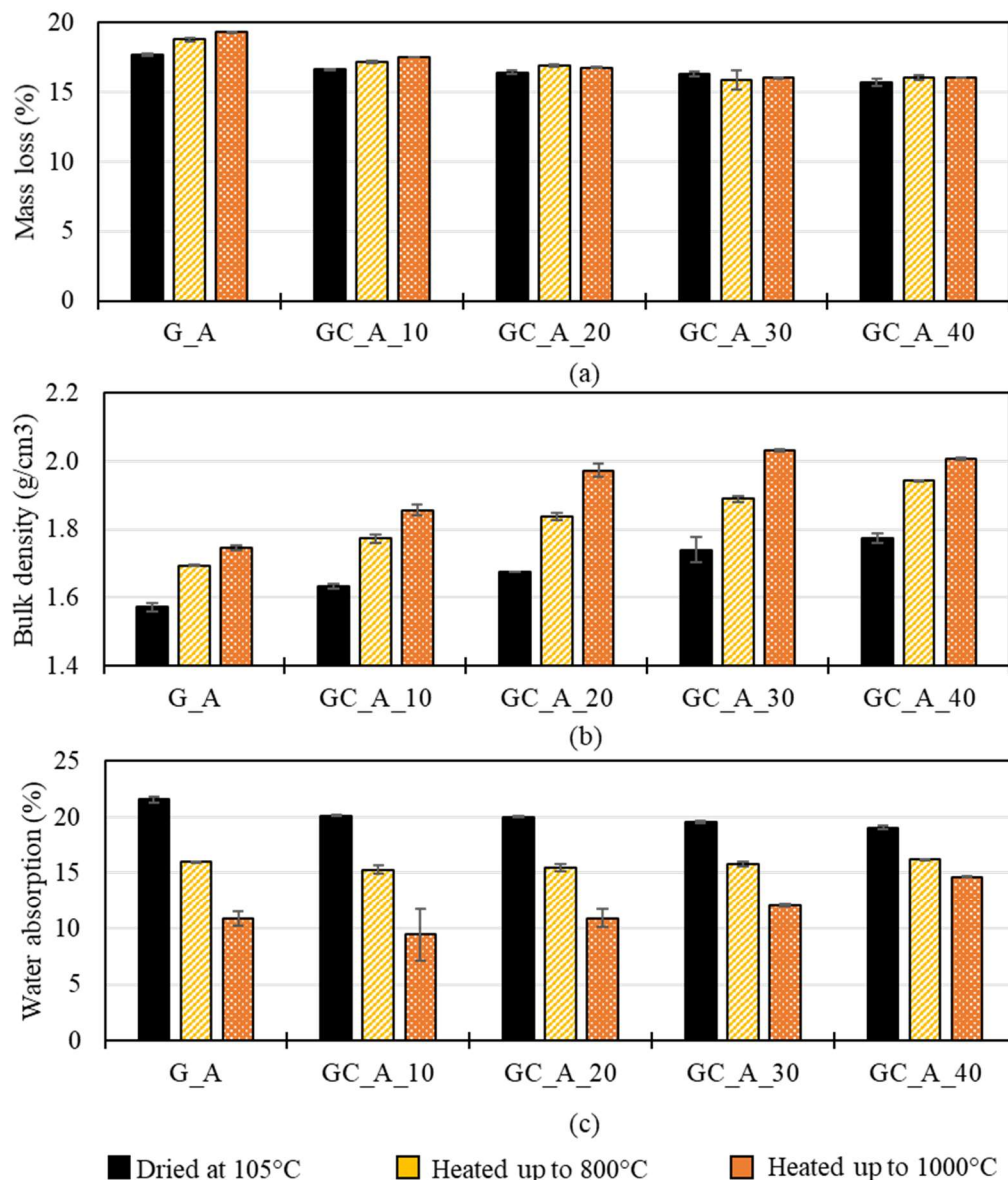
Figure 6.10: Quantification of mass loss (a), bulk density (b), and water absorption (c) of the specimens after drying (T = 105 °C) and thermal treatment (T = 800 °C and 1000 °C) (values are reported as average of two measurements) [176].

<u>Influence of thermal curing on the thermal behaviour of fly ash based geopolymers</u>

Results presented in this section aim to investigate the influence of the curing method on the thermal behaviour of G_A and GC_A specimens. The heat-cured specimens (cured in oven at T = 70 ± 1 °C for the first 24 h, see paragraph 3.2.2) are indicated with a subscript **T** (i.e. G_A$_T$) in the relevant label.

In terms of mechanical strength, it was possible to assess a beneficial effect of the heat-curing on the material performance. Indeed, G_A$_T$ exhibited a compressive strength of 25.8 ± 6.7 MPa which was more than double of the one showed by G_A (11.3 ± 1.5 MPa). Also in this case, the test was performed on cubic specimens (40 mm side) and results are reported as average of two measurements. This behaviour was somehow expected since it is known that heat curing usually boost the activation process, increasing the degree of reaction and therefore favouring the rapid development of a more resistant gel in terms of mechanical properties [45]. After 7 days of curing, specimens were exposed to high temperature and the resulting crack formation is visible in the Figure 6.11.
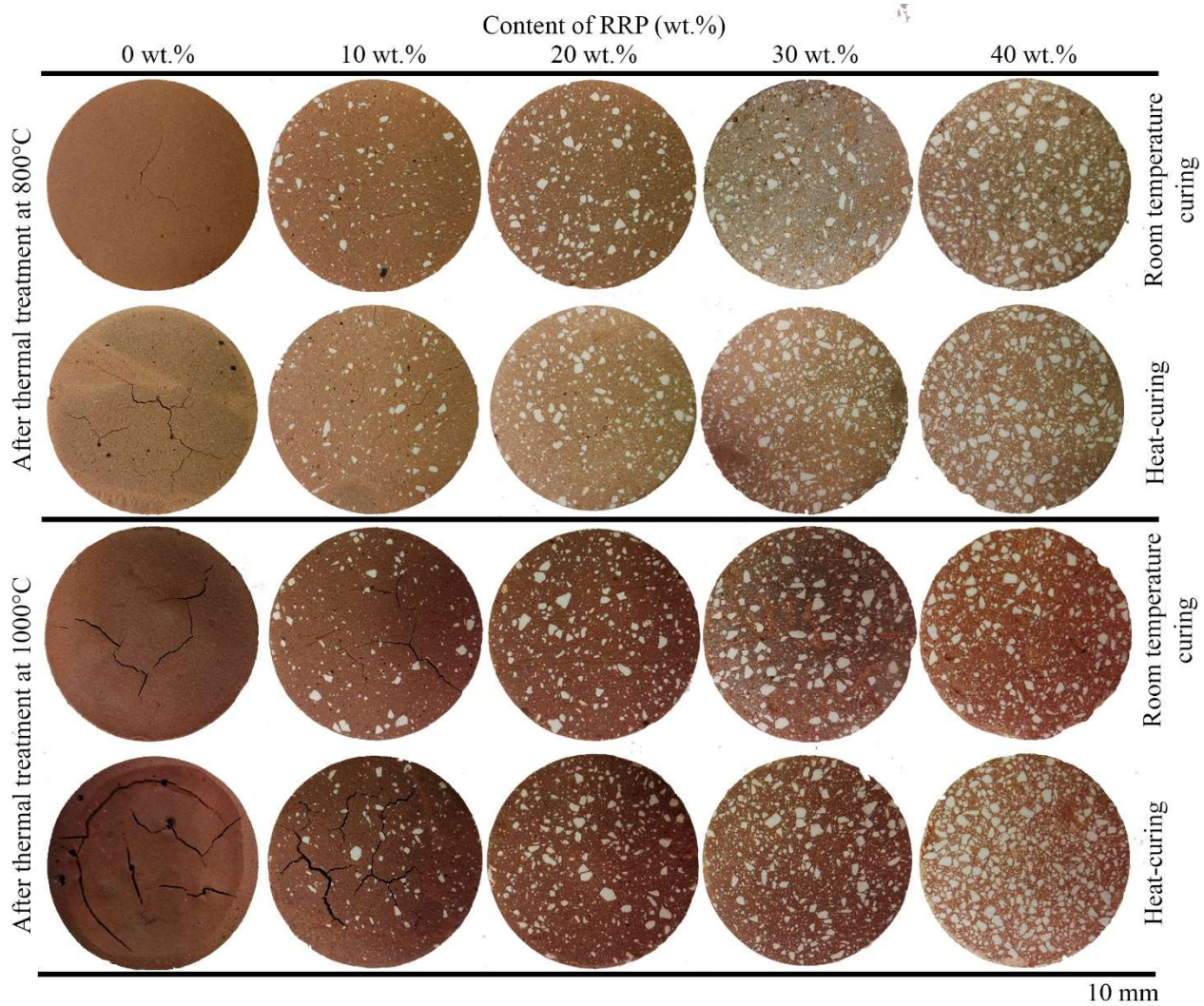
Figure 6.11: Pictures of the specimens after thermal treatment at 800°C (upper rows) and 1000°C (lower rows) [176].

Changes of the samples colour from grey to reddish and more intense red, when heated at 800 and 1000°C, respectively, were clearly observed. As discussed in the paragraph 6.2, when G_A is exposed to temperature higher than 550 °C, it undergoes crack formation during both heating and cooling period. However, cracks observed on heat-cured specimens appeared to be more severe than the ones of the room temperature-cured specimens. The different level of damage can be connected to the different pore size distribution of the two specimens influenced by the curing method. Indeed, the heat curing favours the development of finer pore structure [40,41,180]. It is possible that when a heat-curing is performed, that leads to a structure richer in small pores, the stronger capillary pressure during dehydration is responsible for the greatest damage observed on the specimens surface when compared to the room temperature specimens one and in this case is more related to a damage which occur during heating instead of cooling.

The use of RRP proved to be a possible solution to avoid cracking. In fact, regardless of the curing conditions, the presence of the particulates favours the progressive reduction of cracking (Figure 6.12). When exposed to 800 °C, 20 wt% of RRP was sufficient to guarantee the integrity of the material. However, when the temperature of exposure increased up to 1000°C, the integrity of the samples is maintained only in specimen cured at room temperature (Figure 6.12). Composites containing 30 wt% and 40 wt% of RRP appeared undamaged after both thermal treatments regardless of the curing condition adopted (Figure 6.12).

<u>Investigation of the thermal dimensional stability of the composites</u>

Heating microscope analysis and dilatometry were used to more precisely investigate the thermal dimensional stability of the developed composites. The heating microscope analysis allows following up the geometrical modification of the samples during heating at a constant rate of 5°C/min up to the complete melting of the material (Figure 6.13). In this way, it was possible to identify the temperature above which the material undergoes significant geometrical modification, which was therefore considered the maximum temperature of its thermal dimensional stability (Tmax in Figure 6.13b). For the sake of brevity, only some of the images obtained through the heating microscope are reported in the Figure 6.13a. Generally, a geometrical thermal stability up to 1000 °C was determined and it was not significantly influenced by the curing conditions. In particular, G_A and G_A$_T$ samples showed a reversible expansion between 600 and 850 °C and a stability up to 1140 °C. When 10 wt% and 20 wt% of RRP were added, Tmax increases up to 1170 °C (GC_A_10 and GC_A$_T$_10) and 1200°C (GC_A_20 and GC_A$_T$_20), respectively. Samples GC_A_30 and GC_A$_T$_30 are stable up to 1225 °C and 1240 °C, respectively. In all the aforementioned cases, above the maximum temperature of stability a swelling of the samples was detected. Finally, the specimens containing the highest amount of RRP considered in this research (GC_A_40 and GC_A$_T$_40) showed dimensional stability up to temperatures comprised in the range of 1210-1220 °C. In these cases, above the determined Tmax, the specimens experienced a shrinkage before swelling. According to the presented findings, the use of RRP up to the amount of 30 wt% appeared to be effective in increasing the temperature range of dimensional stability of the studied fly ash-based geopolymers. Above this amount, the effectiveness of the particulates was no longer

substantial. Moreover, from the heat curing no interesting benefits in terms of dimensional stability at high temperature were found which could justify the additional costs of this curing condition.
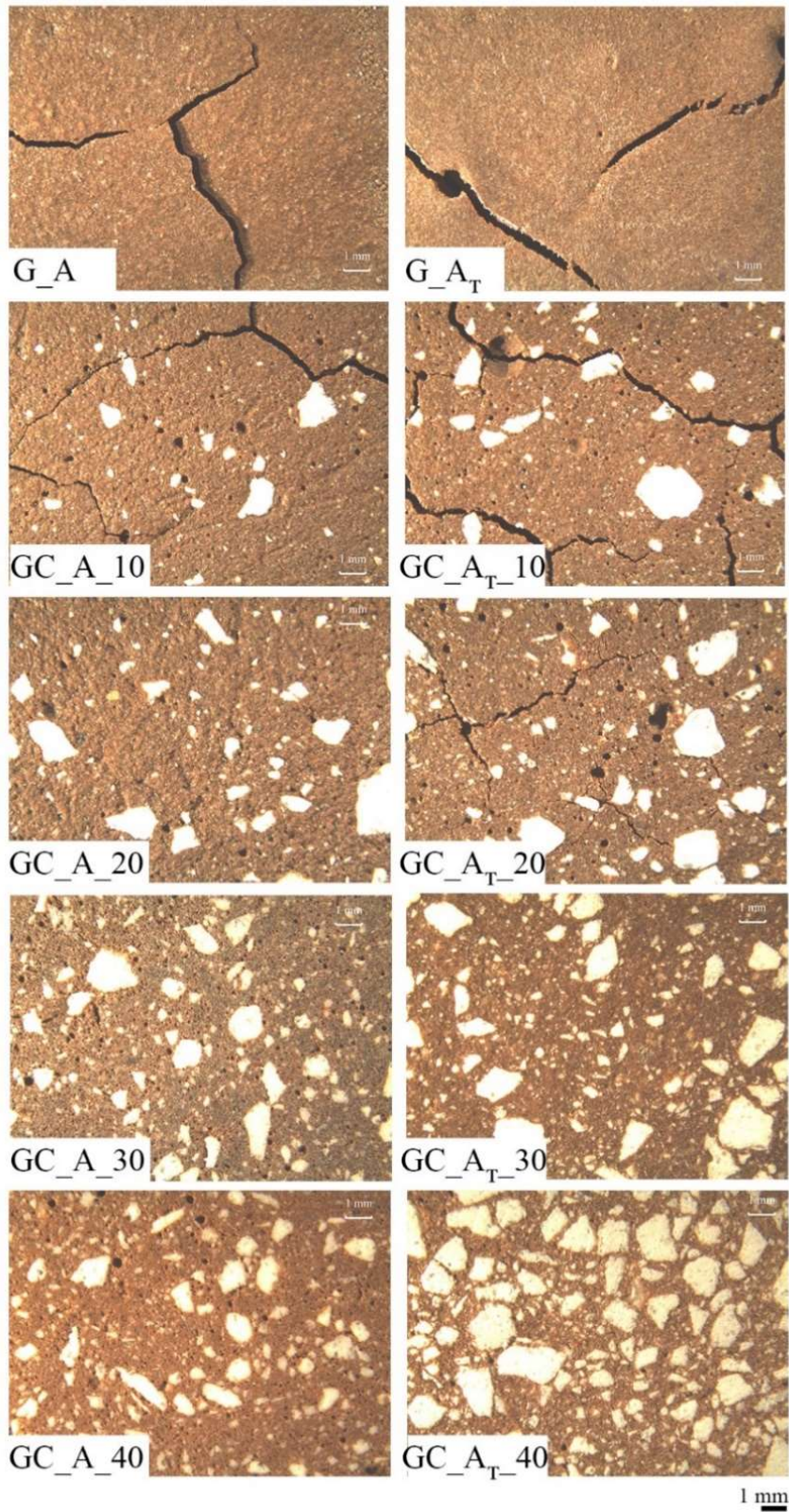

Figure 6.12: Optical micrographs (10X) of matrices (G_A and G_A$_T$) and composites containing 10, 20, 30, and 40 wt% RRP, after thermal treatment at 1000 °C [176].
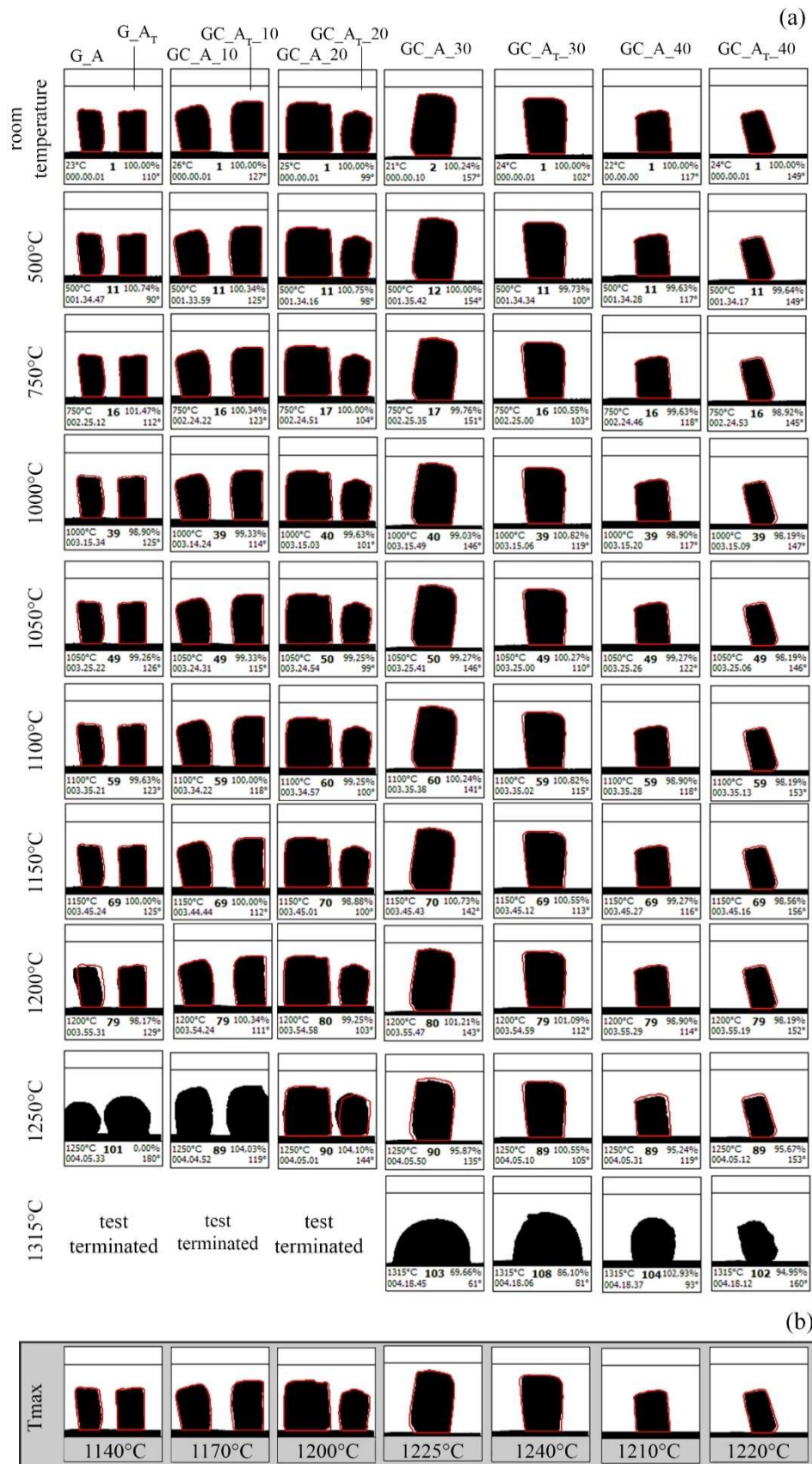
Figure 6.13: Samples geometrical modifications over increasing temperature obtained with heating microscope analysis (a). Images of the specimens at T_{max} (i.e. temperature above which the geometry of the sample started to significantly change) (b) [176].

In order to better investigate the dimensional stability of the composites, the dimensional changes during heating up to 1000°C were assessed in situ through a dilatometer. According to the previous results, the focus was put on room temperature cured samples (G_A, GC_A_10, GC_A_30, and GC_A_40). Results were consistent with the heating microscope analysis since all samples showed high dimensional stability up to 1000 °C with dimensional changes comprised in ± 2 % (Figure 6.14).
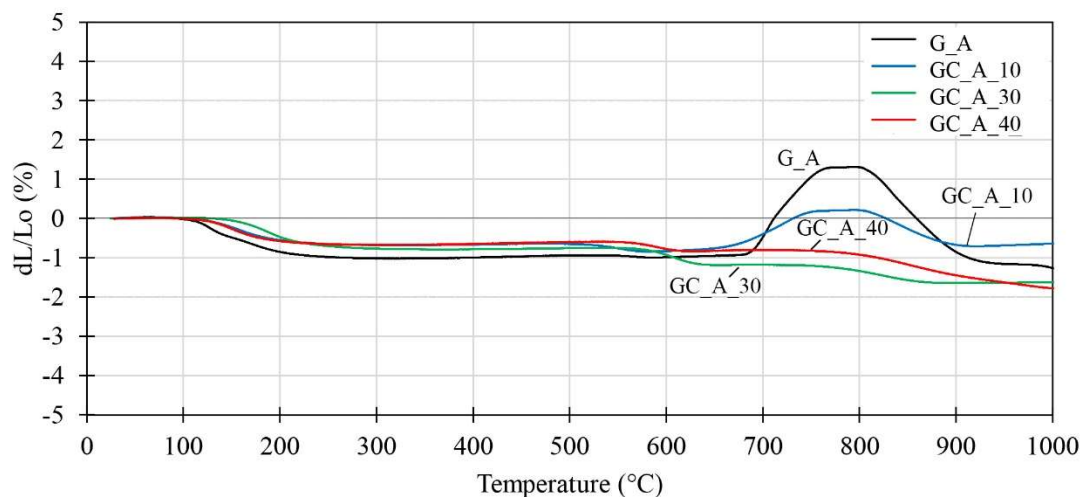
Figure 6.14: Linear dimensional changes of the G_A, GC_A_10, GC_A_30, and GC_A_40 samples during dilatometry measurements [176].

The curves were also consistent with the thermal expansion and shrinkage of low calcium-based alkali activated materials, extensively investigated in literature [64,66,68,181]. After the dehydration shrinkage recorded in the temperature range of 110-230 °C, all samples showed stability up to above 530 °C. The dehydration identified through mass loss measurements, which occurs for temperature below 105 °C, did not seem to cause shrinkage. Between 530 and 640 °C a shrinkage was observed, mainly linked to a densification of the sample [67,170]. The densification found in this range of temperature could justify the increased values of density measured after the thermal treatment in the muffle furnace. The most evident difference among the investigated samples was found in the region going from 660 to 770°C. In this range of temperature, the literature does not report a clear trend in linear dimensional changes, which vary according to the materials composition. However, it is not uncommon to measure a thermal expansion, as the one measured in the case of G_A and GC_A_10 samples, usually linked to the bloating of residual silicate phases and/or crack formation [66,68]. It is interesting to note that the reactions leading to the expansion were hindered or influenced by the presence of the grains of the refractory. Indeed, by adding 10 wt% of refractory particles and therefore reducing the total amount of silicates contained in the sample, a decrease in the expansion was found. The expansion totally disappeard when 30 and 40 wt% of RRP were used. From these results appeared that the use of RRP can prevent both the bloating of silicate phases and crack formation, increasing the range of the thermal dimensional stability characterized by a total shrinkage lower than 1% up to 800°C in the case of GC_A_40 sample. GC_A_30 and GC_A_40 composites presented similar dimensional changes which were mainly characterized by three areas of shrinkage in the temperature ranges of 110-230 °C, 550-630 °C, and 770-860 °C. In the case of GC_A_30 the dehydration shrinkage was retarded compared to GC_A_40 and started for

slightly higher temperature (~130°C). Up to around 860°C, the GC_A_30 total shrinkage was higher than the one of GC_A_40. Above this temperature, GC_A_30 returned to be dimensionally stable, whereas GC_A_40 underwent a further shrinkage up to 1000°C. The shrinkage from 800 to 1000 °C may be due to the further local densification or sintering of the matrix gel.

6.4   Main remarks

The results here discussed allow drawing the following conclusions:

– the acoustic emission measurements allowed obtaining insight into the cracking mechanism in fly ash-based geopolymer activated at room temperature. During heating up to 800 °C the cracking was associated exclusively to the dehydration of the material in the temperature range of 90 – 360 °C. No further AEs were recorded on heating.

– The temperature of 550 °C was considered significant in terms of microstructural changes of the investigated geopolymer system. Indeed, for temperature of exposure higher than 550 °C, AEs were recorded also on cooling: the higher the temperature of exposure, the higher the AE activity. It can be said that, starting from 550 °C a localized sintering of the geopolymer matrix occurred. The activity detected on cooling can be associated to a stress caused by the shrinkage of the sintered phases experiencing a rapid quenching as the temperature in the furnace started to decrease.

– The thermal treatment at 650 °C did not cause changes in the mineralogical nature of the geopolymer. However, after the exposure to temperatures ≥ 800 °C, crystallization of nepheline and plagioclase feldspar occurred, which in the case of composites (GC_A series) favoured the compressive strength increasing.

– The use of recycled refractory powder for the production of geopolymer composites resulted a suitable path for improving the high-temperature performance of fly ash-based geopolymers. Indeed, the addition of RRP did not hinder the alkali activation process, improved the linear dimensional stability during heating (linear shrinkage inferior to 2 % at 1000 °C) and increased the maximum temperature of dimensional stability from 1140 °C to 1240 °C. In addition, the amount of 30 wt% RRP was sufficient to inhibit the cracking after 2 h exposure to 1000 °C.

– No significant benefits were obtained from the heat curing in terms of thermal dimensional stability of geopolymer composites. On the contrary, when exposed to high temperature, heat-cured specimens with low amounts of dispersed RRP (0, 10, 20 wt%) showed greater cracking.

Chapter 7:
Investigation of lightweight geopolymer mortars
as passive fire protection systems for steel structures

The contents of this chapter formed the basis of the following publication:

7.1   Background and research aims

Fire represents a serious problem for steel-based structures such as high-rise buildings where steel is often used as the skeleton system. Steel is an excellent material at ambient temperature but when exposed to high temperature, it is subjected to a rapid degradation of strength and elastic modulus (i.e. steel loses about one-half of the strength at 500 °C) [120]. Therefore, severe fires can cause initial localized failure or abnormal loading which could lead to a progressive collapse of a building [182].

A preventive solution to reduce fire damages is represented by passive fire protection (PFP) systems. The idea behind these systems is to bond a protective layer to the steel surface, in order to maintain the temperature of the steel component below the critical temperature. The final goal is to provide time to evacuate the building and to control or extinguish the fire, thus avoiding losses. There are some important factors to consider when a fireproofing system is selected such as the weight limitations imposed by the strength of the steel supports, the fire resistance rating selected, the material's adhesion strength and durability, the corrosiveness of the atmosphere and of fireproofing materials to the substrate and cost [183]. Currently, the most used PFP systems are intumescent paints and cementitious fireproofing coatings. Intumescent paints have two key components: a resin binder and a mixture of chemicals that decomposes and releases a gas when heated. The origin of the name is Latin 'intumescere' which means 'to swell up'. When heated beyond a critical temperature, an intumescent material begins to swell and then to expand approximately 15 times to 30 times its initial thickness. A gas-producing reaction is triggered at a temperature corresponding to an appropriate resin melt viscosity. The result of this process is a foamed, cellular charred surface layer which insulates the steel from fire [184,185]. Conversely, fireproofing coatings are generally spray-applied systems that behave like thermal barrier to the transfer of heat to the substrate. Spray applied fireproofing coatings are generally cementitious-based systems grouped under two categories: gypsum-based comprising of gypsum and vermiculite, and Portland cement based composed of Portland cement and vermiculite. They are usually a more inexpensive means to protect structural elements [182,184,186,187]. The term "fireproofing" is widely used to describe these types of coatings, however it does not indicate a material totally safe from the effects of fire but it refers to the materials that provides a degree of fire resistance for protected substrates.

Although geopolymers are characterized by a remarkable thermal resistance as already discussed in Chapter 2 and 6, there is only a limited number of studies on testing the performance of geopolymers as passive fire protection systems under fire like conditions available (e.g., [79,81,84,188,189]).

In this Chapter, the possibility of using fly ash-based geopolymers as passive fire protection (PFP) systems for steel components is investigated. A comprehensive study is presented. The first part of the study aims to the optimization of the mix design in order to produce a lightweight geopolymer (LWG) mortar with increased thermal insulation and low weight load. Physical, mechanical and thermal properties are investigated. In particular, thermal conductivity measurements as function of temperature (up to 700 °C) were carried out in order to provide data on the heat transfer to the substrate during heating. According to the experimental

findings, the most promising formulation was analysed by means of finite volume method simulations to investigate the behaviour of the fireproofing geopolymer during a fire accident. In the second part of the study, the effectiveness of the LWG mortars as passive fire protection system was assessed by means of medium-scale fire test setup. Furthermore, acoustic emission measurements were adopted to analyse cracking phenomena due to the high temperature exposure.

7.2   Development of a lightweight geopolymer mortar: physical and mechanical properties

For this study, the two matrices G_A and G_B were adopted as reference matrices. As reported more in the detail in 3.2.1, the two mix differ for the ratio between the two alkaline solutions adopted (i.e. Sodium silicate solution and 8 M NaOH solution), adjusted in order to modify the compositional Si/Al ratio. In particular, mixtures based on G_A composition have higher Si/Al ratio (Si/Al = 2.9) than the ones developed starting from the G_B composition (Si/Al = 2.5). The mix design of both matrices was optimized by using expanded perlite (EP) and hydrogen peroxide according to the formulations reported in Table 3.8, thus obtaining a lightweight geopolymer mortars (LWG) with increased thermal insulation and reduced weight load. Results presented in this section refer to geopolymers at 7 days of curing. The cross section of a representative specimen for each formulation is reported in Figure 7.1.
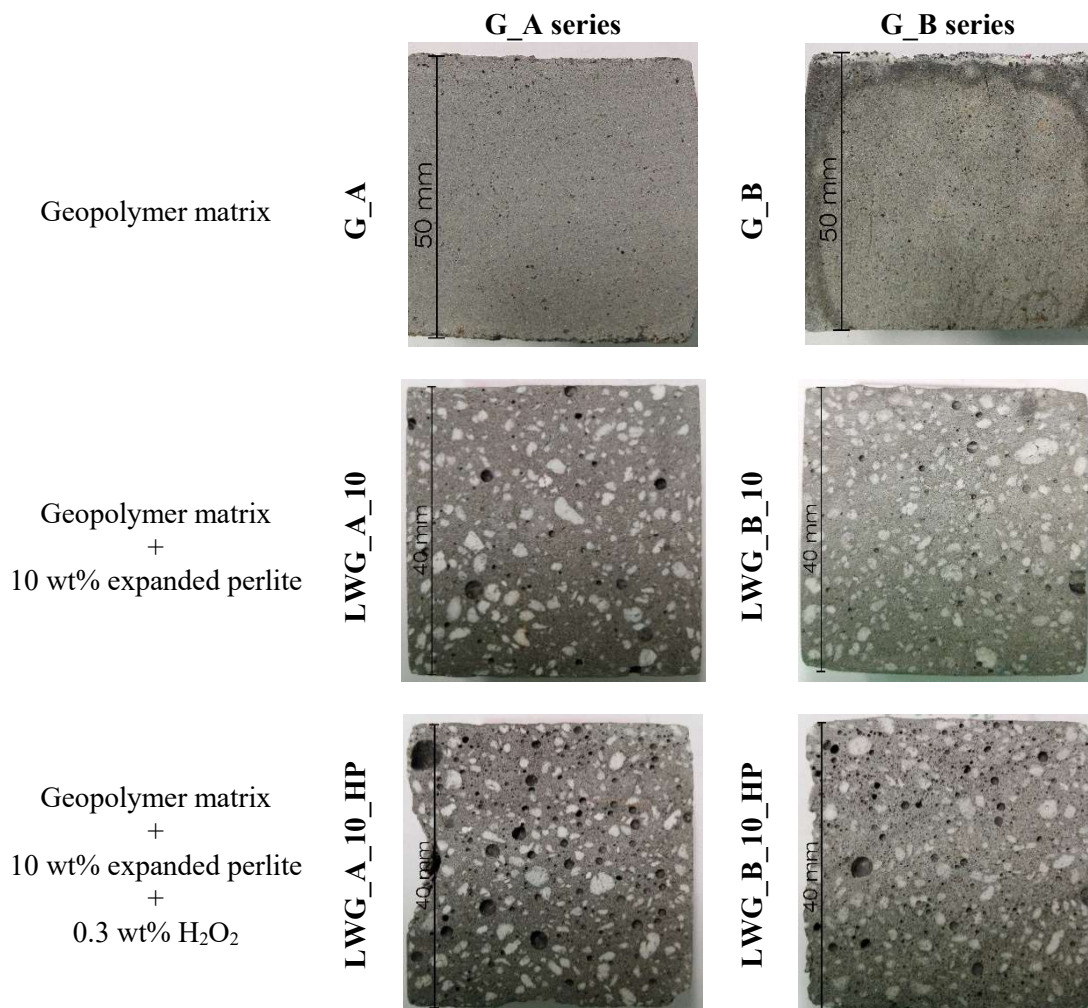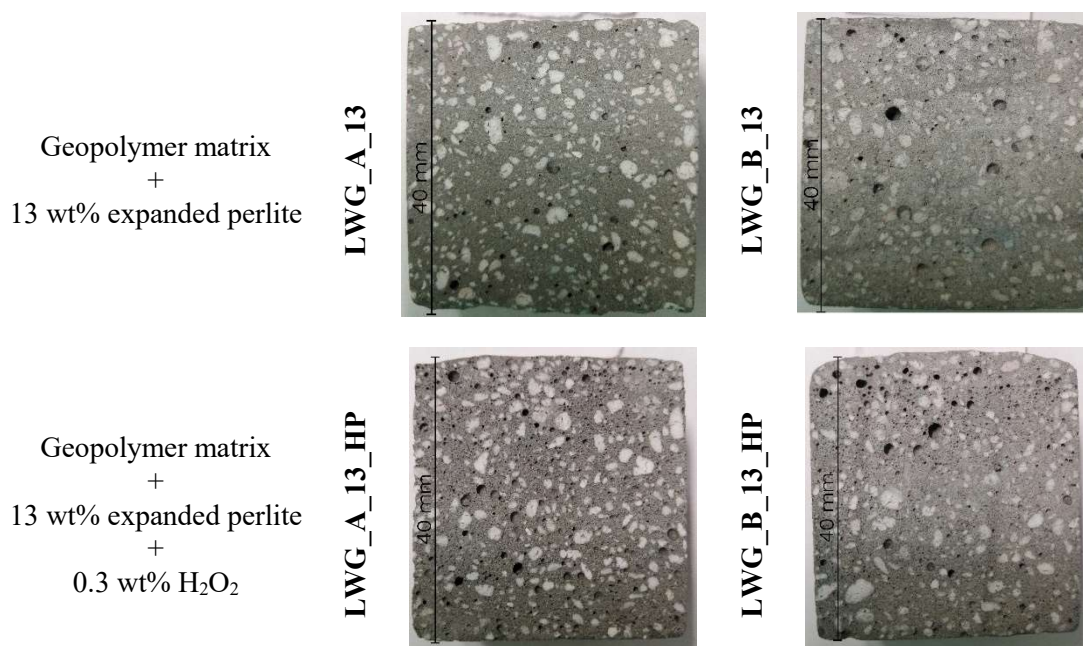
Figure 7.1: Photos of the cross section of the specimens at 7 days.

Table 7.1 reports physical and mechanical properties of all specimens. The comparison between the two different matrices (G_A and G_B) produced without additional components (i.e. expanded perlite and/or H_2O_2) showed that G_A was characterized by higher density and lower water absorption than G_B, indicating a less porous structure of the matrix.

Table 7.1 Physical and mechanical features of geopolymers at 7 days (values are reported as average of two measurements).

Sample	ρ_{bulk} (g/cm^3)	WA (%)	WA$_v$ (%)	Specific intruded Hg volume (mm^3/g)	E$_d$ (GPa)	Rc (MPa)
G_A	1.53 ± 0.01	19.0 ± 0.1	21.3 ± 0.1	207.3	6.20 ± 0.06	6.01
LWG_A_10	1.23 ± 0.01	25.0 ± 0.1	42.8 ± 0.2	343.5	1.71 ± 0.01	2.74
LWG_A_13	1.06 ± 0.01	25.3 ± 0.1	44.1 ± 0.4	365.1	1.54 ± 0.01	2.65
LWG_A_10_HP	0.90 ± 0.01	25.3 ± 0.4	49.1 ± 0.8	338.0	0.67 ± 0.09	1.99
LWG_A_13_HP	0.79 ± 0.01	26.0 ± 0.1	46.6 ± 0.1	403.7	0.49 ± 0.05	2.34
G_B	1.39 ± 0.02	23.2 ± 0.3	24.9 ± 0.2	223.1	5.00 ± 0.01	3.29
LWG_B_10	1.06 ± 0.01	27.4 ± 0.1	43.6 ± 0.3	331.0	1.30 ± 0.01	1.87
LWG_B_13	0.97 ± 0.01	29.0 ± 0.1	46.6 ± 0.1	374.5	0.84 ± 0.10	1.33
LWG_B_10_HP	0.81 ± 0.01	28.9 ± 0.2	52.0 ± 0.3	504.7	0.58 ± 0.06	1.14
LWG_B_13_HP	0.77 ± 0.01	30.8 ± 0.4	57.7 ± 0.4	579.4	0.31 ± 0.01	0.73

As expected, regardless the Si/Al ratio, the introduction of EP and EP + H_2O_2 led to a decrease in the bulk density. A drop of about 20 % of the bulk density was always found when 10 wt% of EP was added, which increased up to 30% when 13 wt% of expanded perlite was used. The use of the foaming agent promoted an additional decrease in the bulk density in all the investigated mixes. LWG_B_13_HP specimen, containing both EP and hydrogen peroxide, showed the lowest value of bulk density (0.77 g/cm^3) among all the specimens.

By adding the same amounts of EP (13 wt%) and H_2O_2 a decrease in bulk density of 49% and 45% is found for G_A and G_B, respectively. Therefore, the use of lightweight aggregate and H_2O_2 for lowering the density of the material results more effective for higher compositional Si/Al ratio.

Because of its high porous structure [190], the addition of expanded perlite had a direct influence also on the water absorption. Regardless the Si/Al ratio, the addition of EP increased the amount of the absorbed water. The highest values of water absorption was found when both EP and foaming agent were used in the G_B matrix (LWG_B_13_HP specimen).

Table 7.1 also reports the compressive strength and dynamic modulus of elasticity of the investigated specimens. As a general trend, the higher Si/Al, the higher compressive strength and E_d. These results agree with previous studies which showed that increased strength and reduced porosity of geopolymers can be found for increased compositional Si/Al ratio [44,191–193]. The use of expanded perlite and its increase in content had a significant effect on compressive strength and dynamic modulus of elasticity of geopolymers, as well. Indeed, for both Si/Al ratio, a decrease of about 60% in compressive strength and 80% in E_d was found when the 13 wt% of EP was added. This behaviour is commonly observed when expanded perlite is used as lightweight aggregate in cement based materials, as well [102]. The mechanical properties dramatically dropped when also hydrogen peroxide was used.

The open porosity of the specimens was further investigated through MIP analysis. Maintaining constant the amount of EP and H_2O_2 in the mix design, similar or higher specific intruded Hg volume that is directly related to the open porosity, was found for specimens with lower Si/Al ratio (Table 7.1). These results are in agreement with the water absorption values previously described. Figure 7.2 shows the pore size distribution of all samples obtained by MIP.
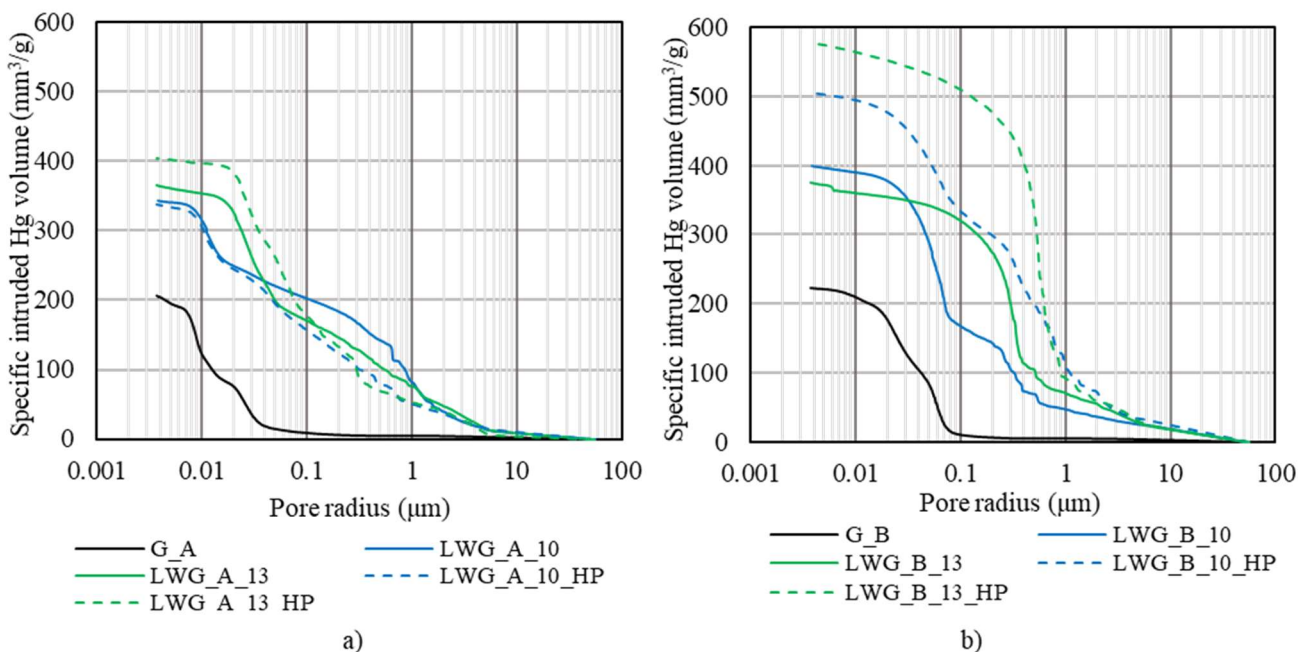
Figure 7.2 Pore size distribution curves of the investigated geopolymers at 7 days: G_A series (a); G_B series (b).

The influence of expanded perlite on increasing the porosity of samples and on enlarging the dimension of pores was evident. When the G_A series is considered (Figure 7.2a), the increasing in the amount of EP from 10 to 13 wt% did not significantly change the pore size distributions of the samples. In addition, the use of H_2O_2 did not strongly modify their total open porosity. Conversely, the use of H_2O_2 led to an increase in both total open porosity and pore dimension of the G_B series geopolymers. This difference can be ascribed to the different viscosity of the fresh mixtures that in G_A was higher than G_B, because of the higher amount of sodium silicate solution used to increase the Si content. Consequently, the use of H_2O_2 in more viscous slurry led to a formation of closed porosity, instead of an open one as happened in LWG_B_10_HP and LWG_B_13_HP samples. This was also supported by the fact that the use of H_2O_2 in G_A series geopolymers was effective in reducing the density without significantly increase the intruded Hg volume and the water absorption.

To characterize more in depth the pore morphology and the development of the pore structure caused by the hydrogen peroxide, optical analysis was performed on LWG_A_13_HP and LWG_B_13_HP samples. In Figure 7.3, optical microscopy images of representative LWG_A_13_HP and LWG_B_13_HP cross sections are presented.
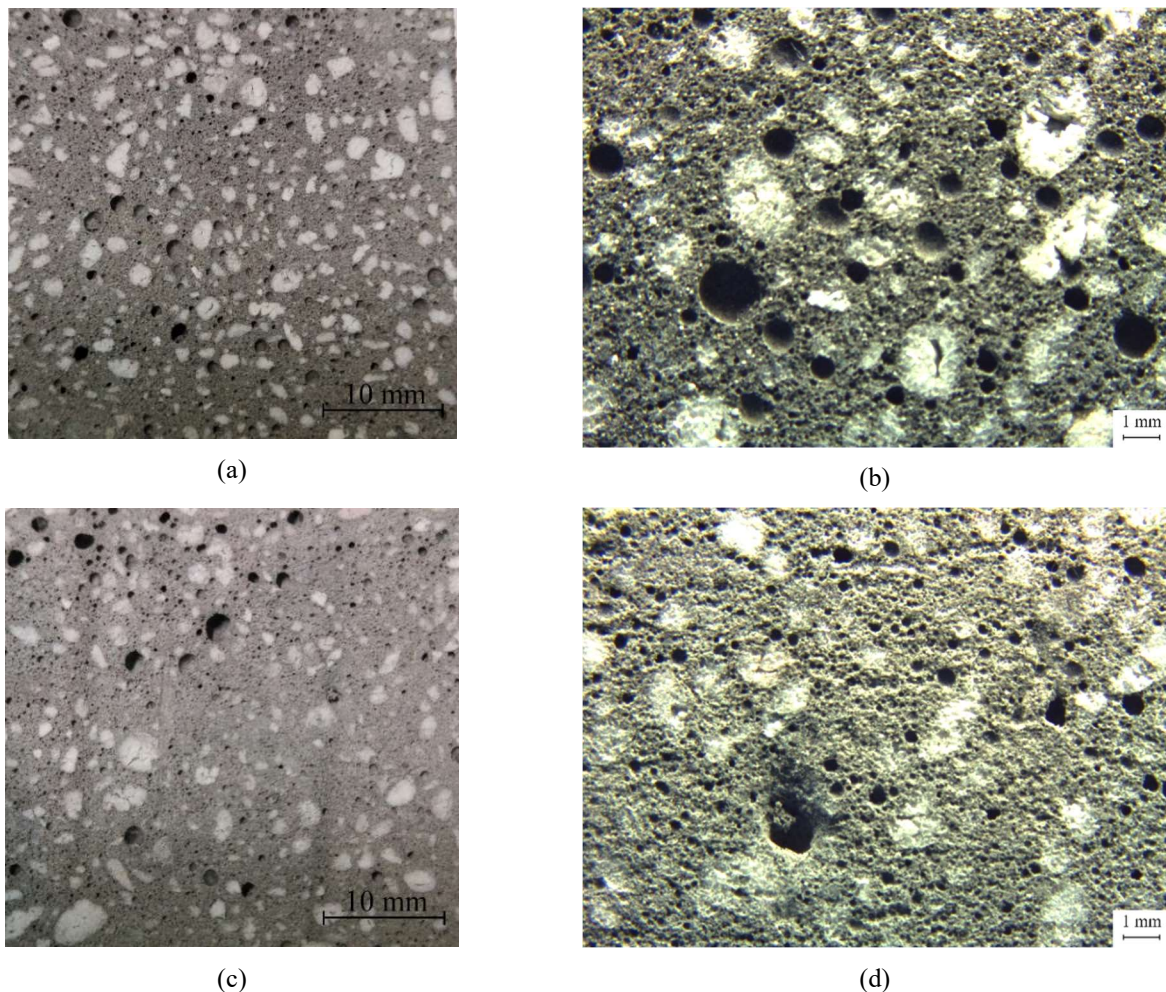
Figure 7.3 Digital and optical images of foamed geopolymers containing 13 wt% of expanded perlite: LWG_A_13_HP (a and b), LWG_B_13_HP (c and d). Vertical section, top on top.

The former revealed a more homogeneously foamed section, confirming that the higher viscosity of the fresh mixture favoured the entrapping of the O_2 bubble in the matrix. On the contrary, the LWG_B_13_HP section showed higher foaming at the top compared to the bottom region. This was likely caused by rising pores collapsing due to the low viscosity of the slurry prior to gel hardening [88]. The optical images were analysed through digital imaging software that allows investigating porosity starting from the minimum diameter of 29 μm. The total porosity (%), the number of pores per mm^2 and the content % of pores arranged per ranges of pore diameters, are reported in Table 7.2. Results confirmed the higher total porosity of LWG_B_13_HP than LWG_A_13_HP. However, the latter showed a major presence of spherical shape pores bigger than 50 μm which can be attributed to the effect of hydrogen peroxide [87,194].

Table 7.2 Pore distribution obtained via image analysis of four images per investigated sample (Investigated area average = 140 ± 16 mm^2).

Sample	Porosity area ratio (%)	Number of pores/mm²	Content of pores (%) per size ranges (μm)				
			29 - 50	50 - 250	250 - 500	500 - 1000	> 1000
LWG_A_13_HP	15.4 ± 1.5	6.6 ± 0.6	20.7 ± 1.6	71.3 ± 0.8	6.2 ± 1.6	1.4 ± 0.5	0.3 ± 0.2
LWG_B_13_HP	19.3 ± 1.3	9.9 ± 1.6	26.3 ± 1.0	65.7 ± 1.2	7.0 ± 1.2	0.8 ± 0.6	0.2 ± 0.04

7.3   Development of a lightweight geopolymer mortar: thermal properties and insulating capacity

The performance of a fireproofing coating are temperature and composition dependant. However, in practice, when fire resistance of structural members is evaluated, only room temperature thermal properties are often taken into account, without any consideration to variation of these properties with temperature. In order to overcome this issue and to better evaluate the fire performance of LWG mortars, data on temperature dependant thermal properties (i.e. thermal conductivity, specific heat, mass loss) of LWG mortars were evaluated both at room temperature and at elevated temperatures.

Figure 7.4 shows the values of thermal conductivity (K) measured at 20°C in correlation with the bulk density of the specimens previously discussed.
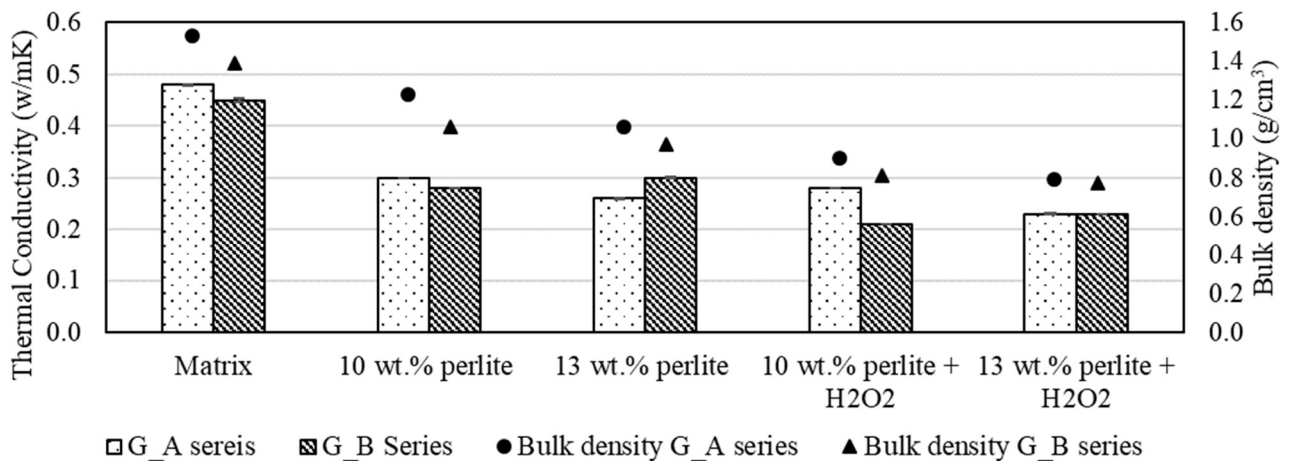
Figure 7.4: Thermal conductivity and relevant bulk density of geopolymers at 20°C.

The thermal conductivity of the samples in this study was observed to the range from 0.48 to 0.21 W/mK. The measured values are in the same trend as other geopolymer foams in the literature [188,195] and slightly higher than that of lightweight cement based fireproofing materials [186,196]. The thermal conductivity of geopolymers followed the same trend of the bulk density, whereas a negligible influence of the Si/Al ratio was found. Similar results were found in previous study [197] were no correlation between the thermal conductivity and the geopolymer gel structure was observed. Conversely, the influence of expanded perlite and H_2O_2 was clearly observed and was expected, since the insulating properties of perlite are well known and H_2O_2 favoured the increasing of porosity.

The variation of thermal conductivity with temperature for G_B, LWG_A_13_HP and LWG_B_13_HP specimens is plotted in Figure 7.5. As expected and already assessed during measurements at room temperature, the thermal conductivity of the matrix G_B was higher than to the one of specimens with expanded perlite and H_2O_2. In addition, no significant differences were found comparing LWG_A_13_HP and LWG_B_13_HP, thus confirming that the role of the geopolymer matrix composition is secondary to the one of expanding agents (i.e. expanded perlite and H_2O_2), as far as the thermal conductivity is concerned. In all cases, a slight increase in thermal conductivity was found for increasing temperature up to 300 °C. At 550 °C a decrease of thermal conductivity was observed in all specimens. The drop in the thermal conductivity possibly indicates a change in the microstructure of the geopolymer matrix. Indeed, as previously reported in paragraph 6.2, above 550 °C localized sintering phenomena occur changing the porosity and the pore distribution of the fly ash-based geopolymer system investigated in this study. In addition, the crystallization of nepheline and plagioclase phases from the amorphous geopolymer matrix, which occurs for temperature close to 800 °C, can further decrease the thermal conductivity since plagioclase is a poor heat conductor mineral and increased feldspar volume fraction tends to decrease the thermal diffusion of the material [198].
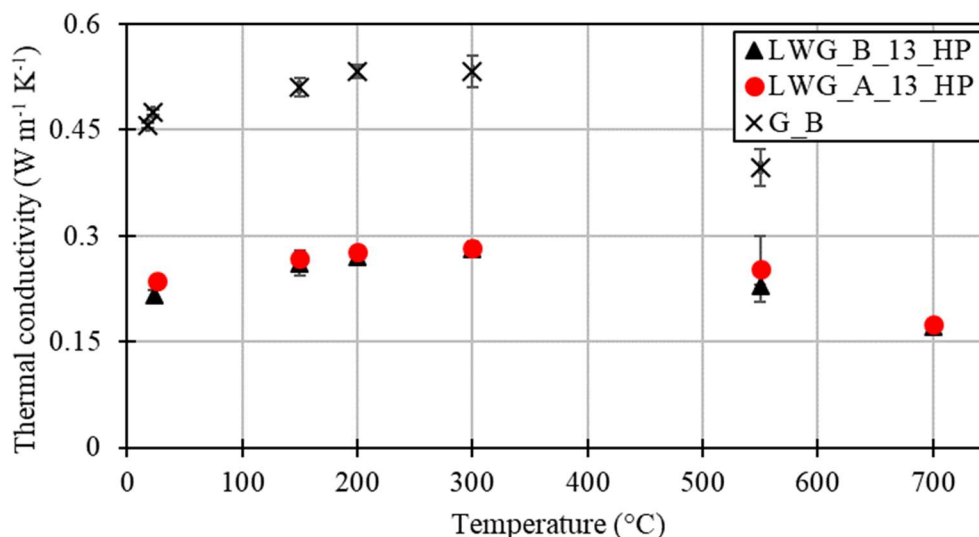
Figure 7.5: Variation of thermal conductivity with temperature.

The mass loss and the thermodynamic processes in geopolymer matrix and lightweight geopolymer mortars were measured using thermogravimetric analysis (TGA) and differential scanning calorimetry (DSC).

Figure 7.6 shows the mass losses determined in air atmosphere of the G_A series (Figure 7.6a) and of the G_B series (Figure 7.7b). The measurements were conducted on crushed and pre-dried (T = 105 °C) samples according to the procedure reported in 3.3.5.

In all cases, the mass loss was contained in the range of 4-8 %. These values are significantly lower compared to the ones of a gypsum and cementitious based fireproofing material (i.e. mass loss of 20-25 %) [186]. A mass loss was always verified in the temperature range of 80-100 °C up to about 300 °C and it can be associated to the dehydration of adsorbed and loosely bound water. This in in agreement to what observed by DSC analysis, where endothermic peaks associated with the dehydration were observed in the same temperature range (Figure 7.7). As the temperature increased, a second mass loss was found at temperature comprised in the range of 450-750 °C. Rickard et al. [67] performed TGA / DTA curves of fly ash-based geopolymers where the fly ash contained 15 wt% of iron oxide and they observed an exothermic spike at approximately 400 °C in the DTA curve and a simultaneous weight loss in the TGA curve. They concluded that the weight loss can be related to the loss of hydroxyl groups during the phase change of poorly ordered iron oxide from the fly ash crystallising to hematite.
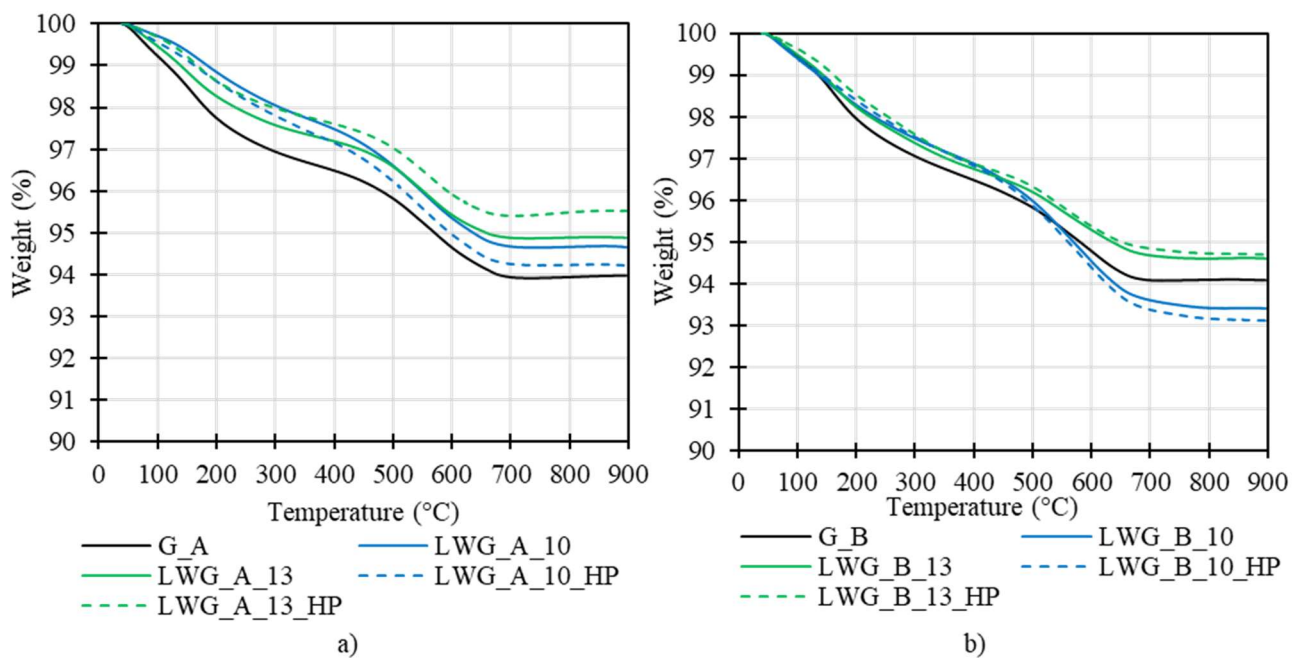
Figure 7.6: TGA measurements of geopolymers: G_A series (a); G_B series (b) (heating rate 10°C/min in air).

From the DSC curves the specific heat (c_p) of samples in the temperature range of 30-200 °C was obtained, according to EN 821-3 [115]. The compositional Si/Al ratio seemed to have negligible influence on the specific heat, which assumed values of about 870 J/ kgK at 30 °C and increased during heating up to about 1645 J/ kgK at 200 °C for both G_A and G_B. By adding expanded perlite and hydrogen peroxide, a decrease in the specific heat was found at high temperature. The specific heat of the foamed and lightweight samples in this study was observed to the range from 787 to 981 J/ kgK at 30 °C and increased during heating up to 1314 – 1571 J/ kgK at 200 °C.
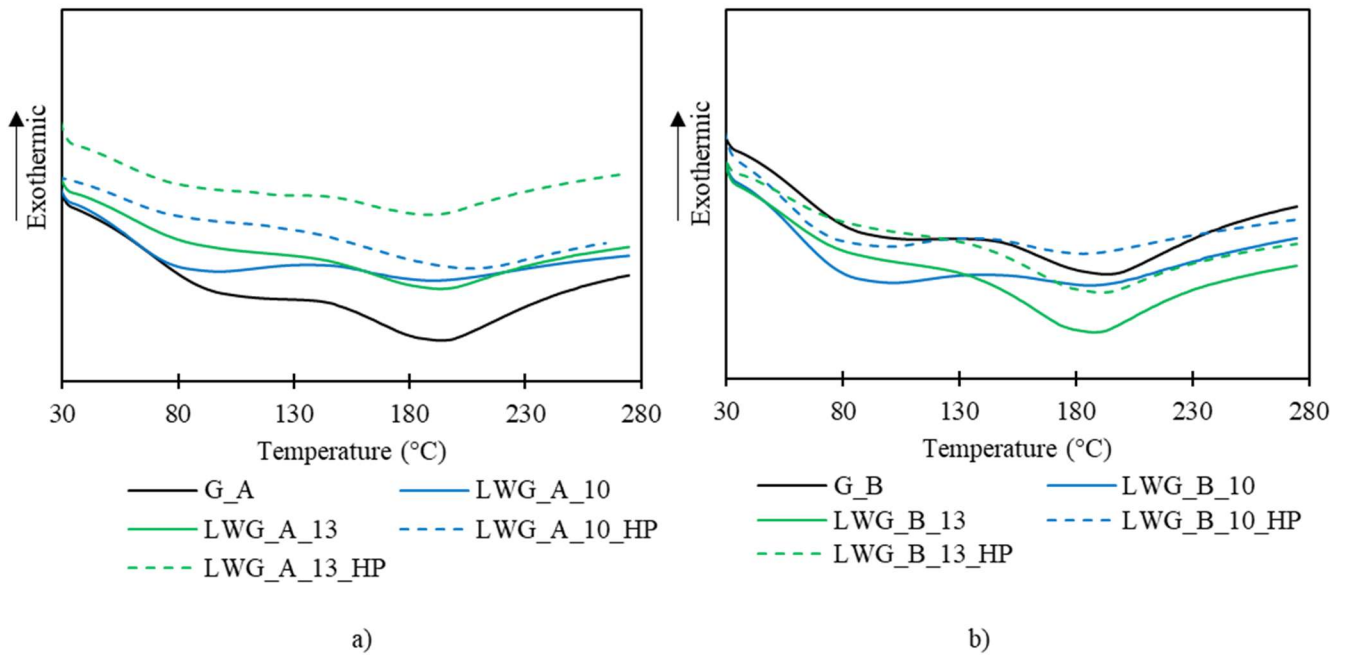
Figure 7.7: DSC measurements of geopolymers: G_A series (a); G_B series (b) (heating rate 20°C/min in nitrogen).

7.4   Finite volume method simulations of the fireproofing performance

In order to evaluate the potentiality of the geopolymers as passive fire protection system of steel structures, a finite volume method simulation was used to simulate a significant geometry for practical fireproofing applications. The performance of a geopolymer mixture (LWG_B_13_HP) was compared with a commercial Portland cement-based fireproofing mortar (named LWC). LWG_B_13_HP mix was chosen because of the lowest density and thermal conductivity showed among all the investigated mixtures in paragraphs 7.2 and 7.3. These features were considered the most important ones to take into account for a fireproofing coating.

The geometry considered a section of an infinite IPE 100 steel beam protected by a fireproofing layer of different thickness: 15, 20 and 25 mm for the LWG_B_13_HP and a 20 mm layer for the LWC. The steel beam was exposed on all of its faces to thermal irradiation. A slice 2D configuration of the element was meshed with tetrahedral cells. The number of cells are reported in Table 7.3, simulation run time was extended to 30 minutes.

Table 7.3: Number of cells for 2D simulation.

Thickness of the fireproofing layer (mm)	15	20	25
Number of cells	254480	352878	46761

Two standardized fire curves were considered as external thermal load: the standard fire curve in ISO 834, which is representative of building fires, and the fire curve RWS – Rijkswaterstaat. The RWS curve is the most harsh fire curve that can be adopted for testing the fire resistance of various elements of construction. The RWS curve was developed by Ministry of Transport in the Netherlands according to the results of testing

carried out by TNO in 1979. This curve is based on the assumption that in a worst-case scenario, a 50 m³ fuel, oil or petrol tanker fire with a fire load of 300 MW could occur, lasting up to 120 minutes.

The simulation used the experimental properties (i.e. bulk density, specific heat, thermal conductivity) of the geopolymers determined through small-scale tests presented in sections 7.2 and 7.3, while for LWC the properties reported in a previous study were used [196]. The thermal properties assumed for steel (S275) are density equal to 7850 kg/m³, heat capacity of 475 J/kg K and thermal conductivity equal to 44.5 W/m K.

The Figure 7.8 shows the temperature-time curves resulting from the simulation of cellulosic fire (Figure 7.8a) and RWS fire (figure 7.8b) conditions. In particular, the temperature rising of the steel surface covered by cementitious fireproofing mortar and different thickness of LWG_B_13_HP is plotted.
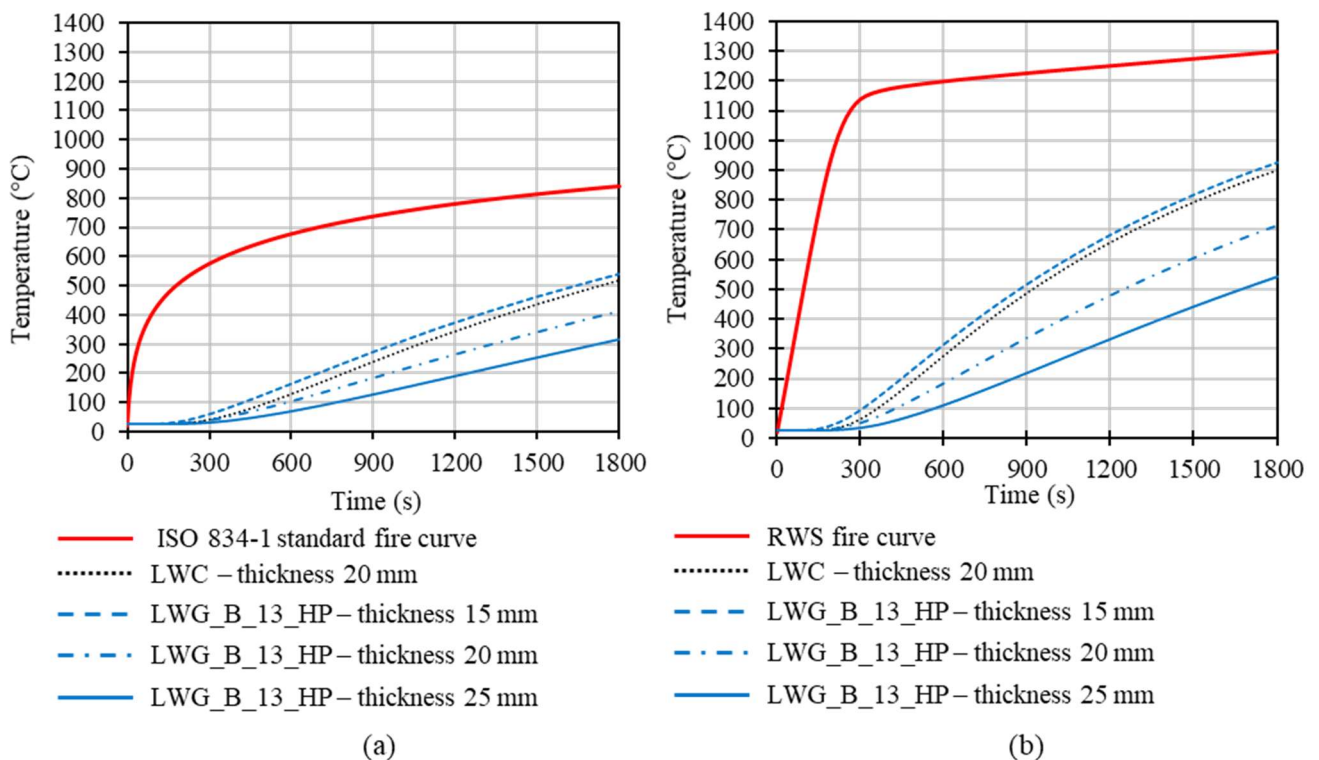
Figure 7.8: : Finite volume method simulations results of the case study considering the ISO 834 standard fire curve (a) and RWS fire curve (b).

In all cases, the mortars are effective in delaying the temperature rising of the steel. In the case of cellulosic fire, all the investigated possibilities allowed to protect the steel surface from reaching the critical temperature of 500°C for all the time of the test (30 minutes). Similar performance were found for a 20 mm thickness of LWC and 15 mm thickness of LWG_B_13_HP, thus suggesting that when lightweight geopolymer mortar is used, a thinner layer (15 mm) of coating can guarantee the same performance of a thicker layer (20 mm) of cementitious-based product. The performance improved for increasing thickness of geopolymer mortars. When RWS fire curve is simulated, the same trend as the one previously described was found. However, in this case, at least a 25 mm thickness of LWG_B_13_HP was found necessary to keep the steel surface under T = 500°C for the 30 minutes of the test.

7.5   Testing of the fireproofing performance: medium-scale fire tests

In this section, prototypes of steel protected by the LWG mortars characterized in paragraphs 7.2 and 7.3 were tested by means of medium-scale fire test setup. The LWG mixtures were selected with the aim to further investigate the influence of the Si/Al molar ratio, the alkali cation (i.e. Na or K) used, and the presence of a foaming agent (i.e. H_2O_2) on the fireproofing behaviour of the mortar. Cellulosic and hydrocarbon (EN 1363-2 [119]) standard fire curves were performed. In addition, a geopolymer mortar containing quartz aggregate (GM_A) was also realized for comparison. Finally, acoustic emission measurements were adopted to analyse cracking phenomena due to the high temperature exposure. Details on specimens preparation and test procedure are reported in section 3.3.6.

Figures 7.9a and 7.9b show the temperature-time curves of the specimens exposed to cellulosic fire as average of at least three measurements. Two different thickness of mortar layer were tested: 15 mm (Figure 7.9a) and 20 mm (Figure 7.9b). It worth to remind that the temperature-time curves were recorded to identify the time after which the temperature of the cold side of the steel plate exceed 500°C which is identified as the critical threshold for the properties of steel.

The bare steel plate showed a rapid increase of the temperature, which exceeded 500 °C after only 9 minutes. The comparison between the bare steel curve and the coated steel curves showed that mortars containing both sand and expanded perlite were always effective in retarding the temperature rise of the cold side of the steel. When a 15 mm-thick layer of mortar was applied, the cold side of the steel plate reached the critical temperature of 500 °C after 28 minutes in the best case. By increasing the thickness of the mortar layer to 20 mm a substantial improvement in terms of steel protection was observed. Indeed, as can be seen in Figure 7.9b, mortars were able to keep the temperature of the steel plate under the critical threshold for at least 30 minutes (GM_A) and up to 40 minutes (LWG_A_K_13).

Figure 7.9c shows the temperature-time curves of the specimens exposed to hydrocarbon fire. Only the 20 mm- thick layer was considered, as the conditions of the test were harsher than the previous one (i.e. the temperature in the furnace exceeded 1000 °C after the first 10 minutes of the test). The best performing mixture resulted to be the (LWG_A_K_13), which was able to protect the steel plate from reaching 500 °C for 16 minutes. As can be noted from the temperature-time curves, in the temperature range of 100–140 °C a plateau related to the endothermic dehydration of water contained in the specimens (as previously discussed in section 7.3) was always identified. The contribution of the dehydration significantly slowed down the temperature rise of the steel. For GM_A the plateau started for slightly higher temperature compared to lightweight mortars. This can be related to the different pore structure of the two types of mortars. In Figure 7.10 are reported the pore size distributions of the GM_A sample and of the lightweight geopolymer mortars. As representative examples, the curves of LWG_A_13 and LWG_B_13 are reported. As can be observed, LWG samples were significantly more porous than GM_A sample. In addition, a great difference in the pore structure was found for porous with a radius higher than 0.3 μm. Generally in geopolymer structure, water is mainly in the form of free water in large pores and bound water in small pores [22]. Therefore, because of its more compact structure, higher

temperature was required for water to evaporate from GM_A specimen. Moreover, it has to be noted that the GM_A specimen was produced by adding lesser overall amount of water (10 wt%) than the lightweight mortars (23-25 wt%), and this can affect the duration of the plateau related to the dehydration reaction.
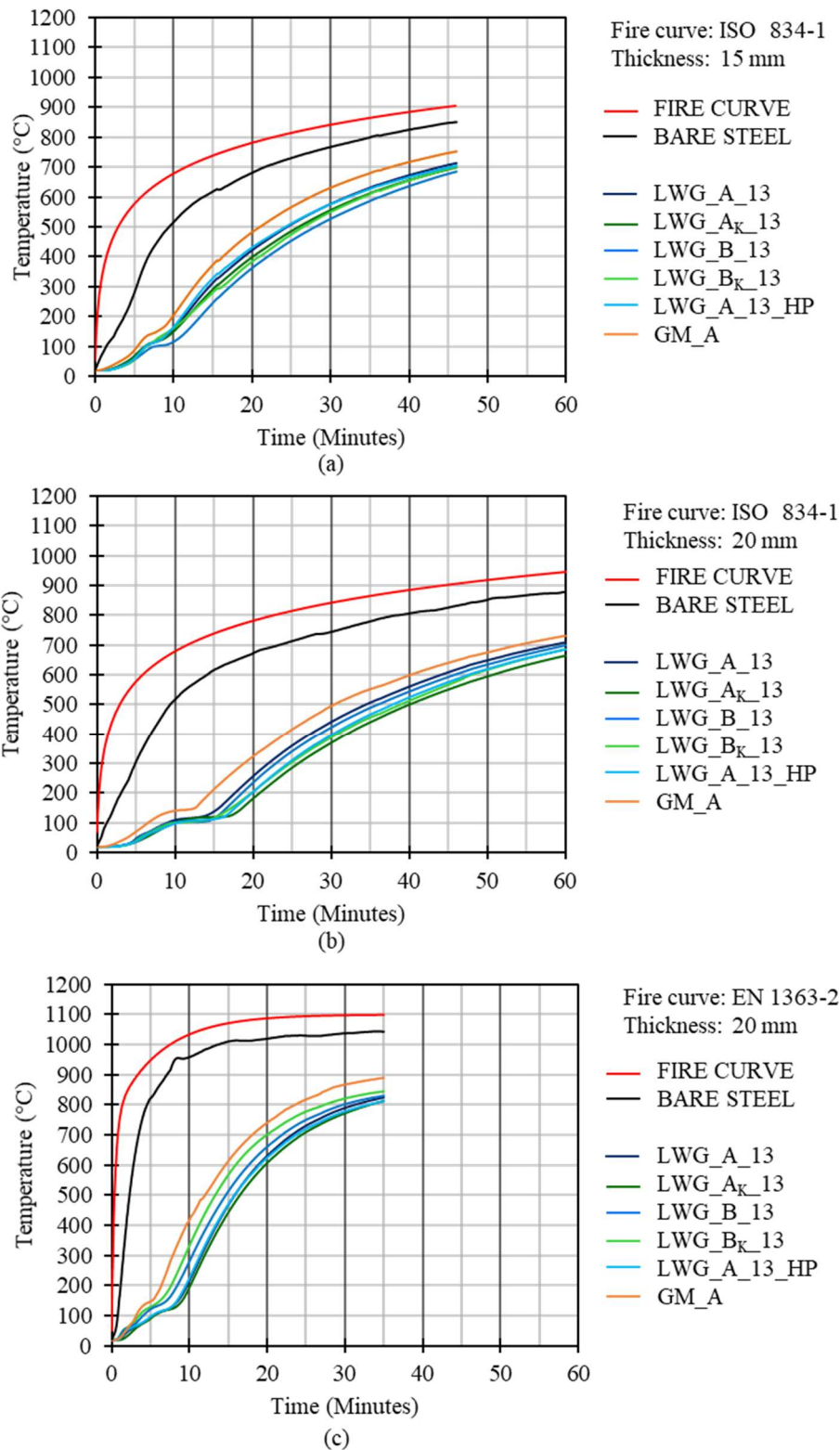
Figure 7.9: Temperature-time curves of the specimens exposed to cellulosic and hydrocarbon fire curves: cellulosic fire curve and layer thickness of 15 mm (a); cellulosic fire curve and layer thickness of 20 mm (b); hydrocarbon fire curve and layer thickness of 20 mm (c).
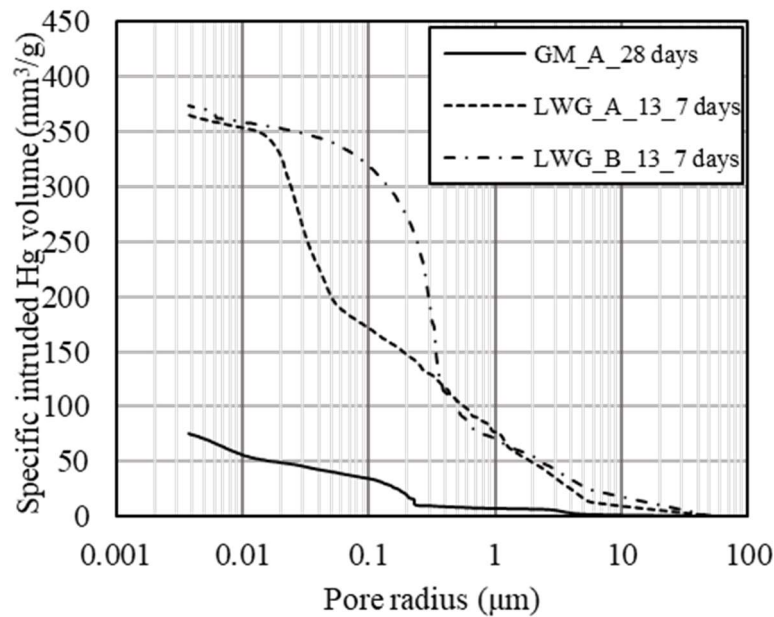
Figure 7.10: Comparison of the pore size distributions curves of the GM_A containing quartz aggregate and lightweight geopolymer mortars containing expanded perlite.

As expected, the expanded perlite was effective in enhancing the insulating properties of the mortar. Indeed, in all cases the GM_A reached higher temperature at shorter time. In the case of the lightweight mortars, it was not possible to indicate a best performing formulation among the ones investigated, since all specimens showed similar trend. The Si/Al ratio did not significantly affect the fire resistance of the material. This is in accordance with the results presented in paragraph 7.3 where no correlation between the thermal conductivity and geopolymer composition (Si/Al ratio) was found. In addition, as found in paragraph 6.2, the use mixed cation type (Na/K) in the alkaline activator seemed not to significantly improve the fireproofing performance of the LWG mortar. Finally, even though it was previously assessed the effectiveness of H_2O_2 as foaming agent and reducer of thermal conductivity of geopolymers (paragraph 7.2), in this case no significant benefits in terms of fire resistance were found by adding 0.3 wt% of hydrogen peroxide to the mixture.

Acoustic emission (AE) measurements during firing and subsequent cooling of the mortars studied here are reported in Figure 7.11. A previous study [199], already assessed the suitability of acoustic emission measurements for studying cracking mechanism occurring in geopolymers during fire tests. The temperature-time curves are correlated with the acoustic emission results obtained for the two different fire tests (i.e. cellulosic and hydrocarbon fire curves), according to the experimental program reported in Table 3.9. In this case, only results on LWG specimens are reported.

During the firing period, in the majority of the cases and for both fire curves, some hits were recorded at the start of the test when a rapid increase of the temperature occurred, and in correspondence with the temperature plateau related to the dehydration. LWG_B_13 specimen behaved differently from the others: although the temperature plateau was present, no significant acoustic emissions were recorded during dehydration. This can indicate a higher permeability of this specimen compared to the others, which favored

the escaping of water during heating without causing significant damage to the specimen. This is also supported by the results presented in section 7.2 where samples of the G_B series showed a more porous structure than G_A series samples, and characterized by a larger dimension of the open pores. The majority of crack formation occurred on cooling. These results agree with the results presented in paragraph 6.2, where crack formation of geopolymer matrix (G_A and G_A$_K$) were found on cooling for temperature higher than 550°C. In the case of cellulosic fire (continuous lines in Fig. 7.11),
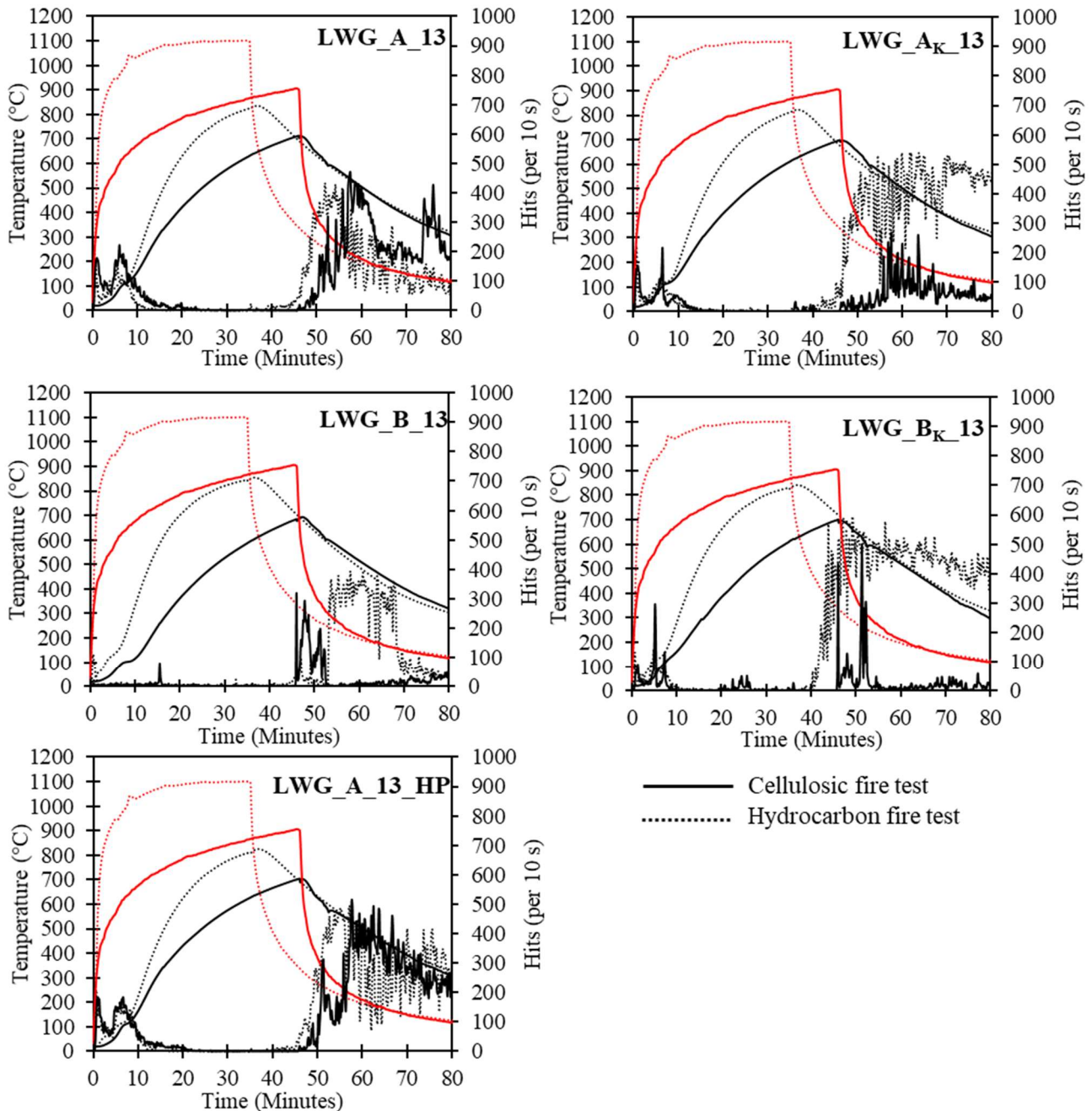
Figure 7.11 Acoustic emission results correlated with temperature-time curves inside the furnace (red curve) and the temperature-time curves of the cold side of the coated steel plates.

AEs were recorded immediately on cooling, when the temperature of the cold side of the covered steel plates was about 650-700 °C. On the contrary, when hydrocarbon fire curve was performed, no AEs were

recorded immediately at the extinguishing of the fire, but they appeared only when the temperature of the steel plates fell below approx. 700 °C. From these results, the temperature of 700 °C appears to be significant in terms of cracking and crack growth on cooling. As previously discussed in Chapter 6, it is assumed that a partial sintering and melting in localized areas of the mortars started to occur during heating and involved increasing portions of the material at increasing temperatures. The phases, which experienced sintering/melting during heating, experienced also a quenching on cooling, possibly when the temperature decreased below 700 °C. Up to this temperature, other regions, e.g. crystalline impurities from the fly ash, remain stable. It is possible that this phenomenon caused stress between the stable and the quenched phases and therefore may be at the origin of the cracking indicated by AE during the cooling period. In addition, the higher acoustic emission activity in the case of HC curve can possibly be related also to the formation of new crystalline phases, that occurs when fly ash-based, Na-activated geopolymers are heated above approx. 800 °C, as discussed in Chapter 6. The formation of these new crystalline phases on heating could induce increased stresses during the cooling period

After the complete cooling of the furnace, the specimens were removed from the sample holders and visually analyzed. In all cases, the specimens maintained their position in the sample holder during the test and only in the moment of their removal the steel plate detached from its coating mortar. Figure 7.12 reports the images of the specimens as cured (first row), 24 h after the cellulosic fire test (second row) and 24 h after the hydrocarbon fire test (third row).

None of the specimens experienced explosive spalling during heating, thus indicating a sufficient degree of permeability, which facilitates the release of the vapor pressure during the heat exposure. This aspect is particularly advantageous compared to ordinary Portland cement (OPC) based materials, which can be prone to spalling phenomena. The post-fire surfaces of the specimens varied as a function of the fire curve used. In accordance with what was observed by AE measurements, after the exposure to the cellulosic fire all specimens exhibited the presence of cracks. This was more evident for the lightweight mortars compared to the GM_A, probably because sand acted as reinforcement particle against crack propagation. Conversely, specimens exposed to the hydrocarbon fire showed almost no cracks on their surfaces, although the AE measurements indicated crack formation. In the case of hydrocarbon fire, the hot surface of the specimens was exposed up to 1100 °C; in this conditions, significant melting can occur which may be responsible for a self-healing process of cracks. It is interesting to note that the post-fire surface of LWG_B_13 specimen showed an increase in the porosity ('bubble formation') compared to the other specimens. It can be deduced that, when temperatures above 900 °C are involved, both, the Si/Al ratio and the alkali cation, influence the sintering process and the properties of the material after firing [61,197,200].
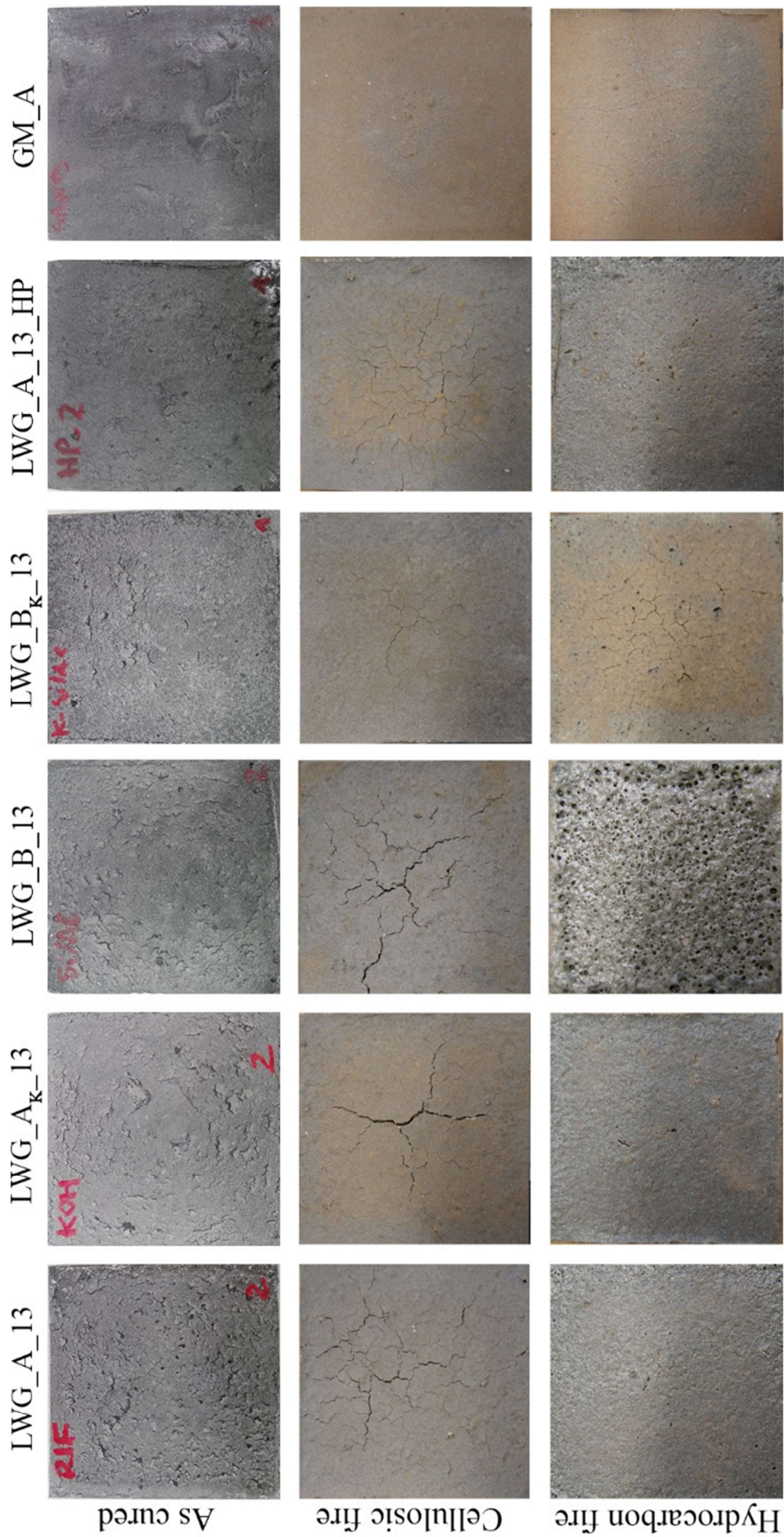
Figure 7.12: Specimen surfaces before and after the fire tests.

7.6   Comparison between simulated and experimental results

In this section, the temperature-time curves obtained from simulations were compared with the experimental data. It worth to remind that the test conditions are slightly different: in the case of the simulations a section of an infinite IPE 100 steel beam protected by different thickness of LWG_B_13_HP is exposed on all of its faces to thermal irradiation. In the experimental setup, a $20 \times 20 \times 2$ mm steel plate protected with several compositions of LWG mortar was considered and only one face was exposed to the flame. Although the conditions in the setup are different, in Figure 7.13 it can be observed a good agreement between the simulated data and the experimental results. Both simulated and experimental data refer to the ISO 834 standard fire curve. The black dot curve is representative of the simulated temperature-time curve of a steel protected by a 20 mm thick layer of cementitious fireproofing coating (LWC), whereas the green dashed line is representative of the simulated temperature-time curve of the steel covered by a 15 mm- (Figure 7.13a) and 20 mm-thick LWG_B_13_HP mortar (Figure 7.13b). The violet area shows the interval in which are included all the experimental temperature-time curves referring to LWG specimens exposed to medium-scale fire test. As can be seen, in both cases the simulated curve did not take into account the plateau related to the endothermic dehydration of water. However, at 30 minutes the temperature reached from the steel in the simulation is very close to the experimental findings.
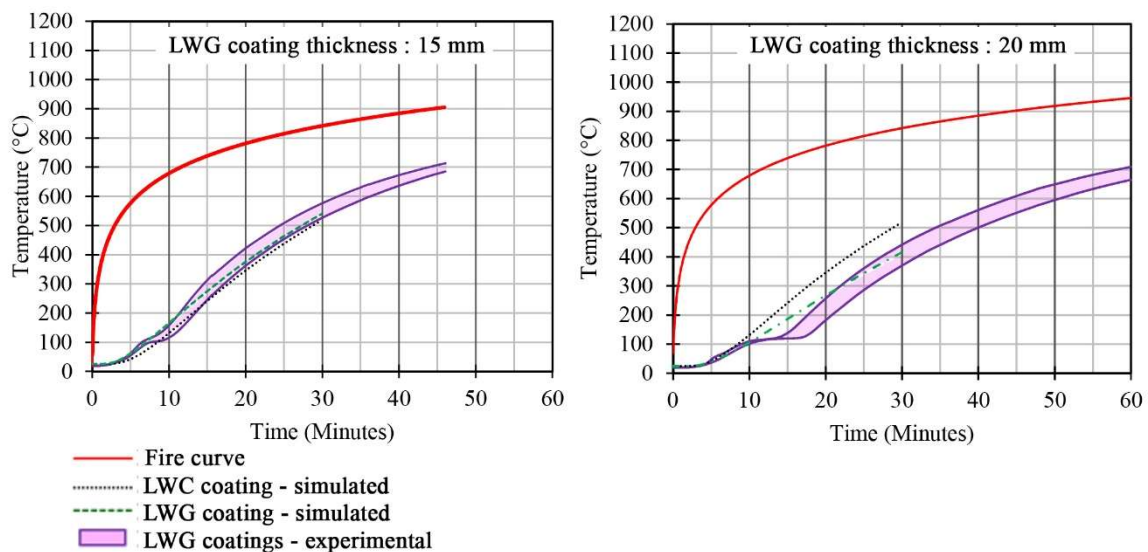
Figure 7.13: Comparison of the Temperature-time curves obtained by means of simulations and experimental data. LWG mortar thickness of 15 mm (a); LWG mortar thickness of 20 mm (b).

7.7   Main remarks

The results here discussed allow drawing the following conclusions:

- geopolymers with higher Si/Al ratio proved to be intrinsically denser, less porous and characterized by a higher compressive strength. However, the role of the geopolymer matrix

composition is secondary to the one of expanded perlite and hydrogen peroxide, as far as the thermal properties are concerned.

- The use of expanded perlite and hydrogen peroxide allowed obtaining a lightweight geopolymer mortar with properties similar to those of commercially available cementitious-based fireproofing coatings. In particular, geopolymer mortars containing 13 wt% of expanded perlite and 0.3 wt% of H_2O_2 showed bulk density values of around 0.78 g/cm^3 and thermal conductivity at T = 20°C of 0.21 W/mK. In addition, regardless the composition, all geopolymers showed high weight stability at high temperature with a total mass loss contained in 8% at 1000°C.

- The fireproofing behaviour of the geopolymer mortars appeared to be more influenced by the water content and thermal conductivity of the aggregate rather than by their composition in terms of Si/Al ratio and alkali cation. The mortars containing expanded perlite as aggregate are more protective towards fire scenarios compared to the mortar produced with quartz aggregate. As expected, a thicker layer of mortar led to the elongation of the dehydration plateau.

- Acoustic emission measurements enabled correlating crack formation and temperature of exposure. Cracking on heating was connected to dehydration processes. More severe events were recorded on cooling owed to the stress caused by cooling/quenching of the geopolymer matrix. The composition of the geopolymers resulted to be more important for the microstructural changes and sintering processes, which occurred at high temperature, as proved by the increased porosity of the surface of LWG_B_13 specimen exposed to the hydrocarbon fire.

General conclusions and perspectives

The research aimed at investigating the suitability of using cement-free fly ash-based geopolymers activated at room temperature in view of their application in civil and building engineering.

Fly-ash based geopolymers proved to be versatile materials that can be tailored according to the desired final performances. In particular, in this study by varying the type of aggregates (i.e., sand, refractory particles, expanded perlite) it was possible to test and characterize traditional and lightweight mortars, as well as composites, for different areas of application. The obtained results proved that in all the investigated cases, optimized fly ash-based geopolymers resulted promising and competitive products when compared to existing analogous cementitious-based materials.

In details, according to the experimental findings, the main and general conclusions can be summarized as follows.

In the absence of specifically designed admixtures for geopolymers, understanding if cement designed superplasticizers can be effective in alkali activated systems is a topic of great importance. Among the superplasticizers studied during this research, polycarboxylic ether-based superplasticizer in 1 wt% by mass of the solid precursor, was the best performing one on fly ash-based-geopolymer mortars as was able to provide good workability without affecting mechanical and microstructural properties of the hardened product.

Fly ash based geopolymer mortars resulted a suitable material for strengthening applications of existing concrete and masonry structures when used to prepare fibre reinforced geopolymer matrix (FRGM) composites. An interdisciplinary approach was used to gain information on physical and mechanical properties of the geopolymer mortars and on the stress mechanism in FRGM-substrate joints. Results showed that the study of the mix design is fundamental to avoid a detrimental interaction between the matrix and the fibres, especially when galvanized steel fibres are used. Even if it was not the aim of the investigation, from the presented results, it was possible to give insight into how the decrease in molar concentration of the activating NaOH solution (from 8 to 4 M) induces a decrease of geopolymers physical and mechanical properties. Nevertheless, GM_A_{4M} mortar still showed satisfactory properties for its use as matrix in FRGM systems with a compressive strength equal to 24 MPa at 28 days, and a dynamic modulus of elasticity equal to 11 GPa. In addition, the decrease of the molar concentration of sodium hydroxide activator produced an improvement of the matrix-fibre adhesion, which in turn enhanced the composite performance. Therefore, GM_A_{4M} was considered the most suitable mortar, among the ones investigated, to cast steel-FRGM composites. An adequate compatibility and adhesion of the composite with both concrete and masonry substrates were found, as well. Indeed, for all the tested specimens, the failure mode was debonding of the external layer of matrix from the internal layer (interlaminar failure) rather than debonding at the matrix-substrate interface. The FRGM composites showed similar performances to those achievable using cementitious mortars, with the average value of the maximum stress in the fibres in direct shear tests equal to 67% of the tensile strength provided by the manufacturer.

An extensive study on the behaviour of fly ash-based geopolymers activated at room temperature and exposed to high temperature was presented. In particular, the investigated geopolymers were assessed for their performance after thermal treatments in muffle furnace up to 1000 °C and after medium-scale fire tests. An extensive study of the cracking mechanism during heating and subsequent cooling was reported. Results showed that when cracking on heating was verified, it was connected to dehydration processes and occurred in the temperature range of 90-360 °C. It was possible to define 550 °C as critical temperature. Indeed, for temperature of exposure higher than 550 °C, acoustic emissions (AEs) were recorded also on cooling: the higher the temperature of exposure, the higher the AEs activity. By correlating acoustic emissions results with SEM and XRD analysis, it was highlighted that starting from 550 °C localized sintering phenomena occurred in the geopolymer matrix. From XRD analysis, it was found that heating up to 650°C did not induce modifications in the mineralogical composition of the material. Therefore, AEs detected above 550°C were not related to the formation of new crystalline phases. SEM micrographs showed no significant changes in the microstructure of the sample heated up to 500°C. On the contrary, crack formation was detected in the sample heated up to 600 °C. In this case, a detachment of the geopolymer gel from the unreacted fly ash particles was observed. After the exposure to 800°C, SEM micrographs showed evidence of sintering in the microstructure. According to the experimental findings, it was assumed that above 550 °C partial sintering and melting in localized areas of the material started to occur during heating and involved increasing portions of the material at increasing temperatures. The phases, which experienced sintering/melting during heating, also experienced a rapid quenching on cooling, whereas other regions, e.g. crystalline impurities from the fly ash, remained stable. The AE activity on cooling was thus associated to a stress between the stable phases and the shrinkage of the quenched phases.

The use of recycled refractory powder (RRP) for the production of geopolymer composites was proposed as a possibility to increase the thermal dimensional stability of fly ash-based geopolymers. Because of its crystalline nature, the inclusion of RRP did not hinder the alkali activation process. Conversely, it was found that the addition of 40 wt% of RRP to fly ash based geopolymers activated at room temperature, improved the linear dimensional stability during heating (linear shrinkage was no more than 2 % at 1000 °C) and increased the maximum temperature of dimensional stability from 1140 °C to 1240 °C. In addition, the amount of 30 wt% RRP resulted sufficient to inhibit the cracking after 2 h exposure to 1000 °C. Furthermore, it was found that, after the exposure to temperatures ≥ 800 °C, crystallization of nepheline and plagioclase feldspar occurred, which in the case of composites favoured the increase in the compressive strength.

Considering the remarkable thermal stability of fly ash-based geopolymers, lightweight geopolymer mortars were developed and characterized as passive fire protection systems for steel elements. A comprehensive study was presented, starting from the optimization of the mix design, up to the testing of the developed mortars by means of medium-scale fire test setup. Several parameters were taken into account to investigate their influence on the physical, mechanical, and thermal properties and, consequently, on the fireproofing behaviour of the obtained product. It was demonstrated that the use of expanded perlite as

lightweight aggregate was feasible for obtaining lightweight geopolymer mortars. Working on the mix design allowed obtaining a lightweight mortar with bulk density of around 0.78 g/cm^3 and thermal conductivity of 0.21 W/mK at T = 20°C. These values made geopolymers comparable to the commercially available cementitious-based fireproofing coatings. Finite volume method simulations and experimental medium-scale fire tests confirmed that the optimized lightweight geopolymer mortars can provide a protection of the steel substrate for more than 30 minutes under a cellulosic fire conditions, thus representing an important safety measure against accidental fires. The experimental findings demonstrated that the role of the geopolymer matrix composition (Si/Al ratio and alkali cation) is secondary to the one of the water content and of the expanded perlite, as far as the thermal properties are concerned. In addition, lightweight geopolymer mortars did not experience explosive spalling during heating, thus indicating a sufficient degree of permeability, which facilitated the release of the vapor pressure during the heat exposure. This aspect is particularly advantageous compared to ordinary Portland cement based materials, which can be prone to spalling phenomena.

The market entry of fly ash-based geopolymer technology can also be promoted by some economic advantages. A preliminary analysis of the costs of production of lightweight geopolymer mortars designed for fire protection (mix LWG_A_13_HP) was carried out and compared to the production costs estimated for a commercial cementitious-based product used as fireproofing coating. The calculation included costs of raw materials as well as transportation costs and management of the end life of the product. More details on the calculation are reported in APPENDIX A. Results showed that production costs of geopolymer and cementitious-based products are very close. It has to be highlighted that the analysis referred to the Italian context. Furthermore, only the production of one type of lightweight geopolymer mortar was investigated. It is highly probable that in a more global market and considering geopolymers for other types of applications (e.g. mortars containing quartz sand for FRGM composites) the benefits in terms of costs of geopolymers compared to cement-based material could be superior. However, as showed by the simulations, in order to obtain the same fire resistance rate, a thicker layer of the cementitious product is necessary. Considering that, the developed geopolymer product can be evaluated competitive in the market also from an economic point of view. In geopolymer production, the highest impact in both economic and sustainability terms is generated by the alkaline solutions that are the most expensive and pollutant components involved. Furthermore, alkaline solutions are not user-friendly and therefore they are often seen as a technical issue to overcome when the commercialization of geopolymers is concerned. However, research is already active on these topics. In particular, on the one hand there is some ongoing research investigating the possibility of replacing sodium silicate with suitable and sustainable silica source [92-94]. On the other hand, academic and industrial research is focusing on the study of the so-called "one part geopolymers" that consists in a mix of solid components that can be activated just adding water [201].

An extensive study on fly ash-based geopolymers activated at room temperature was reported in this thesis together with the proposal of different applications for this type of product in civil engineering supported by

encouraging and promising results. However, further research need to be done on the topic before obtaining market-ready products. Some suggestions for future research can be summarized as follows:

– further research on superplasticizers is essential, since superplasticizers are a very effective tool in promoting the practical use of geopolymers in civil engineering and results obtained so far in the academic community are not yet conclusive;

– the possibility of using other types of textiles (e.g. basalt, carbon, glass, and Poliparafenilenbenzobisoxazolo-PBO fabrics) in combination with fly ash-based geopolymer mortar to obtain FRGM composites for strengthening existing structures is a topic of great interest;

– among all the areas of civil engineering, geopolymers are certainly mostly competitive in the ones that involve high temperature resistance. To further increase the performance of fly ash-based geopolymers, additional studies are necessary to understand and control the reactions and the microstructural modifications linked to the compositional parameters that are induced by the high temperature exposure;

– finally, all the aspects related to standardisation and the analysis of durability and long-term performance are key issues to promote the acceptance of geopolymers as a new class of materials in the market.

References

[1] Jackson RB, Quéré CL, Andrew RM, Canadell JG, Peters GP, Roy J, et al. Warning signs for stabilizing global CO_2 emissions. Environmental Research Letters 2017;12:110202.

[2] Imbabi MS, Carrigan C, McKenna S. Trends and developments in green cement and concrete technology. International Journal of Sustainable Built Environment 2012;1:194–216.

[3] McLellan BC, Williams RP, Lay J, van Riessen A, Corder GD. Costs and carbon emissions for geopolymer pastes in comparison to ordinary portland cement. Journal of Cleaner Production 2011;19:1080–90.

[4] Provis JL. Alkali-activated materials. Cement and Concrete Research 2017 http://dx.doi.org/10.1016/j.cemconres.2017.02.009

[5] Davidovits J. Geopolymers inorganic polymeric new material. Journal of Thermal Analysis 1991;37:1633–56.

[6] Provis JL, van Deventer JSJ, editors. Alkali Activated Materials: State-of-the-Art Report, RILEM TC 224-AAM, Dordrecht: Springer Netherlands 2014.

[7] Kühl, H. Slag cement and process of making the same. US Patent 900,939 (1908).

[8] Purdon, A. The action of alkalis on blast furnace slag. Journal of the Society of Chemical Industry 1940;59:191–202.

[9] Glukhovsky, V.D. Gruntosilikaty (Soil Silicates). Gosstroyizdat, Kiev (1959).

[10] Krivenko P. Why Alkaline Activation – 60 Years of the Theory and Practice of Alkali-Activated Materials. Journal of Ceramic Science and Technology 2017;8:323–34.

[11] Pacheco-Torgal F, Castro-Gomes J, Jalali S. Alkali-activated binders: A review: Part 1. Historical background, terminology, reaction mechanisms and hydration products. Construction and Building Materials 2008;22:1305–14.

[12] Yang K, White CE. Modeling the Formation of Alkali Aluminosilicate Gels at the Mesoscale Using Coarse-Grained Monte Carlo. Langmuir 2016;32:11580–90.

[13] Shi C, Jiménez AF, Palomo A. New cements for the 21st century: The pursuit of an alternative to Portland cement. Cement and Concrete Research 2011;41:750–63.

[14] Provis JL, Bernal SA. Geopolymers and Related Alkali-Activated Materials. Annual Review of Materials Research 2014;44:299–327.

[15] Palomo, A, Krivenko, P, Garcia-Lodeiro, I, Kavalerova, E, Maltseva, O, Fernández-Jiménez, A. A review on alkaline activation: new analytical perspectives. Materiales de Construccion 2014;64;e022.

[16] Duxson P, Fernández-Jiménez A, Provis JL, Lukey GC, Palomo A, Deventer JSJ van. Geopolymer technology: the current state of the art. Journal of Materials Science 2006;42:2917–33.

[17] Provis JL. Geopolymers and other alkali activated materials: why, how, and what? Materials and Structures 2013;47:11–25.

[18] Duxson P, Provis JL, Lukey GC, Separovic F, van Deventer JSJ. 29Si NMR Study of Structural Ordering in Aluminosilicate Geopolymer Gels. Langmuir 2005;21:3028–36.

[19] Fernández-Jiménez A, Palomo A, Sobrados I, Sanz J. The role played by the reactive alumina content in the alkaline activation of fly ashes. Microporous and Mesoporous Materials 2006;91:111–9.

[20] Bernal SA, Provis JL. Durability of Alkali-Activated Materials: Progress and Perspectives. Journal of American Ceramic Society 2014;97:997–1008.

[21] Loewenstein W The distribution of aluminum in the tetrahedra of silicates and aluminates. American Mineralogist 1954;39;92–96

[22] White CE, Provis JL, Proffen T, Van Deventer JSJ. The Effects of Temperature on the Local Structure of Metakaolin-Based Geopolymer Binder: A Neutron Pair Distribution Function Investigation. Journal of the American Ceramic Society 2010;93:3486–92.

[23] Rashad AM. Metakaolin as cementitious material: History, scours, production and composition – A comprehensive overview. Construction and Building Materials 2013;41:303–18.

[24] Bell JL, Driemeyer PE, Kriven WM. Formation of Ceramics from Metakaolin-Based Geopolymers. Part II: K-Based Geopolymer. Journal of the American Ceramic Society 2009;92:607–15.

[25] Kamseu E, Rizzuti A, Leonelli C, Perera D. Enhanced thermal stability in K_2O-metakaolin-based geopolymer concretes by Al_2O_3 and SiO_2 fillers addition. Journal of Materials Science 2010;45:1715–24.

[26] Jamieson E, McLellan B, van Riessen A, Nikraz H. Comparison of embodied energies of Ordinary Portland Cement with Bayer-derived geopolymer products. Journal of Cleaner Production 2015;99:112–8.

[27] Williams RP, van Riessen A. Determination of the reactive component of fly ashes for geopolymer production using XRF and XRD. Fuel 2010;89:3683–92.

[28] Yao ZT, Ji XS, Sarker PK, Tang JH, Ge LQ, Xia MS, et al. A comprehensive review on the applications of coal fly ash. Earth-Science Reviews 2015;141:105–21.

[29] Blissett RS, Rowson NA. A review of the multi-component utilisation of coal fly ash. Fuel 2012;97:1–23.

[30] ASTM C618 Standard Specification for Coal Fly Ash and Raw or Calcined Natural Pozzolan for Use in Concrete 2017.

[31] EN 450-1 Fly ash for concrete. Definition, specifications and conformity criteria 2012.

[32] Halse Y, Pratt PL, Dalziel JA, Gutteridge WA. Development of microstructure and other properties in flyash OPC systems. Cement and Concrete Research 1984;14:491–8.

[33] Ahmaruzzaman M. A review on the utilization of fly ash. Progress in Energy and Combustion Science 2010;36:327–63.

[34] Rattanasak U, Chindaprasirt P. Influence of NaOH solution on the synthesis of fly ash geopolymer. Minerals Engineering 2009;22:1073–8.

[35] Fernández-Jiménez A, Palomo A, Criado M. Microstructure development of alkali-activated fly ash cement: a descriptive model. Cement and Concrete Research 2005;35:1204–9.

[36] Duxson P, Provis JL. Designing Precursors for Geopolymer Cements. Journal of the American Ceramic Society 2008;91:3864–9.

[37] Fernández-Jiménez A, Palomo A. Characterisation of fly ashes. Potential reactivity as alkaline cements. Fuel 2003;82:2259–65.

[38] Zhang Z, Provis JL, Zou J, Reid A, Wang H. Toward an indexing approach to evaluate fly ashes for geopolymer manufacture. Cement and Concrete Research 2016;85:163–73.

[39] Ma Y, Hu J, Ye G. The pore structure and permeability of alkali activated fly ash. Fuel 2013;104:771–80.

[40] Zhang Z, Provis JL, Reid A, Wang H. Fly ash-based geopolymers: The relationship between composition, pore structure and efflorescence. Cement and Concrete Research 2014;64:30–41.

[41] Sindhunata, van Deventer JSJ, Lukey GC, Xu H. Effect of Curing Temperature and Silicate Concentration on Fly-Ash-Based Geopolymerization. Industrial & Engineering Chemistry Research 2006;45:3559–68.

[42] Bignozzi MC, Manzi S, Natali ME, Rickard WDA, van Riessen A. Room temperature alkali activation of fly ash: The effect of Na_2O/SiO_2 ratio. Construction and Building Materials 2014;69:262–70.

[43] Criado M, Fernández-Jiménez A, Palomo A. Alkali activation of fly ash. Part III: Effect of curing conditions on reaction and its graphical description. Fuel 2010;89:3185–92.

[44] Duxson P, Provis JL, Lukey GC, Mallicoat SW, Kriven WM, van Deventer JSJ. Understanding the relationship between geopolymer composition, microstructure and mechanical properties. Colloids and Surfaces A: Physicochemical and Engineering Aspects 2005;269:47–58.

[45] Part WK, Ramli M, Cheah CB. An overview on the influence of various factors on the properties of geopolymer concrete derived from industrial by-products. Construction and Building Materials 2015;77:370–95.

[46] Zhuang XY, Chen L, Komarneni S, Zhou CH, Tong DS, Yang HM, et al. Fly ash-based geopolymer: clean production, properties and applications. Journal of Cleaner Production 2016;125:253–67.

[47] Pacheco-Torgal F, Castro-Gomes J, Jalali S. Alkali-activated binders: A review. Part 2. About materials and binders manufacture. Construction and Building Materials 2008;22:1315–22.

[48] Singh B, Ishwarya G, Gupta M, Bhattacharyya SK. Geopolymer concrete: A review of some recent developments. Construction and Building Materials 2015;85:78–90.

[49] Hardjito D, Wallah SE, Sumajouw DMJ, Rangan BV. On the Development of Fly Ash-Based Geopolymer Concrete. MJ 2004;101:467–72.

[50] Bakria AMMA, Kamarudin H, BinHussain M, Nizar IK, Zarina Y, Rafiza AR. The Effect of Curing Temperature on Physical and Chemical Properties of Geopolymers. Physics Procedia 2011;22:286–91.

[51] Puertas F, Palomo A, Fernández-Jiménez A, Izquierdo JD, Granizo ML. Effect of superplasticisers on the behaviour and properties of alkaline cements. Advances in Cement Research 2003;15:23–8.

[52] Criado M, Palomo A, Fernández-Jiménez A, Banfill PFG. Alkali activated fly ash: effect of admixtures on paste rheology. Rheologica Acta 2009;48:447–55.

[53] Laskar, A. I., Bhattacharjee, R. Effect of Plasticizer and Superplasticizer on Rheology of Fly-Ash-Based Geopolymer Concrete. Materials Journal 2013;110.

[54] Duxson P, Provis JL, Lukey GC, van Deventer JSJ. The role of inorganic polymer technology in the development of "green concrete." Cement and Concrete Research 2007;37:1590–7.

[55] Monticelli C, Natali ME, Balbo A, Chiavari C, Zanotto F, Manzi S, et al. Corrosion behavior of steel in alkali-activated fly ash mortars in the light of their microstructural, mechanical and chemical characterization. Cement and Concrete Research 2016;80:60–8.

[56] Monticelli C, Natali ME, Balbo A, Chiavari C, Zanotto F, Manzi S, et al. A study on the corrosion of reinforcing bars in alkali-activated fly ash mortars under wet and dry exposures to chloride solutions. Cement and Concrete Research 2016;87:53–63.

[57] Criado M. The corrosion behaviour of reinforced steel embedded in alkali-activated mortar. In: Pacheco-Torgal F, Labrincha J, Leonelli C, Palomo, Chindaprasit P, editors. Handbook of Alkali-Activated Cements, Mortars and Concretes, Oxford: Woodhead Publishing; 2015, p. 333–72.

[58] Panias D, Balomenos E, Sakkas K. 16 The fire resistance of alkali-activated cement-based concrete binders. In: Pacheco-Torgal F, Labrincha J, Leonelli C, Palomo, Chindaprasit P, editors. Handbook of Alkali-Activated Cements, Mortars and Concretes, Oxford: Woodhead Publishing; 2015, p. 423–61.

[59] Rickard WDA, Gluth GJG, Pistol K. In-situ thermo-mechanical testing of fly ash geopolymer concretes made with quartz and expanded clay aggregates. Cement and Concrete Research 2016;80:33–43.

[60] Rickard WDA, Temuujin J, van Riessen A. Thermal analysis of geopolymer pastes synthesised from five fly ashes of variable composition. Journal of Non-Crystalline Solids 2012;358:1830–9.

[61] Kong DLY, Sanjayan JG, Sagoe-Crentsil K. Factors affecting the performance of metakaolin geopolymers exposed to elevated temperatures. Journal of Materials Science 2008;43:824–31.

[62] Duxson P, Lukey GC, van Deventer JSJ. The thermal evolution of metakaolin geopolymers: Part 2 – Phase stability and structural development. Journal of Non-Crystalline Solids 2007;353:2186–200.

[63]   Barbosa VFF, MacKenzie KJD. Thermal behaviour of inorganic geopolymers and composites derived from sodium polysialate. Materials Research Bulletin 2003;38:319–31.

[64]   Duxson P, Lukey GC, Deventer JSJ van. Physical evolution of Na-geopolymer derived from metakaolin up to 1000 °C. J Mater Sci 2007;42:3044–54.

[65]   Rahier H, Mele BV, Wastiels J. Low-temperature synthesized aluminosilicate glasses. Part II Rheological transformations during low-temperature cure and high-temperature properties of a model compound. Journal of materials science 1996;31:80–5.

[66]   Rickard WDA, Kealley CS, van Riessen A. Thermally Induced Microstructural Changes in Fly Ash Geopolymers: Experimental Results and Proposed Model. Journal of American Ceramic Society 2015;98:929–39.

[67]   Rickard WDA, Riessen A van, Walls P. Thermal Character of Geopolymers Synthesized from Class F Fly Ash Containing High Concentrations of Iron and α-Quartz. International Journal of Applied Ceramic Technology 2010;7:81–8.

[68]   Provis JL, Yong CZ, Duxson P, van Deventer JSJ. Correlating mechanical and thermal properties of sodium silicate-fly ash geopolymers. Colloids and Surfaces A: Physicochemical and Engineering Aspects 2009;336:57–63.

[69]   Hertz KD. Concrete strength for fire safety design. Magazine of Concrete Research 2005;57:445–53.

[70]   White CE, Provis JL, Llobet A, Proffen T, van Deventer JSJ. Evolution of Local Structure in Geopolymer Gels: An In Situ Neutron Pair Distribution Function Analysis. Journal of the American Ceramic Society 2011;94:3532–9.

[71]   Vickers L, van Riessen A, Rickard WDA. Fire-Resistant Geopolymers - Role of Fibres and Fillers to Enhance Thermal Properties, Springer; 2015.

[72]   Pan Z, Sanjayan JG. Factors influencing softening temperature and hot-strength of geopolymers. Cement and Concrete Composites 2012;34:261–4.

[73]   Bakharev T. Thermal behaviour of geopolymers prepared using class F fly ash and elevated temperature curing. Cement and Concrete Research 2006;36:1134–47.

[74]   Zhao R, Sanjayan JG. Geopolymer and Portland cement concretes in simulated fire. Magazine of Concrete Research 2011;63:163–73.

[75]   Kong DLY, Sanjayan JG, Sagoe-Crentsil K. Comparative performance of geopolymers made with metakaolin and fly ash after exposure to elevated temperatures. Cement and Concrete Research 2007;37:1583–9.

[76]   Masi G, Rickard WDA, Bignozzi MC, van Riessen A. The effect of organic and inorganic fibres on the mechanical and thermal properties of aluminate activated geopolymers. Composites Part B: Engineering 2015;76:218–28.

[77]   Krivenko, P. V., Pushkareva, Ye.K., Sukhanevich, M. V. and Guziy, S. G. Fireproof Coatings on the Basis of Alkaline Aluminum Silicate Systems. In: H.-T. Lin, K. Koumoto, W. M. Kriven, E. Garcia, I. E. Reimanis and D. P. Norton, editors. Developments in Strategic Materials: Ceramic Engineering and Science Proceedings, Vol. 29, John Wiley & Sons, Inc., Hoboken, NJ, USA, 2008.

[78]   Krivenko PV, Guzii SG, Bodnarova L, Valek J, Hela R, Zach J. Effect of thickness of the intumescent alkali aluminosilicate coating on temperature distribution in reinforced concrete. Journal of Building Engineering 2016;8:14–9.

[79]   Watolla MB, Gluth GJG, Sturm P, Rickard WDA, Krüger S, Schartel B. Intumescent Geopolymer-Bound Coatings for Fire Protection of Steel. Journal of Ceramic Science and Technology n.d.;8:351–64.

[80]   Sakkas K, Sofianos A, Nomikos P, Panias D. Behaviour of Passive Fire Protection K-Geopolymer under Successive Severe Fire Incidents. Materials 2015;8:6096–104.

[81] Sakkas K, Panias D, Nomikos PP, Sofianos AI. Potassium based geopolymer for passive fire protection of concrete tunnels linings. Tunnelling and Underground Space Technology 2014;43:148–56.

[82] Sakkas K, Nomikos P, Sofianos A, Panias D. Sodium-based fire resistant geopolymer for passive fire protection. Fire and Materials 2015;39:259–70.

[83] ISO 834-1Fire-resistance tests - Elements of building construction -Part 1: General requirements 1999.

[84] Temuujin J, Minjigmaa A, Rickard W, Lee M, Williams I, van Riessen A. Fly ash based geopolymer thin coatings on metal substrates and its thermal evaluation. Journal of Hazardous Materials 2010;180:748–52.

[85] Temuujin J, Minjigmaa A, Rickard W, Riessen A van. Thermal properties of spray-coated geopolymer-type compositions. Journal of Thermal Analysis and Calorimetry 2011;107:287–92.

[86] Abidi S, Nait-Ali B, Joliff Y, Favotto C. Impact of perlite, vermiculite and cement on the thermal conductivity of a plaster composite material: Experimental and numerical approaches. Composites Part B: Engineering 2015;68:392–400.

[87] Novais RM, Buruberri LH, Ascensão G, Seabra MP, Labrincha JA. Porous biomass fly ash-based geopolymers with tailored thermal conductivity. Journal of Cleaner Production 2016;119:99–107.

[88] Masi G, Rickard WDA, Vickers L, Bignozzi MC, van Riessen A. A comparison between different foaming methods for the synthesis of light weight geopolymers. Ceramics International 2014;40:13891–902.

[89] Feng J, Zhang R, Gong L, Li Y, Cao W, Cheng X. Development of porous fly ash-based geopolymer with low thermal conductivity. Materials & Design 2015;65:529–33.

[90] Turner LK, Collins FG. Carbon dioxide equivalent (CO_2-e) emissions: A comparison between geopolymer and OPC cement concrete. Construction and Building Materials 2013;43:125–30.

[91] Passuello A, Rodríguez ED, Hirt E, Longhi M, Bernal SA, Provis JL, et al. Evaluation of the potential improvement in the environmental footprint of geopolymers using waste-derived activators. Journal of Cleaner Production 2017;166:680–9.

[92] Kamseu E, Beleuk à Moungam LM, Cannio M, Billong N, Chaysuwan D, Melo UC, et al. Substitution of sodium silicate with rice husk ash-NaOH solution in metakaolin based geopolymer cement concerning reduction in global warming. Journal of Cleaner Production 2017;142:3050–60.

[93] Tchakouté HK, Rüscher CH, Kong S, Kamseu E, Leonelli C. Geopolymer binders from metakaolin using sodium waterglass from waste glass and rice husk ash as alternative activators: A comparative study. Construction and Building Materials 2016;114:276–89.

[94] Toniolo N, Boccaccini AR. Fly ash-based geopolymers containing added silicate waste. A review. Ceramics International 2017.

[95] Habert G, d'Espinose de Lacaillerie JB, Roussel N. An environmental evaluation of geopolymer based concrete production: reviewing current research trends. Journal of Cleaner Production 2011;19:1229–38.

[96] Schweizerisches Ingenieur and Architektenverein (SIA). Anforderungen an neue Zemente (Merkblatt 2049), Zürich, Switzerland 2014

[97] British Standards Institute. BSI PAS 8820 Construction Materials – Alkali-activated Cementitious Material and Concrete – Specification, London, UK 2016

[98] ASTM C1157/C1157M Standard Performance Specification for Hydraulic Cement 2017

[99] Standardization Administration of China. GB/T 29423 Corrosion-resistant Products for Alkali-activated Slag Cement Fly Ash Concrete, Beijing 2012

[100] Natali ME, White CE, Bignozzi MC. Elucidating the atomic structures of different sources of fly ash using X-ray and neutron PDF analysis. Fuel 2016;177:148–56.

[101] EN 196-1 Methods of testing cement – part 1: Determination of strength 2005

[102]   Rashad AM. A synopsis about perlite as building material – A best practice guide for Civil Engineer. Construction and Building Materials 2016;121:338–53.

[103]   Technical data sheet Peralit 20. http://www.perlite.it/vedit/15/img_download/Scheda-tecnica-Peralit%2020-rev08.pdf (accessed October 15, 2017).

[104]   Technical data sheet GeoSteel G600. http://products.kerakoll.com/gestione/immagini/prodotti/00075GeoSteel%20G600%202014%20IIxEN_(EN).pdf (accessed October 03, 2017).

[105]   Koehler EP, Fowler DW. Summary of Concrete Workability Test Methods. Summary of Concrete Workability Test Methods, Research Report 105-1 2016.

[106]   EN 1015-3 Methods of test for mortar for masonry. Determination of consistence of fresh mortar (by flow table) 1999.

[107]   EN 1015-7 Methods of test for mortar for masonry. Determination of air content of fresh mortar 1999.

[108]   GSAS Notes. https://www.ncnr.nist.gov/xtal/software/gsas.html (accessed June 30, 2017).

[109]   Washburn EW. The Dynamics of Capillary Flow. Physical Review Letters 1921;17:273–83.

[110]   EN 15801 Conservation of cultural property. Test methods. Determination of water absorption by capillarity 2009.

[111]   EN 13057 Products and systems for the protection and repair of concrete structures. Test methods. Determination of resistance of capillary absorption 2002.

[112]   EN 12617-4 Products and systems for the protection and repair of concrete structures - Test methods. Determination of shrinkage and expansion 2002.

[113]   Carabba L, Santandrea M, Carloni C, Manzi S, Bignozzi MC. Steel fiber reinforced geopolymer matrix (S-FRGM) composites applied to reinforced concrete structures for strengthening applications: A preliminary study. Composites Part B: Engineering 2017;128:83–90.

[114]   EN 1542 Products and systems for the protection and repair of concrete structures. Test methods. Measurement of bond strength by pull-off 1999.

[115]   EN 821-3 Advanced technical ceramics. Monolithic ceramics. Thermo-physical properties. Determination of specific heat capacity 2005.

[116]   ISO 22007-2 Plastics - Determination of thermal conductivity and thermal diffusivity - Part 2: Transient plane heat source (hot disk) method 2015.

[117]   Instruction Manual Hot Disk® 6.0.

[118]   EN 1363-1 Fire resistance tests - Part 1: General Requirements 2012.

[119]   EN 1363-2 Fire resistance tests. Alternative and additional procedures 1999.

[120]   American Petroleum Institute Publication 2218 : Fireproofing Practices in Petroleum and Petrochemical Processing Plants, Second edition 1999.

[121]   Rixom R, Mailvaganam N. Chemical admixtures for concrete. London, United Kingdom: E & FN Spon; 1999.

[122]   Jolicoeur C, Simard MA. Chemical admixture-cement interactions: Phenomenology and physico-chemical concepts. Cement and Concrete Composites 1998;20:87–101.

[123]   Collepardi M. Admixtures used to enhance placing characteristics of concrete. Cement and Concrete Composites 1998;20:103–12.

[124]   Winnefeld F, Becker S, Pakusch J, Götz T. Effects of the molecular architecture of comb-shaped superplasticizers on their performance in cementitious systems. Cement and Concrete Composites 2007;29:251–62.

[125] Hanehara S, Yamada K. Interaction between cement and chemical admixture from the point of cement hydration, absorption behaviour of admixture, and paste rheology. Cement and Concrete Research 1999;29:1159–65.

[126] Ramachandran VS. Chemical Admixtures—Recent Developments. Concrete Admixtures Handbook, Park Ridge, NJ: William Andrew Publishing; 1996, p. 137–84.

[127] Rashad AM. A comprehensive overview about the influence of different admixtures and additives on the properties of alkali-activated fly ash. Materials & Design 2014;53:1005–25.

[128] Nematollahi B, Sanjayan J. Effect of different superplasticizers and activator combinations on workability and strength of fly ash based geopolymer. Materials & Design 2014;57:667–72.

[129] Palacios M, Puertas F. Effect of superplasticizer and shrinkage-reducing admixtures on alkali-activated slag pastes and mortars. Cement and Concrete Research 2005;35:1358–67.

[130] Nematollahi B, Sanjayan J. Efficacy of available superplasticizers on geopolymers. Research Journal of Applied Sciences, Engineering and Technology 2014;7:1278–82.

[131] Łaźniewska-Piekarczyk B. The methodology for assessing the impact of new generation superplasticizers on air content in self-compacting concrete. Construction and Building Materials 2014;53:488–502.

[132] Khatib JM, Mangat PS. Influence of superplasticizer and curing on porosity and pore structure of cement paste. Cement and Concrete Composites 1999;21:431–7.

[133] Carabba L, Manzi S, Bignozzi MC. Superplasticizer Addition to Carbon Fly Ash Geopolymers Activated at Room Temperature. Materials 2016;9:586.

[134] Collepardi M. Chemical admixtures today. Proceedings of Second International Symposium on Concrete Tecnology for Sustainable, Hyderabad, India: 2005, p. 527–41.

[135] Kashani A, Provis JL, Xu J, Kilcullen AR, Qiao GG, Deventer JSJ van. Effect of molecular architecture of polycarboxylate ethers on plasticizing performance in alkali-activated slag paste. Journal of Materials Science 2014;49:2761–72.

[136] Puertas F, Palacios M, Provis JL. Admixtures. In: Provis JL, van Deventer JSJ, editors. Alkali Activated Materials RILEM TC 224-AAM, Springer Netherlands; 2014, p. 145-156.

[137] Janowska-Renkas E. The effect of superplasticizers' chemical structure on their efficiency in cement pastes. Construction and Building Materials 2013;38:1204–10.

[138] Palacios M, Puertas F. Stability of superplasticizer and shrinkage-reducing admixtures Stability of superplasticizer and shrinkage-reducing admixtures in high basic media. Materiales de Construcción 2004;54:65–86.

[139] Pia G, Sassoni E, Franzoni E, Sanna U. Predicting capillary absorption of porous stones by a procedure based on an intermingled fractal units model. International Journal of Engineering Science 2014;82:196–204.

[140] D'Antino T, Carloni C, Sneed LH, Pellegrino C. Matrix–fiber bond behavior in PBO FRCM composites: A fracture mechanics approach. Engineering Fracture Mechanics 2014;117:94–111.

[141] Carloni C, Bournas DA, Carozzi FG, D'Antino T, Fava G, Focacci F, et al. Fiber reinforced composites with cementitious (Inorganic) matrix. RILEM State-of-the-Art Reports 2016;19:349–92.

[142] Donnini J, Corinaldesi V, Nanni A. Mechanical properties of FRCM using carbon fabrics with different coating treatments. Composites Part B: Engineering 2016;88:220–8.

[143] Carloni C, Verre S, Sneed LH, Ombres L. Loading rate effect on the debonding phenomenon in fiber reinforced cementitious matrix-concrete joints. Composites Part B: Engineering 2017;108:301–14.

[144] Ombres L. Analysis of the bond between Fabric Reinforced Cementitious Mortar (FRCM) strengthening systems and concrete. Composites Part B: Engineering 2015;69:418–26.

[145] Carloni C, D'Antino T, Sneed LH, Pellegrino C. Role of the matrix layers in the stress-transfer mechanism of FRCM composites bonded to a concrete substrate. Journal of Engineering Mechanics 2015;141.

[146] Van Balen K, Papayianni I, Van Hees R, Binda L, Waldum A. Introduction to requirements for and functions and properties of repair mortars. Materials and Structures 2005;38:781–5.

[147] Sassoni E, Pahlavan P, Franzoni E, Bignozzi MC. Valorization of brick waste by alkali-activation: A study on the possible use for masonry repointing. Ceramics International 2016;42:14685–94.

[148] Pacheco-Torgal F, Castro-Gomes JP, Jalali S. Adhesion characterization of tungsten mine waste geopolymeric binder. Influence of OPC concrete substrate surface treatment. Construction and Building Materials 2008;22:154–61.

[149] Geraldes CFM, Lima AM, Delgado-Rodrigues J, Mimoso JM, Pereira SRM. Geopolymers as potential repair material in tiles conservation. Applied Physics A 2016;122:197.

[150] Pacheco-Torgal F, Barroso de Aguiar J, Ding Y, Tahri W, Baklouti S. Performance of alkali-activated mortars for the repair and strengthening of OPC concrete. In: Pacheco-Torgal F, Labrincha J, Leonelli C, Palomo, Chindaprasit P, editors. Handbook of Alkali-Activated Cements, Mortars and Concretes, Oxford: Woodhead Publishing; 2015, p. 627–41.

[151] Mobili A, Belli A, Giosuè C, Bellezze T, Tittarelli F. Metakaolin and fly ash alkali-activated mortars compared with cementitious mortars at the same strength class. Cement and Concrete Research 2016;88:198–210.

[152] Pacheco-Torgal F, Abdollahnejad Z, Miraldo S, Baklouti S, Ding Y. An overview on the potential of geopolymers for concrete infrastructure rehabilitation. Construction and Building Materials 2012;36:1053–8.

[153] Zhang HY, Kodur V, Qi SL, Wu B. Characterizing the bond strength of geopolymers at ambient and elevated temperatures. Cement and Concrete Composites 2015;58:40–9.

[154] Bencardino F, Condello A, Ashour AF. Single-lap shear bond tests on Steel Reinforced Geopolymeric Matrix-concrete joints. Composites Part B: Engineering 2017;110:62–71.

[155] Katakalos K, Papakonstantinou CG. Fatigue of Reinforced Concrete Beams Strengthened with Steel-Reinforced Inorganic Polymers. Journal of Composites for Construction 2009;13:103–12.

[156] Menna C, Asprone D, Ferone C, Colangelo F, Balsamo A, Prota A, et al. Use of geopolymers for composite external reinforcement of RC members. Composites Part B: Engineering 2013;45:1667–76.

[157] Zhang H, Hao X, Fan W. Experimental Study on High Temperature Properties of Carbon Fiber Sheets Strengthened Concrete Cylinders Using Geopolymer as Adhesive. Procedia Engineering 2016;135:47–55.

[158] Tamburini S, Natali M, Garbin E, Panizza M, Favaro M, Valluzzi MR. Geopolymer matrix for fibre reinforced composites aimed at strengthening masonry structures. Construction and Building Materials 2017;141:542–52.

[159] Singh B, Rahman MR, Paswan R, Bhattacharyya SK. Effect of activator concentration on the strength, ITZ and drying shrinkage of fly ash/slag geopolymer concrete. Construction and Building Materials 2016;118:171–9.

[160] Carabba L, Santandrea M, Manzi S, Carloni C, Bignozzi MC. Geopolymer mortars for strengthening existing reinforced concrete structures, Proceedings of the 4th Workshop on New Boundaries of Structural Concrete Capri Island: 2016.

[161] Sneed LH, D'Antino T, Carloni C. Investigation of Bond Behavior of PBO Fiber-Reinforced Cementitious Matrix Composite-Concrete Interface. ACI Materials Journal 2014;111:569–80.

[162] Chindaprasirt P, Jaturapitakkul C, Chalee W, Rattanasak U. Comparative study on the characteristics of fly ash and bottom ash geopolymers. Waste Management 2009;29:539–43.

[163] Nath P, Sarker PK. Use of OPC to improve setting and early strength properties of low calcium fly ash geopolymer concrete cured at room temperature. Cement and Concrete Composites 2015;55:205–14.

[164] Zhang XG. Corrosion and electrochemistry of zinc, Plenum Press, New York, NY, 1996.

[165] De Santis S, Ceroni F, de Felice G, Fagone M, Ghiassi B, Kwiecień A, et al. Round Robin Test on tensile and bond behaviour of Steel Reinforced Grout systems. Composites Part B: Engineering 2017;127:100–20.

[166] Bernal SA, Krivenko PV, Provis JL, Puertas F, Rickard WDA, Shi C, et al. Other Potential Applications for Alkali-Activated Materials. In: Provis JL, van Deventer JSJ, editors. Alkali Activated Materials RILEM TC 224-AAM, Springer Netherlands; 2014, p. 339–79.

[167] Natali Murri A, Rickard WDA, Bignozzi MC, van Riessen A. High temperature behaviour of ambient cured alkali-activated materials based on ladle slag. Cement and Concrete Research 2013;43:51–61.

[168] Temuujin J, van Riessen A. Effect of fly ash preliminary calcination on the properties of geopolymer. Journal of Hazardous Materials 2009;164:634–9.

[169] Nazari A, Bagheri A, Dao M, Mallawa C, Zannis P, Zumbo S, et al. The behaviour of iron in geopolymer under thermal shock. Construction and Building Materials 2017;150:248–51.

[170] Rahier H, Simons W, Mele BV, Biesemans M. Low-temperature synthesized aluminosilicate glasses: Part III Influence of the composition of the silicate solution on production, structure and properties. Journal of Materials Science 1997;32:2237–47.

[171] Duxson P, Lukey GC, van Deventer JSJ. Thermal evolution of metakaolin geopolymers: Part 1 – Physical evolution. Journal of Non-Crystalline Solids 2006;352:5541–55.

[172] Bernal SA, Bejarano J, Garzón C, Mejía de Gutiérrez R, Delvasto S, Rodríguez ED. Performance of refractory aluminosilicate particle/fiber-reinforced geopolymer composites. Composites Part B: Engineering 2012;43:1919–28.

[173] Musil SS, Kriven WM. In Situ Mechanical Properties of Chamotte Particulate Reinforced, Potassium Geopolymer. Journal of American Ceramic Society 2014;97:907–15.

[174] Vickers L, Rickard WDA, van Riessen A. Strategies to control the high temperature shrinkage of fly ash based geopolymers. Thermochimica Acta 2014;580:20–7.

[175] Ribero D, Kriven WM. Properties of Geopolymer Composites Reinforced with Basalt Chopped Strand Mat or Woven Fabric. Journal of American Ceramic Society 2016;99:1192–9.

[176] Carabba, L., Manzi, S., Rambaldi, E., Ridolfi, G., Bignozzi, M.C. High temperature behaviour of alkali activated composites based on fly ash and recycled refractory particles. Journal of Ceramic Science and Technology 2017;8:377–88.

[177] Kuenzel C, Grover LM, Vandeperre L, Boccaccini AR, Cheeseman CR. Production of nepheline/quartz ceramics from geopolymer mortars. Journal of the European Ceramic Society 2013;33:251–8.

[178] Fernández-Jiménez A, Pastor JY, Martín A, Palomo A. High-Temperature Resistance in Alkali-Activated Cement. Journal of the American Ceramic Society 2010;93:3411–7.

[179] Sabbatini A, Vidal L, Pettinari C, Sobrados I, Rossignol S. Control of shaping and thermal resistance of metakaolin-based geopolymers. Materials & Design 2017;116:374–85.

[180] Aredes FGM, Campos TMB, Machado JPB, Sakane KK, Thim GP, Brunelli DD. Effect of cure temperature on the formation of metakaolinite-based geopolymer. Ceramics International 2015;41:7302–11.

[181] Mohd Salahuddin MB, Norkhairunnisa M, Mustapha F. A review on thermophysical evaluation of alkali-activated geopolymers. Ceramics International 2015;41:4273–81.

[182] Porcari G-LF, Zalok E, Mekky W. Fire induced progressive collapse of steel building structures: A review of the mechanisms. Engineering Structures 2015;82:261–7.

[183] American Petroleum Institute, Fireproofing Practices in Petroleum and Petrochemical Processing Plants, API Publication 2218, 1999.

[184] Goode MG. NIST GCR 04-872, Fire Protection of Structural Steel in High-Rise Buildings. U.S. Department of Commerce Technology Administration National Institute of Standards and Technology, 2004.

[185] Alongi J, Han Z, Bourbigot S. Intumescence: Tradition versus novelty. A comprehensive review. Progress in Polymer Science 2015;51:28–73.

[186] Kodur VKR, Shakya AM. Effect of temperature on thermal properties of spray applied fire resistive materials. Fire Safety Journal 2013;61:314–23.

[187] Kodur V, Arablouei A. Effective properties of spray-applied fire-resistive material for resistance to cracking and delamination from steel structures. Construction and Building Materials 2015;84:367–76.

[188] Rickard WDA, van Riessen A. Performance of solid and cellular structured fly ash geopolymers exposed to a simulated fire. Cement and Concrete Composites 2014;48:75–82.

[189] Rickard WDA, Vickers L, van Riessen A. Performance of fibre reinforced, low density metakaolin geopolymers under simulated fire conditions. Applied Clay Science 2013;73:71–7.

[190] Lanzón M, García-Ruiz PA. Lightweight cement mortars: Advantages and inconveniences of expanded perlite and its influence on fresh and hardened state and durability. Construction and Building Materials 2008;22:1798–806.

[191] Ozer I, Soyer-Uzun S. Relations between the structural characteristics and compressive strength in metakaolin based geopolymers with different molar Si/Al ratios. Ceramics International 2015;41:10192–8.

[192] Duxson P, Mallicoat SW, Lukey GC, Kriven WM, van Deventer JSJ. The effect of alkali and Si/Al ratio on the development of mechanical properties of metakaolin-based geopolymers. Colloids and Surfaces A: Physicochemical and Engineering Aspects 2007;292:8–20.

[193] Komljenović M, Baščarević Z, Bradić V. Mechanical and microstructural properties of alkali-activated fly ash geopolymers. Journal of Hazardous Materials 2010;181:35–42.

[194] Narayanan N, Ramamurthy K. Structure and properties of aerated concrete: a review. Cement and Concrete Composites 2000;22:321–9.

[195] Zhang Z, Provis JL, Reid A, Wang H. Mechanical, thermal insulation, thermal resistance and acoustic absorption properties of geopolymer foam concrete. Cement and Concrete Composites 2015;62:97–105.

[196] Moricone R, Tugnoli A. Investigating the properties of fireproofing materials for an advanced design of equipment protection. Chemical Engineering Transactions 2015;43:2389–94.

[197] Duxson P, Lukey GC, van Deventer JSJ. Thermal Conductivity of Metakaolin Geopolymers Used as a First Approximation for Determining Gel Interconnectivity. Industrial & Engineering Chemistry Research 2006;45:7781–8.

[198] Hanley EJ, Dewitt DP, Roy RF. The thermal diffusivity of eight well-characterized rocks for the temperature range 300–1000 K. Engineering Geology 1978;12:31–47.

[199] Gluth GJG, Rickard WDA, Werner S, Pirskawetz S. Acoustic emission and microstructural changes in fly ash geopolymer concretes exposed to simulated fire. Materials and Structures 2016;49:5243–54.

[200] Sotiriadis K, Guzii S, Kumpová I, Mácová P, Viani A. The Effect of Firing Temperature on the Composition and Microstructure of a Geocement-Based Binder of Sodium Water-Glass. Solid State Phenomena 2017;267:58–62.

[201] Luukkonen T, Abdollahnejad Z, Yliniemi J, Kinnunen P, Illikainen M. One-part alkali-activated materials: A review. Cement and Concrete Research 2017.

[202] Ruberto A. Master Thesis, Analisi del ciclo di vita di geopolimeri per applicazioni di fireproofing (in italian). University of Bologna 2016.

List of Figures

List of Tables

List of Papers on peer reviewed journals

- **Carabba L.**, Manzi S., Bignozzi M.C., *Superplasticizer addition to carbon fly ash geopolymers activated at room temperature*, Materials 2016, 9 (7), 586.

- **Carabba L.**, Santandrea M., Carloni C., Manzi S., Bignozzi M.C., *Steel fiber reinforced geopolymer matrix (S-FRGM) composites applied to reinforced concrete structures for strengthening applications: a preliminary study*, Composites part B: Engineering, 128, 83 - 90, 2017.

- **Carabba L.**, Manzi S., Rambaldi E., Ridolfi G., Bignozzi M.C., *High temperature behaviour of alkali activated composites based on fly ash and recycled refractory particles*, Journal of Ceramic Science and Technology, 8 (3), 377 - 388, 2017.

- Dal Pozzo A., **Carabba L.**, Bignozzi M.C., Tugnoli A*., Life cycle assessment of a geopolymer mixture for fireproofing applications* – submitted to The International Journal of Life Cycle Assessment on 19th February 2018.

- **Carabba L.**, Moricone R., Scarponi G.E., Tugnoli A., Bignozzi M.C., *Coal fly ash based geopolymers for fireproofing applications: a preliminary study of the performance* – submitted to Fuel on 14th March 2018.

List of Proceedings of national and international conferences

- **Carabba L.**, Manzi S., Bignozzi M.C., *Fly ash geopolymers: effect of admixtures on fresh and hardened properties*, Proceedings of the 1st International Workshop on Durability and Sustainability of Concrete Structures, <u>Bologna</u> (Italy), 1st – 3rd October 2015, published as paper in ACI Special Publication, SP-305, Eds. M.A. Chiorino, L. Coppola, C. Mazzotti, R. Realfonzo, P. Riva, American Concrete Institute, 2015, pp 297-301 – *oral presentation.*

- Manzi S., **Carabba L.**, Bignozzi M.C., *Study of the influence of different admixtures on the properties of alkali-activated materials*, Proceedings of the 14th International Congress of the Chemistry of the Cement, <u>Beijing</u> (China), 13th – 16th October 2015 – *oral presentation.*

- **Carabba L**., Santandrea M., Manzi S., Carloni C., Bignozzi M.C., *Assessing the suitability of fly ash geopolymer for strengthening existing reinforced concrete structure*, Proceedings of the 13th National Congress AIMAT, <u>Ischia Porto</u> (Italy), 13th – 15th July 2016, published as abstract in Journal of applied biomaterials & functional materials, 2016, 14, pp. e344 - e344 – *oral presentation.*

- **Carabba L.**, Ridolfi G., Manzi S., Bignozzi M.C., *Thermal properties of fly ash based geopolymers containing refractory powder*, Proceedings of National Forum of Young Researcher of Materials Science and Technology, <u>Ischia Porto</u> (Italy), 11th – 13th July 2016, published as abstract in Journal of applied biomaterials & functional materials, 2016, 14, pp. e319 - e319 – *oral presentation.*

- **Carabba L.**, Santandrea M., Manzi S., Carloni C., Bignozzi M.C., *Geopolymer mortars for strengthening existing reinforced concrete structures,* Proceedings of The New Boundaries of Structural Concrete 2016, <u>Capri Island</u> (Italy), 29th September – 1st October 2016 – *oral presentation.*

- **Carabba L.**, Manzi S., Bignozzi M.C., Santandrea M., Carloni C., *Materiali compositi fibrorinforzati a matrice geopolimerica per il rinforzo di strutture in calcestruzzo armato o in muratura*, Proceedings of Giornate di Studio sui Geopolimeri – IX edizione – Geopolimeri e Compositi, <u>Napoli</u> (Italy), 26th – 27th January 2017.

- **Carabba L.**, Ridolfi G., Manzi S., Bignozzi M.C., *Geopolymers containing refractory powder for high temperature applications*, Proceedings of the 92nd DKG Annual Conference & Symposium on High-Performance Ceramics 2017, TU Berlin (Germany), 19th - 22nd March 2017 – *oral presentation.*

- **Carabba L.**, Manzi S., Bignozzi M.C., Santandrea M., Carloni C., *Preliminary studies on the suitability of coal fly ash geopolymer mortars for strengthening existing concrete and masonry structures*, Proceedings of the 2nd European Geopolymer Network, Madrid (Spain), 14th July 2017.

- **Carabba L.**, Gluth G.J.G., Pirskawetz S.M., Krüger S., Bignozzi M.C., *Fly ash-based lightweight geopolymer mortars for fire protection*, submitted for the 2nd International Workshop on Durability and Sustainability of Concrete Structures DSCS 2018, Moscow (Russia), 6th - 7th June 2018 – *accepted as oral presentation.*

- **Carabba L.,** Moricone R., Scarponi G.E., Tugnoli A., Bignozzi M.C., *Investigation of lightweight geopolymer mortars as fireproofing coatings,* submitted for the ECI conference, International Conference on Alkali Activated Materials and Geopolymers, Tomar (Portugal), 27th May - 1st June 2018 – *accepted as oral presentation.*

- **Carabba L.**, Rambaldi E., Ridolfi G., Bignozzi M.C., *Geopolymer matrix composites as innovative sustainable refractories*, Proceedings of ECerS2017 - 15th Conference & Exhibition of the European Ceramic Society, 9th –13th July 2017, Budapest (Hungary) – *poster.*

- Bedon A., **Carabba L.**, Bignozzi M.C., Natile M.M., Glisenti A., *Environmentally friendly LSGF-functionalized fly-ash geopolymers for pollutants abatement in industrial processes*, Proceedings of Europacat 2017, 27th – 31st August 2017, Florence (Italy) – *poster.*

Oral presentations at conferences

- 14th International Congress of the chemistry of cement (14th ICCC), 13-16 October 2015, Beijing- China.

- International Workshop on durability and sustainability of concrete structures (DSCS 2015), 1st-3rd October 2015, Bologna- Italy.

- National Forum of Young Researchers, 11th-13th July 2016, Ischia-Italy.

- XIII National Congress AIMAT, 13th-15th July 2016, Ischia – Italy.

- 4th Workshop on The New Boundaries of Structural Concrete (NBSC 2016), 29th September- 01st October 2016, Capri – Italy.

- 92nd DKG Annual Meeting & Symposium on High-Performance Ceramics 2017 (92.DKG), 19th-22nd March 2017, Berlin – Germany.

APPENDIX A

A preliminary investigation of the production costs of one type of lightweight geopolymer mortar (LWG_A_13_HP) studied as passive fire protection system (see Chapter 7), was carried out. The cost analysis of analogous commercial cementitious-based fireproofing coating (LWC) was also reported for comparison.

The cost analysis refer to the Italian market and Italian territory and the unit costs of raw materials reported in Table A.1 are based on commercial offers by suppliers. Fly ashes are waste materials and for this reason their cost was considered negligible in the calculation of raw materials cost. Instead, the transportation costs of fly ashes were considered.

Table A.1: Cost of raw materials used for producing 1 m³ of geopolymer and cement-based product

Cost of raw materials – transportation costs excluded						
Lightweight geopolymer mortar - LWG						
Component	Mix design		Unit cost		Cost of raw materials	
Fly ash	410.4	kg/m³	0.00	€/kg	0.0	€/m³
8M NaOH solution	31.2	kg/m³	0.60	€/kg	18.7	€/m³
Sodium silicate solution	154.3	kg/m³	0.21	€/kg	32.4	€/m³
Perlite	102.7	kg/m³	1.15	€/kg	118.1	€/m³
Water	89.3	kg/m³	0.002	€/kg	0.2	€/m³
Hydrogen peroxide	2.4	kg/m³	0.50	€/kg	1.2	€/m³
Total	790.3	kg/m³			**170.6**	**€/m³**
Commercial cementitious-based fireproofing coating - LWC						
Component	Mix design		Unit cost		Cost of raw materials	
Portland cement	274.4	kg/m³	0.12	€/kg	32.9	€/m³
Vermiculite	102.3	kg/m³	1.30	€/kg	133.0	€/m³
CaCO₃	88.4	kg/m³	0.11	€/kg	9.7	€/m³
Water	310.0	kg/m³	0.002	€/kg	0.5	€/m³
Total	775.1	kg/m³			**176.2**	**€/m³**

According to a preliminary study [202], the transportation costs (including fuel) were considered higher in the case of geopolymer products because the raw materials necessary for geopolymers production were assumed less distributed in the territory, thus increasing the transportation distances. The transportation costs of raw materials to the production site were estimated equal:

- 3% of the raw materials cost for geopolymers;
- 1% of the raw materials cost for cementitious based material.

Other costs such as transportation costs to the working site and management of the end life of 1 m³ of material were assumed equal for both products and calculated as reported in Table A.2 [202].

Table A.1: Other costs

	Amount	Unit	Unit cost		Costs	
Fuel costs for the transportation to the working site (in case it is different from the production site)	50	km	0.033	€/km	1.6	€/m³
Demolition and transportation to the landfill	1	m³	90	€/ m³	90.0	€/m³
Landfilling	790	kg	0.008	€/kg	6.3	€/m³
Total					**97.9**	**€/m³**

According to the results, the production costs of lightweight geopolymer mortars (LWG) and cementitious-based fireproofing coatings (LWC), including the cost of raw materials as well as transportation costs and management of the end life of the products, can be summarized as follows:

LWG : 274 €/m³ and 0.35 €/kg

LWC : 276 €/m³ and 0.36 €/kg

Lorenza Carabba

Via San Felice, 83 – 40122 Bologna, Italia

lorenza.carabba@gmail.com

https://www.unibo.it/sitoweb/lorenza.carabba3

https://www.researchgate.net/profile/Lorenza_Carabba

lorenza_ca

November 2017 – October 2018	**Postdoctoral Research fellow** University of Bologna - Department of Civil, Chemical, Environmental and Materials Engineering – Via Terracini, 28 – 40131, Bologna, Italy Research project: *Study and development of innovative materials with high content of wastes for applications in civil and building engineering* Supervisor: Prof. M. C. Bignozzi
November 2014 –October 2017	**PhD student in Civil, Chemical, Environmental and Materials Engineering curriculum: Materials Science and Technology** University of Bologna - Department of Civil, Chemical, Environmental and Materials Engineering – Via Terracini, 28 – 40131, Bologna, Italy Expected date for Doctoral degree: May 2018 Title of the PhD thesis: *Cement-free building materials: mix design and properties in view of their application in civil engineering* Supervisor: Prof. M. C. Bignozzi Co-supervisors: Dr. S. Manzi
October 2016 – April 2017	**Visiting PhD Student** BAM - Bundesanstalt für Materialforschung und –prüfung (division 7.4) Unter den Eichen, 87 – 12205, Berlin, Germany Supervisor: Dr. Ing. Gregor Gluth
October 2013	**M.Sc. degree in Building Engineering and Architecture (110/110)** B-ECTS scale University of Bologna - Via Risorgimento, 2– 40126, Bologna, Italy Title of the Master thesis: *Durability, mechanical behaviour and microstructure of new cement-free building materials* Supervisor: Prof. M.C. Bignozzi Co-supervisors: Prof. C. Monticelli, Dr. S. Manzi, Dr. M. E. Natali, Dr. M. Abbottoni Subject: Technology of Materials and Applied Chemistry
April – September 2013	**Internship within Department of Civil, Chemical, Environmental and Materials Engineering - Laboratory of Materials Science and Technology - LASTM** University of Bologna– Via Terracini, 28 – 40131, Bologna, Italy **Collaboration with Corrosion and Metallurgy Center "A. Daccò" of the University of Ferrara in the frame of the Master thesis project** University of Ferrara - Via Saragat, 4/a – 44122, Ferrara, Italy